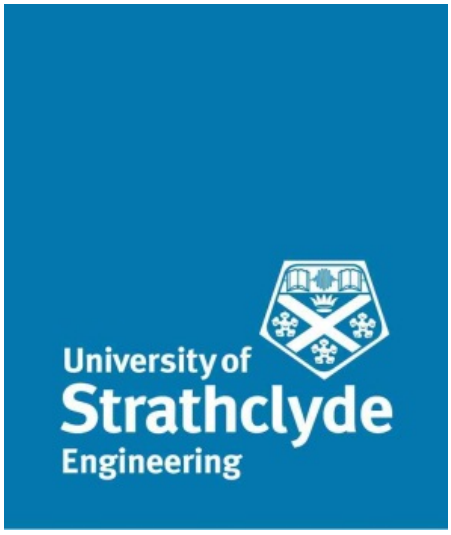

Investigating fibre/matrix interface and sizing components in thermoplastic composites

A thesis in fulfilment of the requirements for the degree of Doctor of Philosophy

By

Roya Akrami

Department of Mechanical and Aerospace Engineering

University of Strathclyde

Glasgow, Scotland

UK

2024

Declaration of Authenticity and Author's Rights

This thesis is the result of the author's original research. It has been composed by the author and has not been previously submitted for examination which has led to the award of a degree.

Signed: R.Akrami

Date: 19.11.2024

Acknowledgments

I would like to express my heartfelt gratitude to my first supervisor, Dr. Liu Yang, for the unwavering guidance and support provided throughout my academic journey. His expertise and mentorship have been invaluable.

I am also deeply thankful to my second supervisor, Professor James Thomason, for generously sharing his time and expertise. His contributions have greatly enriched my research.

I extend my appreciation to all the current and former members of the Advanced Composites Group at the University of Strathclyde, especially Dr David Bryce. Their advice and assistance have been instrumental in shaping my work, and it has been a privilege to collaborate with such talented individuals.

I would like to acknowledge the financial support received from Şişecam and the University of Strathclyde. Their funding has played a crucial role in enabling the successful completion of this research.

Lastly, I am profoundly grateful to my parents, brothers, and my love, Mohammad, for their unconditional love, unwavering support, and constant encouragement throughout my studies. Their belief in me has been a driving force behind my achievements.

To everyone mentioned above, I am sincerely thankful. I am indebted to each and every one of you for your contributions to my academic and personal growth.

Thank you.

Roya

Publications

Several results of this thesis have been published or are under review in the form of journal articles and conference contributions.

Akrami, Roya, Liu Yang, and James L. Thomason. "Investigating the effect of silane coupling agent on glass fibre/thermoplastic interfacial adhesion." The 20th European Conference on Composite Materials (ECCM20). 2022.

Akrami, Roya; Yang, Liu; Thomason, James L. "Investigating the effect of amino silane pH on glass fibre/thermoplastic interfacial adhesion". The 6th Brazilian Conference on Composite Materials (BCCM6). 2022.

Akrami, Roya, Liu Yang, and James L. Thomason. " Exploring a New Laboratory-Scale Approach for Glass Fibre Sizing Analysis Using Spin Coating Method." Under review, Journal of material science 2024

Akrami Roya, Liu Yang, and James L. Thomason. "Investigating on silane coupling agent variations on glass fibre thermoplastic composites." In perpetration to be submitted to Composites Part A: Applied Science and Manufacturing 2024.

James L. Thomason, Akrami Roya, Liu Yang, and. A new method to prepare more representative coated glass fibres for screening and development of sizings at the laboratory scale. The 21st European Conference on Composite Materials (ECCM21), 2024.

Abstract

Glass fibre sizing, a critical thin coating applied during glass fibre manufacturing, significantly influences the quality and performance of the final composite products. This sizing is integral not only to the fibre's processability and profitability but also to optimizing the fibre/matrix interface in composites. Recognizing the necessity to enhance our understanding of fibre sizing and its impact on this interface, this thesis aims to provide a thorough study of the glass fibre thermoplastic interface, focusing on the role of different sizing components in the interphase performance of glass fibre-reinforced thermoplastics.

A pivotal aspect of this study is the development of a novel laboratory-based coating method, using the spin coating technique, designed to closely mimic the properties of industrial sized fibres. This method was assessed against traditional dip coating for the lab research and industrial sizing techniques, examining variables such as Loss of ignition (LOI), surface chemistry, adhesion, and surface morphology. Findings indicate that spin coating not only achieves an LOI% similar to industrial standards but also allows for precise control over LOI% by adjusting the spinning speed. This method yields a thin coating layer, crucial for achieving the desired thicknesses.

The research evaluates the efficacy of silane variations, i.e., γ-aminopropyltriethoxysilane (APS), γ-glycidoxypropyltrimethoxysilane (GPS), and γ-methacryloxypropyltrimethoxysilane (MPS), in the performance of glass fibre-reinforced thermoplastics. The interfacial shear strength (IFSS) of fibres sized with different components was measured using microbond tests with thermoplastics like Homo-Polypropylene (PP), Maleic Anhydride Grafted Polypropylene (MAPP), Polyamide 6 (PA6), and Polybutylene Terephthalate (PBT). The study also investigates the impact of pH levels and APS solution concentrations (as the most compatible silane for thermoplastics [1]) on IFSS. Results demonstrate a general increase in IFSS with APS sizing across the studied matrix systems, though pH level variations showed minimal impact. The PP-compatible sizing was selected for investigation, as PP is one of the most widely used thermoplastics due to its excellent corrosion resistance, ease of processing, and low cost [2]. The effect of the PP film-former and full-sizing (PP film former + APS) was also examined to understand the interfacial properties of the sized fibre with PP and MAPP matrices. The study revealed that using the film former alone does not enhance the IFSS in comparison to the bare fibre. Nonetheless, a combination of silane and the film former leads to an increase in IFSS for both PP and MAPP matrices.

In summary, this thesis provides a comprehensive exploration of glass fibre thermoplastic interfaces, emphasizing the critical role of sizing in optimizing stress-transfer capability and overall performance in glass fibre-reinforced thermoplastics. The findings highlight the spin coating technique's potential in laboratory research and the pivotal role of silane coupling agents and film former in fibre sizing, setting the stage for developing more realistic sizing in the laboratory and providing efficient and effective sizing formulations for advanced composite materials.

Table of Contents

Declaration of Authenticity and Author's Rights i

Acknowledgments ii

Publications iii

Abstract iv

Table of Contents vi

Abbreviations ix

List of Figures x

List of Tables xvi

CHAPTER 1: INTRODUCTION 1

1.1. Project background 1

1.2. Originality 3

1.3. Aims and objectives 3

1.4. Outline of the thesis 4

CHAPTER 2: LITERATURE REVIEW 5

2.1. Introduction to glass fibres 5

2.2. Composition of glass fibres and their surface 7

2.3. Glass fibre manufacturing 9

2.4. Glass fibre sizing 9

2.4.1. Silane coupling agent 11

2.4.2. Film formers 14

2.4.3. Auxiliary components 15

2.5. Glass fibre-reinforced thermoplastic composites 16

CHAPTER 3: EXPERIMENTAL METHODS 19

3.1. Microbond test 19

3.1.1. Thermoplastic droplet sample preparation 21

3.1.2. Thermoset droplet sample preparation 22

3.1.3 Microbond test procedure 23

3.2. Hot stage microscopy set up 25

3.3. TGA 27

3.4. SEM 28

3.5. AFM 30

3.6. FTIR 31

CHAPTER 4: A NEW LABORATORY-SCALE APPROACH TO GLASS FIBRE SIZING USING A SPIN COATING METHOD 33

4.1. Introduction 33

4.2. Literature review 36
4.2.1. Glass fibre sizing techniques 36
.4.2.2 Spin coating 39
4.2.3. Sizing characterization 40
4.2.4. Literature conclusion 40

4.3. Experimental procedures 41
4.3.1. Materials 41
4.3.2. Sizing techniques 42
4.3.3. TGA of sizing layer 44
4.3.4. Morphological analysis using SEM and AFM 45
4.3.5. Microbond test 46

4.4. Results and discussion 46
4.4.1. TGA study 46
4.4.2. SEM observation 54
4.4.3. AFM results 57
4.4.4. Microbond test results 58

4.5. Conclusions 61

CHAPTER 5: CHARACTERIZATION AND ADHESION PERFORMANCE OF SILANE-SIZED GLASS FIBRES IN THERMOPLASTIC COMPOSITES 62

5.1. Introduction 62

5.2. Literature review: 63
5.2.1. Silane coupling agent and its role in composite material 63
5.2.2. Adhesion between glass fibre and matrix 63
5.2.3. Silane effect on glass fibre/matrix interphase 69
5.2.4. Chemical interactions of silanes with thermoplastics 75
5.2.5. Literature conclusion 76

5.3. Experimental procedure 76
5.3.1. Materials 76
5.3.2. Silane treatment 76
5.3.3. TGA 78
5.3.4. Spectroscopic characterisation of silane sized glass fibres 78
5.3.5. Hot stage microscopy 78
5.3.6. Microbond 78

5.4. Results and discussion **78**
5.4.1. TGA results of silane sized glass fibre 78
5.4.2. Spectroscopic characterisation of silane sized glass fibres 79
5.4.3. Droplet formation observation 82
5.4.4. Successful debonding 86
5.4.5. Microbond results 88

5.5. Conclusion **95**

CHAPTER 6: CHARACTRIZING THE EFFECT OF FILM FORMER AND FULL SIZING IN GLASS FIBRE/PP, MAPP MATRICES **97**

6.1. Introduction **97**

6.2. Literature review **98**
6.2.1. The role of film former and full sizing in interphase 98
6.2.2. Sizing thermal stability and chemistry 101
6.2.3. Sizing film formation 102
6.2.4. Literature conclusion 103

6.3. Experimental Procedure **104**
6.3.1. Material 104
6.3.2. Film former and full sizing coating procedures 104
6.3.3. Effect of silane on sizing emulsion stability 106
6.3.4. TGA 106
6.3.5. FTIR 106
6.3.6. Microbond 106
6.3.7. Sizing film formation 106

6.4. Results and discussion **107**
6.4.1. Sizing emulsion stability characterization 107
6.4.2. TGA of fully sized glass fibre 109
6.4.3. FTIR Analysis 111
6.4.4. Microbond results 118
6.4.5. Film former and sizing film formation 121

6.5. Conclusion **127**

CHAPTER 7: SUMMARY AND RECOMMENDATIONS FOR FUTURE WORK **128**

7.1. Statement on the novelty of the work presented **128**

7.2. Summary of conclusions **128**

7.3. Recommendations for future work **133**

References **135**

Abbreviations

ABS	Acrylonitrile Butadiene Styrene
AFM	Atomic Force Microscopy
APS	γ-aminopropyltriethoxysilane
APTMS	γ -Aminopropyltrimethoxysilane
DSC	Differential Scanning Calorimetry
FTIR	Fourier-Transform Infrared Spectroscopy
FE-SEM	Field-emission scanning electron microscopy
GFRP	Glass Fibre Reinforced Polymer
GPS	γ-glycidoxypropyltrimethoxysilane
GSLX	Poly(glycidyloxypropyl)siloxan
IFSS	Interfacial Shear Strength
LOI	Loss On Ignition
ILSS	Interlaminar Shear Strength
MAPP	Maleic Anhydride Grafted Polypropylene
MPS	γ-methacryloxypropyltrimethoxysilane
NMR	Nuclear Magnetic Resonance
NIR	Near-infrared
Homo-PP	Polypropylene
PVA	Polyvinyl Acetate
K	Potassium
PTMS	Propyltrimethoxysilane
TEOS	Tetraethoxysilane
Na	Sodium
SFPO	Single Fibre Pull Out
STS	N-β(N-vinylbenzylaminoethyl)-γ-aminopropyltrimethoxysilane hydrogen chloride
SFM	Scanning Force Microscopy
TTS	Isopropyltriisostearoyl titanate
TCVS	Trichlorosilane
UD	Unidirectional
VTES	Vinyltriethoxysilane
XPS	X-ray Photoelectron Spectroscope

List of Figures

Figure 2.1. Examples of glass fibre composites usage in different industrial sectors [21, 22]. 6

Figure 2.2. Schematic diagram illustration of local-to-global multiscale parameters affecting composite materials properties [23]. 6

Figure 2.3. Schematic diagram illustration of: (a) a crystalline structure; (b) a simple glass; and (c) a multicomponent glass [24]. 7

Figure 2.4. Schematic representation of a glass fibre production line. Adapted from [28]. 9

Figure 2.5. Simplified illustration of important components in sizing 10

Figure 2.6. Interpenetrating network structure at the interface between glass fibre sizing and polymer matrix [29]. 11

Figure 2.7. Chemical structure of APS, GPS and MPS [31]..... 12

Figure 2.8. Simplified illustration of important parameters for creating aqueous solution silane coupling agents..... 13

Figure 2.9. Hydrolyzation and condensation process of silane coupling agents. reproduced from [32]. 13

Figure 2.10. Bonding of self-condensed silane coupling agent with substrate surface (such as glass). Reproduced from [32]..... 14

Figure 2.11. Schematic of 3D network structure of hydrolysed APS on glass fibre [33]..... 14

Figure 2.12. Thermoplastics vs. thermoset plastics [34]..... 16

Figure 2.13. Materials trends in aerospace systems flyaway weight requirements [38]..... 17

Figure 2.14. Molecular structure of the investigated polymers. 17

Figure 3.1. Schematic of thermoplastic droplet sample preparation. a) thermoplastic fibre. b) knot around the fibre with thermoplastic fibre. c) Droplet formed after processing 21

Figure 3.2. Thermoplastic sample preparation process. a) Fibre mounted on the steel washer and polymer thread tied around fibre. b) Specimens placed on the steel hooks to be placed in the vacuum oven. c) Specimens in the vacuum oven 22

Figure 3.3. Thermoset droplet sample preparation. 23
Figure 3.4. An example of a PP droplet and measurements. 24
Figure 3.5. a) Thermoplastic microbond sample b) thermoplastic microbond test set up and c) thermoset microbond sample d) thermoset microbond test set up. 24
Figure 3.6. Microbond load versus displacement plot showing a) successful debonding and b) premature fibre fracture..... 25
Figure 3.7 a) Hot stage microscopy setup with sample in place, b) Schematic of hot-stage microscopy sample with microdroplet shown..... 27
Figure 3.8 Fibre bundle in TGA pan. 28
Figure 3.9. a) Gold coated Fibre bundle SEM specimen. b) gold coated single fibre with microbond droplet SEM specimens. 30
Figure 3.10. Schematic of an AFM plate with mounted fibres..... 31
Figure 3.11. AFM 3-D height image of Industrial fuuly sized fibre, a) before flattering and b) after flattering to remove curvature..... 31
Figure 4.1. An example of the dip coating and drying process of a glass fibre bundle. a) Dip coating of glass fibre bundle, usually for 15 min. b) Placed in an aluminium tray for drying in a conventional oven usually at 110 C. c) Dried fibre. 34
Figure 4.2. An example of the dip coated fibre bundles hanged for drying. 35
Figure 4.3.a) Schematic and b) picture of a glass fibre forming position [4]. 36
Figure 4.4. A picture of a sizing applicator in glass fibre production [1]. 37
Figure 4.5. A picture of a sizing applicator in glass fibre production [113]. 40
Figure 4.6. PP compatible sizing process steps..... 42
Figure 4.7. Schematic of the a,c) dip coating and b,d) spin coating methods..... 43
Figure 4.8. a) Sizing was placed at the middle of the slide right b) sizing was placed all over the slide as placed on the fibre bundle. 43

Figure 4.9. a) Spin coated and dip coted bundle in an aluminium tray before placed in the oven b) Spin coted and dip coated fibre bundles after 120 min drying. 44
Figure 4.10. Glass fibre sizing layer model graph. 45
Figure 4.11. Comparison of a) TGA and b) DTG graphs, of the S1A samples with the coating method of dip coated, spin coated, No spin (0.2 ml of sizing applied without spinning), Comparison of c) TGA and d) DTG graphs, of the S3A samples with the coating method of dip coated, spin coated and S3A fibre samples. 47
Figure 4.12. a) Comparison of TGA and DGT graphs of the IS and spin coated S1A at 10000 rpm. b) Comparison of TGA and DTG graphs of the ISE and spin coated S3A (4000 rpm). 49
Figure 4.13. Comparison of average LOI% of a) PP compatible industrial sized fibre (IS), spin coated (S1A). b) Epoxy compatible industrial sized fibre (ISE) and spin coated (S3A). 50
Figure 4.14. Comparison of TGA analysis different parts of spin coated S1A at 10000 rpm a) TGA and LOI%, b) DGT 51
Figure 4.15. Comparison of TGA analysis different parts of spin coated S3A at 4000 rpm a) TGA and LOI%, b) DTG. 52
Figure 4.16. Comparison of TGA results of S1A (1%) dip coated, S1A (10%) spin coated and IS a) TGA weight change b) DGT differential weight change. 53
Figure 4.17. SEM images of fibre bundles i.e., a,b) Dip coated S1A 10 wt%, c,d) Dip coated S1A 1wt%, e,f Spin coated S1A 10 wt%, and g,h) Industrial-sized 55
Figure 4.18. SEM images of microscope slide, a) Dip coated S1A 10 wt%, b) Spin coated (10000rpm) S1A 10 wt% 56
Figure 4.19. SEM images of different part of the spin coated 10000 rpm microscope slide with S1A 10% wt% sizing, a) End1 b) Middle c) End2 56
Figure 4.20. AFM images of BF, IS, dip and spin coated S1A. 58
Figure 4.21. IFSS results for the dip coated fibres with varying sizing concentrations (10%, 1%) and the spin coated fibres (10%). 59

Figure 4.22. IFSS results for the dip coated, spin coated and Industrial PP sizing compatible coated fibre. 59
Figure 4.23. IFSS results for the dip coated, spin coated and Industrial epoxy compatible sized fibre. 60
Figure 5.1. Single-fibre fragmentation test. 64
Figure 5.2. Single-fibre pull-out test. 65
Figure 5.3. Schematic diagram of the indentation test. 66
Figure 5.4. Schematic diagram of the microbond test. 67
Figure 5.5 Illustration of how different meniscus angles affect stress distribution across the fibre [129]. 68
Figure 5.6. a) Silane solution, b) Immersed fibre bundles in the silane solution. 77
Figure 5.7. a) TGA results of silane coated fibre, b) DTG results of silane coated fibre. 79
Figure 5.8. presents the FTIR spectra of unsized glass fibres. 80
Figure 5.9. Shows the FTIR spectra for silane-coated glass fibres. 81
Figure 5.10. HomoPP droplet formation steps under hot-stage microscopy. a) Melt: 163° C, b) Formed: 170°C, c) Max temp: 220°C, d) Cooled: 30°C 82
Figure 5.11. MAPP droplet formation steps under hot-stage microscopy. a) Melt: 157° C, b) Formed: 158°C, c) Max temp: 200°C, d) Cooled: 30°C. 83
Figure 5.12. PA6 droplet formation. steps under hot-stage microscopy. a) Melt: 225° C, b) Formed: 230°C, c) Max temp: 260°C, d) Cooled: 30°C 83
Figure 5.13. PBT droplet formation. steps under hot-stage microscopy. a) Melt: 223° C, b) Formed: 230°C, c) Max temp: 260°C, d) Cooled: 30°C 84
Figure 5.14. Examples of PP, MAPP, PA6 and PBT droplets. 85
Figure 5.15. Embedded length (Le) and diameter (De). 86
Figure 5.16. Examples of PP, MAPP, PA6 and PBT droplets, and the associated force displacement graphs. 87

Figure 5.17. IFSS results for the investigated systems. 88
Figure 5.18. IFSS results for the industrial and dip coated APS sized fibre at different pH. 91
Figure 5.19. IFSS results for the dip coated APS sized fibre with different concentration pH levels. 92
Figure 5.20. IFSS results for the APS spin coated fibre. 94
Figure 6.1.a) APS solution b) Film former added c) pH check. 105
Figure 6.2. a) Nonpolarized and b) polarised microscope image comparison. 107
Figure 6.3. Sizing emulsion with different APS concentration at different times. 108
Figure 6.4. Comparison of TGA and DTG results i.e., a) TGA of 4 different spin coated fibre and IS, b) DTG of 4 different spin coated fibre and IS c) TGA of 4 different dip coated fibre and IS d) DTG of 4 different dip coated fibre and IS. 110
Figure 6.5. FTIR spectra of the PP compatible industrial sized (IS) fibre. 112
Figure 6.6. FTIR spectra of the dip coated MAPP film former only fibres. 113
Figure 6.7. FTIR spectra of the investigated PP compatible sized glass fibres, which were dip and spin coated. 115
Figure 6.8. FTIR spectra of the investigated full sizing after drying. 116
Figure 6.9. The IFSS BF, fibres sized with FF only, APS, and S1A-sized fibres, with PP and MAPP. 120
Figure 6.10. IFSS results for sizing systems containing the different film former emulsions with the MAPP matrix 120
Figure 6.11. IFSS results for sizing systems containing the different film former emulsions with the PP matrix. 121
Figure 6.12. Film formers dried at 110 °C 122
Figure 6.13. a) Film former melted at 165 °C b) After cooling c) final films. 122
Figure 6.14. Full sizing dried at a) 110 and b)165 °C. 123
Figure 6.15. S1A sizing in glass container. 124

Figure 6.16. Investigated sizing structures on microscope slides, left 100x, right 200x. 125

Figure 6.17. S2A sizing crystallisation a) 100x and b) 200x. 126

Figure 6.18. S2A sizing on bare glass fibre (200x)..... 126

List of Tables

Table 2.1. Composition of some commonly used glass fibres. 8

Table 2.2. Properties of some commonly used glass fibres. 8

Table 2.3. Properties of the investigated polymers [39] 18

Table 4.1. Commercial and in house PP compatible sized fibres 42

Table 4.2. LOI% and sizing layer thickness. 54

Table 5.1. Summary of the studied fibres, including industrial APS sized fibre with different pH, in house silane sized fibre i.e., different silane types, different APS pH and concentration. 77

Table 5.2. Droplets dimension and aspect ratio. 86

Table 5.3. Summary of IFSS values for in-house silane sized fibre. 89

Table 5.4. Two-tailed Student's t.test between BF and silane sized fibres 90

Table 5.5. Summary of microbond testing of industrial and dip coated APS sized fibre at different pH. 91

Table 5.6. Summary of Microbond Testing Results of the dip coated APS sized fibre with different concentration and pH. 93

Table 5.7. IFSS results for the APS spin coated fibre. 94

Table 5.8. Summary of all the microbond testing results. 96

Table 6.1. Summary of fully sized industrial and in house sized fibres. 105

Table 6.2. TGA LOI of fully sized glass fibres using spin and dip coating. 111

Table 6.3. Spectral characteristics of film former coated glass fibres. 114

Table 6.4. Spectral characteristics of fully sized spin and dip coated glass fibres. 115

Table 6.5. Spectral characteristics summary of APS sized, FF only sized, fully sized spin and dip coated glass fibres and dried full sizing. 117

CHAPTER 1: INTRODUCTION

1.1. Project background

The escalating demand for glass fibre-reinforced polymers (GFRPs) across diverse industries, including automotive and wind energy, has intensified the need for innovative composite materials. These materials must demonstrate consistent performance under various conditions, enduring both high static and dynamic loads over a broad temperature range throughout their operational lifespan [3]. For example, wind turbine blade manufacturers are continually challenged by the need to develop longer, better performing turbine blades and the exposure of wind turbine blades to high static and dynamic loads over a broad temperature range requires high performance composite materials which will perform reliably over the lifetime of the structure.

Currently, glass fibre products dominate the composites industry, constituting the majority of the utilized fibre reinforcements [4, 5]. This prevalence is primarily attributed to their highly favourable performance-to-price ratio. Despite the perception of glass fibres as relatively low-tech in the realm of composite reinforcements, their production has evolved into a sophisticated technology. A pivotal element in the production of glass fibres and their composites is the fibre size [1, 3, 6]. Sizing, involving the coating of fibres with a size, is a crucial process. The region at the fibre/matrix interface holds paramount importance in determining the mechanical performance of GFRPs. Consequently, optimizing the stress-transfer capability in this region becomes exceptionally significant. Fibre sizing emerges as a key parameter governing the stress-transfer capabilities of the interface and plays a critical role in defining numerous parameters that impact the long-term performance of composites [4, 6] .

Considering the crucial role of fibre sizing, particularly silane as a key determinant of interface strength, in the optimization of the fibre/matrix interface, it is imperative to enhance our understanding of how fibre sizing influences the interfacial strength. A pressing challenge persists as commercial glass fibres are often provided with minimal sizing-related details, typically limited to indications of chemical compatibility with a broad class of matrix polymers and a Loss of Ignition (LOI)% value representing the amount of organic sizing present on the glass fibre product [6]. This lack of comprehensive information regarding the physical and chemical nature of the sizing becomes a significant concern for users across various domains, whether focused on quality control in manufacturing processes or delving into the fundamental

understanding of the fibre/matrix interphase. Given the complexities involved, researchers in polymer composites require practical tools to unravel the nature and role of sizing on glass fibres, ultimately enhancing the efficiency and efficacy of composite materials. Nonetheless, a key obstacle stems from the scarcity of systematic research and development dedicated to sizing analysis and characterization [7]. This challenge is notably influenced by two primary factors. Firstly, a considerable confidentiality barrier shrouds the chemical formulations of sizing utilized in commercial glass fibre products. Secondly, achieving a comprehensive understanding of sizing requires the capability to formulate and apply them to glass fibres under conditions reflective of real-world glass fibre production. In practice, this implies having access to a well-established, operated, and maintained (pilot) glass fibre forming facility. Unfortunately, the financial, engineering, and resource challenges associated with operating such facilities have resulted in their scarcity, particularly for researchers outside the glass fibre manufacturing industry. Therefore, most researchers have used dip-coating of glass fibre samples with small scale laboratory produced sizing emulsions [8-12]. While this approach allows for investigating similar chemistries used in sizing formulations, it lacks a genuine connection to the high-speed, high-shear application and distribution involved in real-world sizing. This raises concerns about the reliability of results obtained from dip coated samples. Dip-coating typically results in a higher LoI and consequently thick sizing layer due to the fibres' exposure to a significant volume of size in the submerging process. Adjusting the sizing layer's thickness often requires creating different (lower) concentrations of sizing solutions or emulsions, which may differ significantly from those used in fibre manufacturing [13-17]. The thickness (from 86 nm to 1280 nm, see the measurement method in chapter 4 section 4.3.3) and distribution of the sizing layer significantly impact the interfacial and mechanical performance of resulting composite materials. For instance, an increase in sizing thickness has been reported to decrease tensile/compressive and shear strength for composites with monofunctional epoxy-coated fibres, while composites with difunctional epoxy-coated glass fibres show an optimum strength at increased thickness [13, 14]. This tendency could be attributed to the excess epoxy, which likely creates a more lubricated interphase, resulting in a lower friction coefficient and reduced shear strength.

The above-mentioned challenges underscore the need for a more accessible and detailed understanding of sizing complex role within the chain of composite producers and users, emphasizing the importance of addressing these challenges to advance the field of polymer composites. This is particularly relevant for thermoplastic resin systems, where systematic

research on the effect of sizing component variations on fibre/matrix interface is limited, and there is a notable emphasis on developing sustainable composite materials with recyclability and a low carbon footprint. Accordingly, the research in this project aimed to develop a new sizing method, ensuring a more accurate representation of the industrial sizing process, and making it cost-effective for most laboratories. Additionally, the study explored the effectiveness of full sizing and various sizing components, i.e., silane and film former. The role of common silane coupling agents (APS, GPS and MPS) was investigated for a range of commonly used thermoplastic resins, PP, MAPP, PA6 and PBT. Furthermore, the effect of different PP film former and full sizing on the interfacial properties was investigated with PP and MAPP resins. Microbond testing, along with Thermogravimetric Analysis (TGA), Scanning Electron Microscopy (SEM), Fourier Transform Infrared Spectroscopy (FTIR), and Atomic Force Microscopy (AFM), was used for an in-depth study. The research focused on conducting a detailed investigation into the differences between macroscale and microscale thermomechanical properties, sized fibre's surface morphology, and to characterize the interface and associated level of adhesion. While there has been extensive research on interface characterization of the glass fibre thermoset resins, there is a gap in such a study for thermoplastics.

1.2. Originality

The novelty of this thesis lies in its focused and extensive examination of the interfacial characteristics within thermoplastic systems. It was determined that fibres coated solely with silane, or a combination of silane and film former, had a more significant effect than those coated only with a film former. The degree of effectiveness varied across different thermoplastic resins. Additionally, the thesis presents an innovative spin-coating technique, developed to overcome the limitations of traditional lab-based fibre sizing methods and better emulate the industrial fibre sizing process. The research concludes that this new spin-coating approach can effectively mimic the results of industrial sizing, offering a straightforward yet insightful means for analysing sizing and the fibre/matrix interface.

1.3. Aims and objectives

To advance the understanding of the sizing effect in GFRPs, especially in thermoplastic resin systems, and address challenges faced by researchers on accurate representation of the industrial sizing process on the laboratory scale, this project outlines the following objectives:

1. Development of a new lab-based sizing method, which gives properties as close as industrial-sized fibre, to have a realistic fundamental study of the interface for both thermoset and thermoplastic polymeric systems.

2. An investigation of the effect of silane coupling agent variation on the interface between glass fibre and thermoplastic matrices.

3. An investigation of the effect of film former and full-sizing (defined as PP film former and APS) on the interface between glass fibre and thermoplastic matrices.

1.4. Outline of the thesis

Chapter 1 is an introduction to the background, objectives, and outline of the thesis. Chapter 2 conducts a general literature review on glass fibre manufacturing, applications and properties. Chapter 3 presents the research methodology and experimental procedures that are utilised in this project. Chapters 4 to 6 elaborate on the research conducted to meet the project objectives, each encompassing a dedicated literature review, results, and discussion sections. Chapter 4 introduces the spin coating method as a novel lab-based fibre coating method, to simulate the high-speed, high-shear application and distribution involved in real-world sizing process (shown in 2.4) for both thermoplastic and thermoset polymers. This chapter extensively investigates the spin coating method, comparing it with dip coating and industrial-sized fibre techniques. Key parameters such as LOI%, coating thickness (which is theoretically derived from LOI% values, densities of the sizing and glass fibre (shown in 4.3.3), and IFSS are measured using various experimental techniques introduced in Chapter 3. Chapter 5 provides a comprehensive study of the silane coated fibre characteristics i.e., thermal stability, surface chemistry and the effect of silane variations on the interface between glass fibre and commonly used thermoplastic matrices. Chapter 6 investigates the film former and fully sized fibre characteristics such as thermal stability and surface chemistry, film formation and the effect of film former and full sizing on the interphase of glass fibre with PP and MAPP thermoplastics. Chapter 7 summarizes the conclusions of the thesis and outlines recommendations for future work.

CHAPTER 2: LITERATURE REVIEW

2. Glass fibres – a review

In this Chapter, an overview of the literature is presented, covering the development, properties, and applications of glass fibres. This Chapter specifically introduces glass fibres and their formulation, the glass fibre sizing process and main components of the size, and the comparison between glass fibre-reinforced thermoset and thermoplastic composites. Subsequent Chapters (3 to 6) offer detailed literature reviews that specifically delve into topics such as characterisation methods, sizing technologies, and advancements in the interfacial properties of glass fibre and different ranges of polymeric matrices.

2.1. Introduction to glass fibres

The evolution of glass fibres, integral to the advancement of composite materials, can be traced back to the mid-20th century. Glass fibres are part of a broader group of materials known as synthetic vitreous fibres. This family includes other materials such as mineral wool and refractory cement. A distinguishing feature of glass fibres within this group is their high content of sodium (Na) and potassium (K). Additionally, glass fibres have relatively lower melting points compared to other synthetic vitreous fibres, which limits their use in environments with temperatures up to 200 °C. However, some glass fibres are specially designed for use in environments with temperatures surpassing 500 °C [9]. Initially employed for insulation purposes, the unique properties of glass fibres, such as their high tensile strength and versatility, have led to their widespread utilization in various industrial sectors [18]. Glass fibres exhibit exceptional mechanical properties, including high tensile strength, stiffness, and resistance to heat and chemicals. These fibres also provide low thermal expansion and dimensional stability, making them crucial for various applications in industries such as automotive, construction, and aerospace [19]. The versatility of glass fibres is highlighted by their applications in diverse industries, with some examples shown in Figure 2.1. In the automotive sector, glass fibres contribute to the development of lightweight and fuel-efficient vehicles. The construction industry benefits from the durability and corrosion resistance provided by glass fibre-reinforced composites. Aerospace applications leverage the high strength-to-weight ratio of these materials. Wind energy relies on glass fibres to enhance the structural integrity of turbine blades [20].

Figure 2.1. Examples of glass fibre composites usage in different industrial sectors [21, 22].

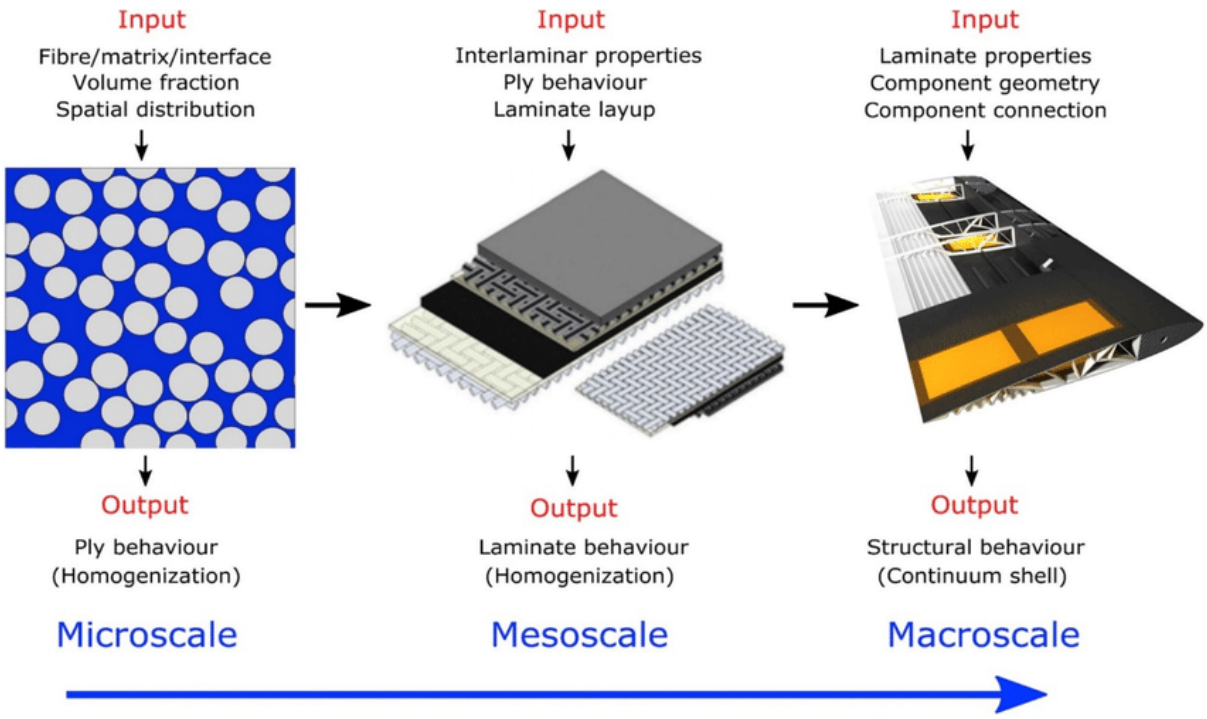

Figure 2.2. Schematic diagram illustration of local-to-global multiscale parameters affecting composite materials properties [23].

By examining each level of this hierarchy, from the micro-scale fibre sizing that affects fibre/matrix adhesion to the macro-scale global composite structure, we can gain deeper insights into the mechanical behaviour and potential failure mechanisms of the composite. Such understanding is vital for refining the properties of the materials, guaranteeing structural integrity, and fostering the development of more effective and durable composites. Consequently, the investigation of fibre sizing and interfacial properties in this thesis could be

instrumental in improving both the performance and dependability of composite material systems.

2.2. Composition of glass fibres and their surface

Commercial glass fibres are readily available in a variety of different chemical compositions. Glass fibres are amorphous and mostly silica-based (~50–60% SiO_2), which is derived from ordinary sand and contains other oxides of different metals as well as, calcium, boron, sodium, aluminium, iron, etc. The differences between a crystal, a simple glass, and a multicomponent glass are shown schematically in Figure 2.3.

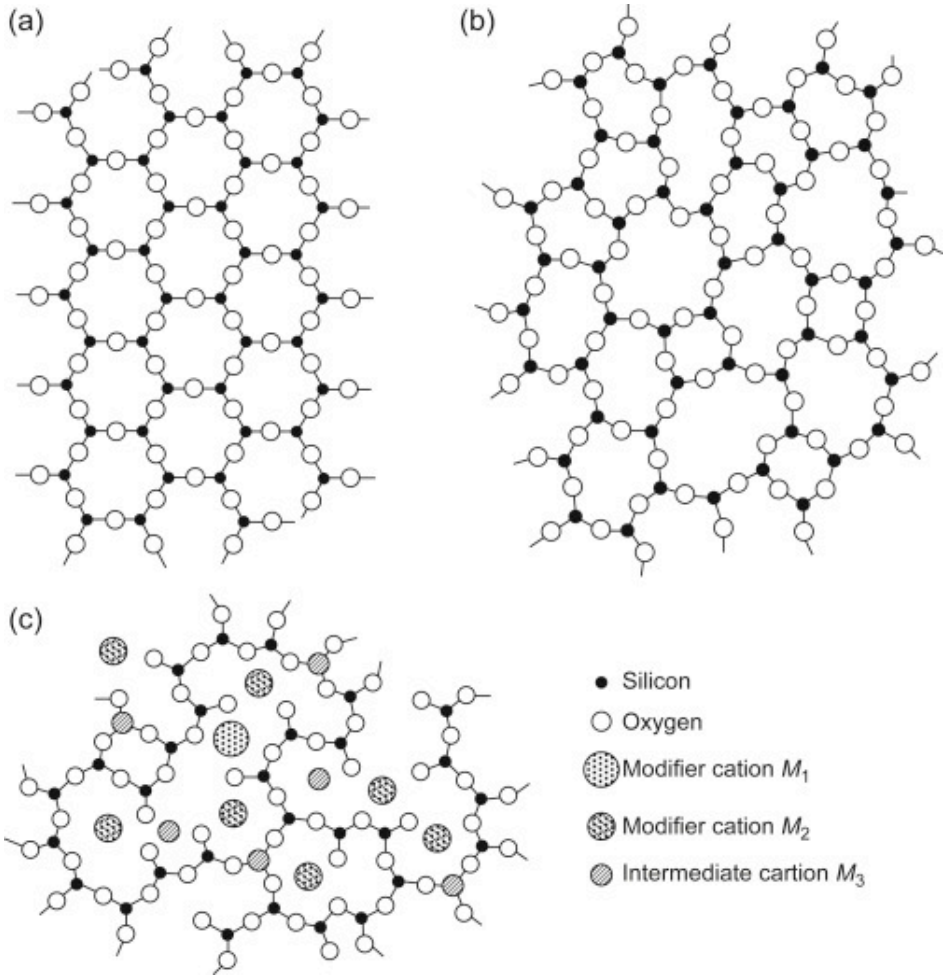

Figure 2.3. Schematic diagram illustration of: (a) a crystalline structure; (b) a simple glass; and (c) a multicomponent glass [24].

The composition of some of the commonly used glass fibres can be seen in Table 2.1. Most types of glass fibre are named according to their specific properties and typically fall into three categories that are popular for use in composite materials. Each glass fibre type, therefore, is

tailored to meet specific industrial requirements, from cost-efficiency to resistance to environmental factors and mechanical performance. Some of the properties of the commonly used glass fibres were summarised in Table 2.2. In this project, only E-glass fibres were investigated. Almost 90% of all reinforcement glass fibres that are produced today in the world are E-grade fibre glass. E-glass fibres are predominantly composed of silica, alumina, and calcium oxide, offering moderate mechanical properties and excellent electrical insulation at a low cost, making them suitable for a wide range of applications including electrical insulation and general-purpose composites. C-glass stands out for its superior chemical resistance, particularly against acids, due to its high silica content along with calcium and boron oxides, which makes it ideal for corrosive environments like chemical plant linings. S-glass fibres, with increased silica, alumina, and magnesia, exhibit exceptional tensile strength and temperature resistance, qualities that come with a higher cost, positioning them for use in demanding sectors such as aerospace and defence where performance is critical [25].

Table 2.1. Composition of some commonly used glass fibres.

Glass fibres	Composition (wt.%)						
	SiO2	A12O3 + Fe2O3	CaO	MgO	Na2O + K2O	B2O3	BaO
E-glass	52.4	14.4	17.2	4.6	0.8	10.6	-
C-glass	64.4	4.1	13.4	3.3	9.6	5.0	0.2
S-glass	64.4	25	-	10.3	0.3	-	-

Table 2.2. Properties of some commonly used glass fibres.

Glass fibre	Density (g/cm^3)	Melting point (°C)	Coefficient of thermal expansion (mm/°C)	Tensile strength (MPa)	Modulus of elasticity (GPa)
E-glass	2.54	1160	4.9	3400	72
C-glass	2.52	1200	4.9	3310	69
S-glass	2.53	1650	2.8	4600	89

The chemical makeup of the surface of glass fibres is not identical to the substance of the glass itself. In contrast to the main glass material, the outer layer of E-glass fibres exhibits decreased levels of magnesium, boron, and calcium, while exhibiting increased concentrations of fluorine, silicon, and aluminium [26].

2.3. Glass fibre manufacturing

Figure 2.4 graphically represents the process of producing glass fibre, which is a blend of the extrusion and thinning of liquid glass. During extrusion, the liquefied glass is drawn by gravity from the melting furnace through the forehearth to a collection of bushings composed of a platinum/rhodium mixture, which have extremely small openings ranging from 200 to 8,000 [27]. The bushing plates are heated by electricity, and the temperature is meticulously regulated to ensure the viscosity of the glass remains steady. The liquid glass then forms droplets at the tips of the bushings and is swiftly drawn out into delicate fibres. Immediately below the bushing, a fine mist of water is applied to the fibres. The attenuation process entails the mechanical stretching of the molten glass streams into filaments, which have diameter from 9 to 24 micrometres, suitable for reinforcing composite materials [1].

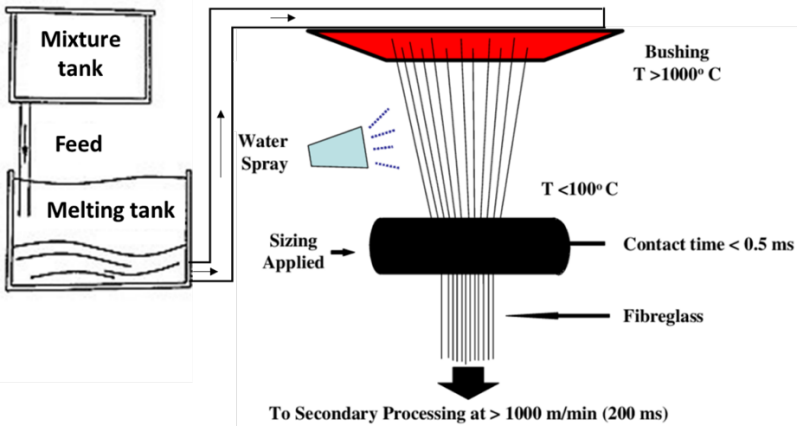

Figure 2.4. Schematic representation of a glass fibre production line. Adapted from [28].

2.4. Glass fibre sizing

The need for high-performance glass fibre composites has pushed the manufacturing of glass fibres into a complex technology to satisfy end user requirements. During the manufacturing, glass fibres are coated with a thin layer that is called “size”. Sizing is considered a key component in manufacturing of glass fibres and it is applied to bare glass fibres so as to improve fibre/matrix interfacial properties as well as protecting the fibres from damage to improve both short-term and long-term composite performances [6]. For sizing, the freshly formed glass fibres are pulled down to the sizing applicator, normally 1-2 m below the bushing plate, as shown in Figure 2.4. The sizing reservoir is routinely circulated and cooled to mitigate the heat generated by the bushing's radiation. As the roller turns at a consistent rate, it acquires a layer of sizing; the layer's thickness corresponds to the speed of rotation. As the fibre brush passes over the roller for a brief distance of roughly 5-10 mm, it collects a layer of this sizing. The

volume of sizing picked up by the fibres depends on the layer's thickness on the roller. These sized fibres are then collected to form a multi-filament strand at a gathering shoe and are then directed to a collection device, typically a fast winder or an in-line chopper [4].

Figure 2.5 shows the important components of sizing for glass fibres. Most commercially used sizings are aqueous chemical systems containing 0.05–10% solids which usually containing a complex mixture of components such as film former, silane coupling agent, anti-static agents, lubricant, emulsifiers and wetting agents. In a size formulation film formers often make up the 70–90% of the size material. Organosilanes is around 10% of the many-component sizing.

Silanes may react with the fibre surface to form a strong bond. This bonding might help connect the glass fibre surface with the matrix polymer. Even if it doesn't bond directly to the matrix, the sizing might still create a network that intertwines, as shown in Figure 2.6. However, since the film former is about 80% of the sizing, it probably takes up more space than we see in the Figure. 2.6. In the following, the details and functionality of each component will be discussed briefly.

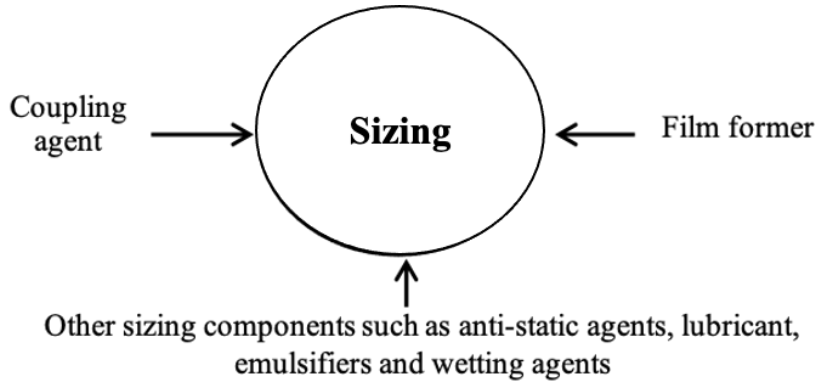

Figure 2.5. Simplified illustration of important components in sizing

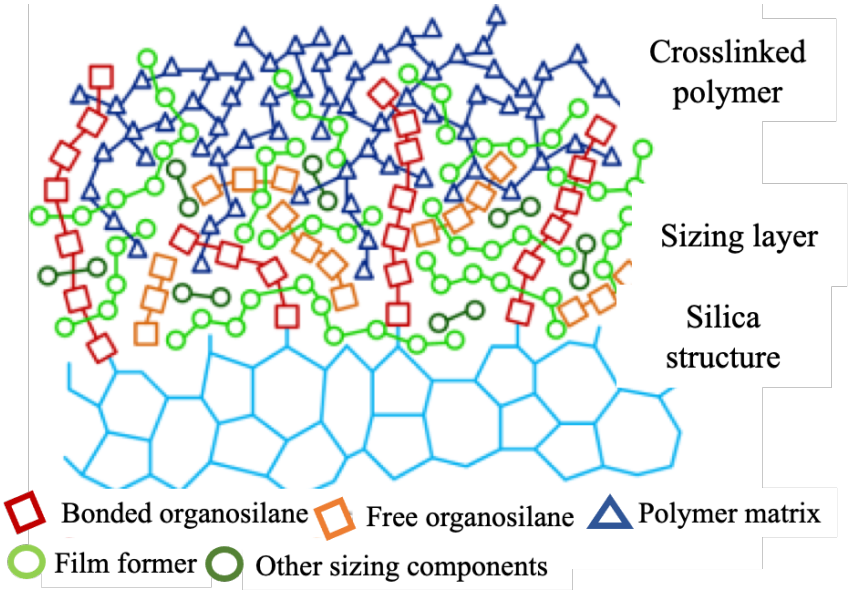

Figure 2.6. Interpenetrating network structure at the interface between glass fibre sizing and polymer matrix [29].

2.4.1. Silane coupling agent

Organofunctional silane, frequently named as a coupling agent, is probably the most important class of chemicals used in glass fibre sizing, and consequently their composites. Organosilanes are noticeable as a link between the inorganic surface of glass fibres and the organic matrix since they contain both silica and organic functional groups being able to form bonds to both materials. Organosilanes improve interphase hydrothermal resistance and strength of the composite interphase, by forming durable siloxane bonds (Si-O-Si) with the fibre surface [1]. Additionally, organosilanes enhance the wetting of glass fibre by modifying its surface energy, which improves adhesion with thermoplastic and thermoset polymers [30]. [X-Si $(OR)_3$] is the general structure of silane coupling agents, where X is an organic functional group capable of bonding with the polymer matrix, and OR is commonly a methoxy or ethoxy group. The aqueous solution silane is hydrolysed to a silanol when used to treat fibres. The silanol, which is unstable, has the potential to form a siloxane network on the fibre's surface through a condensation reaction that involves the release of a water molecule. The Si-OH groups are also involved in this process, leading to the formation of covalent bonds between the siloxane network and the fibre surface. Furthermore, the X groups on the silane remain accessible for reactions with active functional groups. This depends on the processing history and the state of any previous chemical interaction between the silane and other size components, and can lead to a strong network bridging the fibre-polymer interphase [4]. Despite existence of many different silane molecules, the majority of the studies [6] reported that four silanes are commonly used in the glass fibre industry are the γ- aminopropyltriethoxysilane (APS), γ-

glycidoxypropyltrimethoxysilane (GPS), γ-methacryloxypropyltrimethoxysilane (MPS) and vinyltriethoxysilane (VTES). APS constitute the majority of employed silanes [6]. APS is particularly prevalent as silane coupling agents because of their compatibility with a broad range of polymer matrix materials, including both thermoplastics and thermosets. GPS are main coupling agent for epoxy and multi-compatible sizes. MPS are the main coupling agent for polyester compatible sizes. VTES is less commonly used silane in the literature. For the research presented in this thesis, APS, GPS and MPS were the chosen coupling agents, due to their popularity in the research community, to evaluate their effectiveness in the interphase properties in thermoplastic composites. The chemical structures of these silane coupling agents are shown in Figure 2.7.

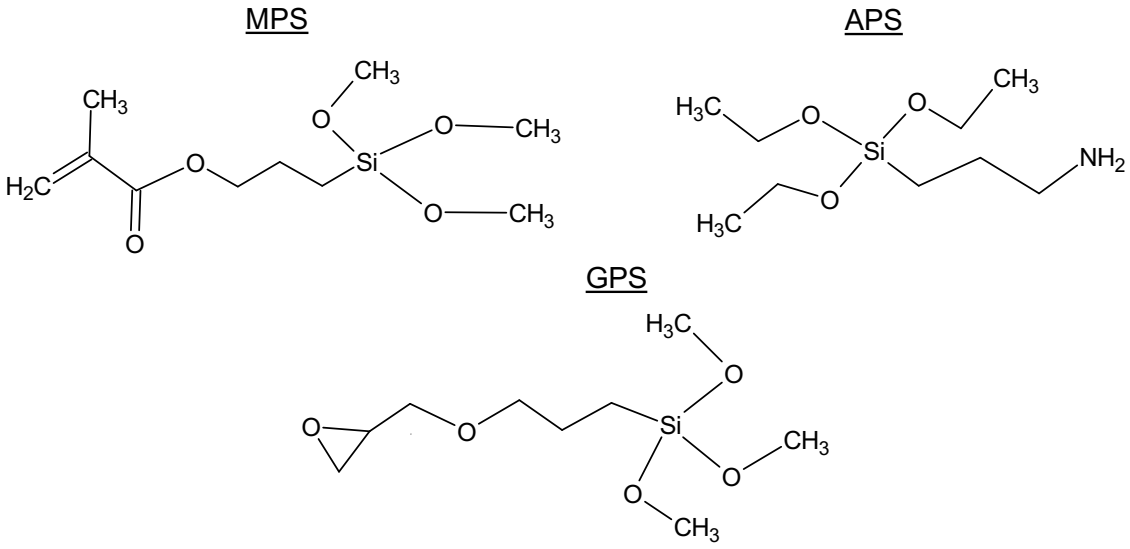

Figure 2.7. Chemical structure of APS, GPS and MPS [31].

The stability and reactivity of aqueous solutions of silanes depend on many factors as shown in Figure 2.8. Silanes are commonly dissolved in water by shaking or stirring vigorously with acidified water until a clear solution is achieved. Organofunctional trialkoxysilanes are hydrolysed in water and then condensed into oligomeric siloxanols.

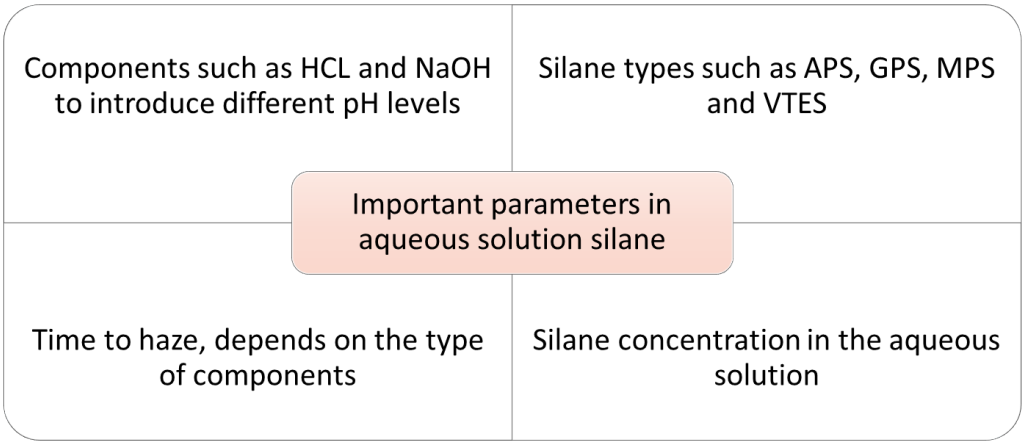

Figure 2.8. Simplified illustration of important parameters for creating aqueous solution silane coupling agents.

For example, in APS, the hydrolysable components are ethyl groups (CH_3CH_2). The organic functional group (X) in APS is a propyl chain ending in a primary amine (NH_2). When APS is dissolved in water, the water molecules remove the ethyl groups from APS, resulting in the formation of ethanol. Subsequently, these ethyl groups are replaced with hydrogen atoms, forming silanol groups in the hydrolysed APS molecules (silanol). These silanol groups then undergo a condensation reaction to create a siloxane structure, as depicted in Figure 2.9. The hydroxyl groups remaining in this siloxane structure then react with the hydroxyl groups on the glass fibre surface, leading to covalent bonds upon drying, as shown in Figure 2.10.

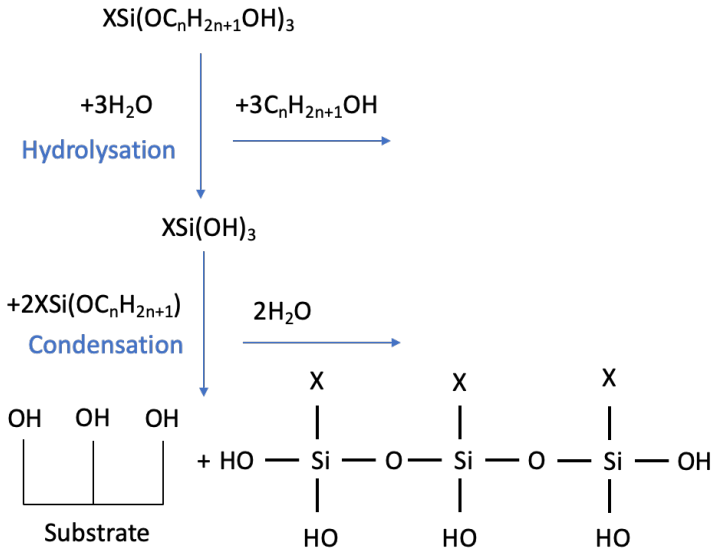

Figure 2.9. Hydrolyzation and condensation process of silane coupling agents. reproduced from [32].

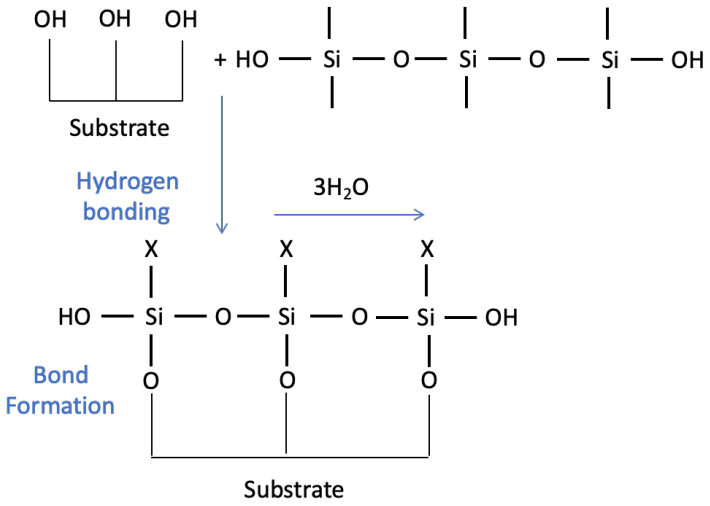

Figure 2.10. Bonding of self-condensed silane coupling agent with substrate surface (such as glass). Reproduced from [32].

While Figure 2.10 might indicate a single layer of coupling agent on the glass surface, the actual structure could be a three-dimensional network composed of siloxane chemically bonded to the glass at the interface, Silanol molecules that have self-condensed into a complex polysiloxane network, and short-chain self-condensed APS (oligomers) loosely attached to the surface, as illustrated in Figure 2.11.

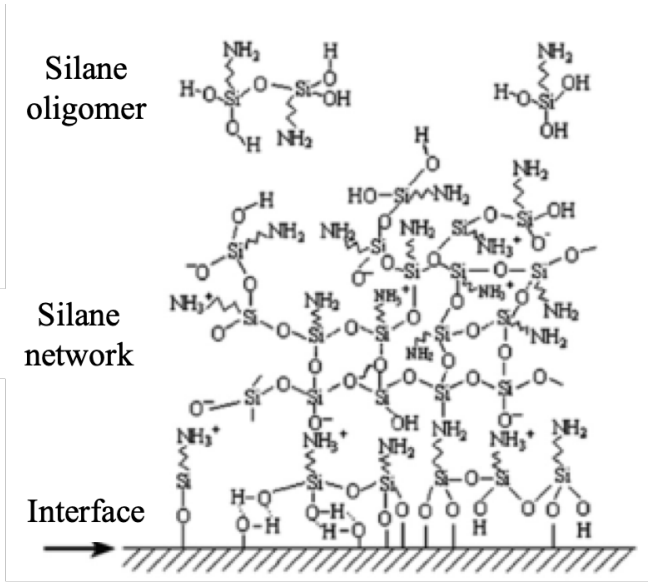

Figure 2.11. Schematic of 3D network structure of hydrolysed APS on glass fibre [33].

2.4.2. Film formers

The primary component in glass fibre sizing by mass (70–90%) is the polymer film former, typically an emulsion consisting of one or multiple polymers [4]. These polymers, being water-

insoluble, require the use of an emulsifier. The choice of polymer(s) for the film former often depends on the resin matrix with which the fibres will be integrated into the final composite product. Consequently, the range of common film-former materials are indicative of the composite matrix materials. For example, in composites based on epoxy resins, the film former within the sizing is likely to be an epoxy-based emulsion. Typical film-former materials encompass a variety of materials such as polyvinyl acetate, polyurethane, polyolefin, polyester, and various forms of epoxy, including those that have been modified [1]. Looking at the sizing formulations in patents and publications, epoxy film former is a common constituent in epoxy-compatible, multi-compatible, unsaturated polyesters and vinyl ester sizings. Epoxy film former is also common in certain thermoplastic-compatible sizes such as PBT. PVA film former and its derivatives are typically used in unsaturated polyester-compatible sizes, while polyurethane and acid-modified polyolefins film formers are favoured for polyamide and PP-compatibility, respectively [1, 4, 6]. The use of emulsion-dispersion methods facilitates the application of these substances, which are often characterized by high molecular weights and are not soluble in water, to the surfaces of glass fibres. The film former's function is to maintain the integrity of the fibre strands during handling and to safeguard the fibres from mechanical damage. Additionally, because the film former's polymer composition is designed to be compatible with the composite matrix, it can also aid in enhancing the bond between the glass fibres and the matrix. However, there is no prior assumption that the film formers are chemically bound to the fibre surface directly (see Figure 2.6).

2.4.3. Auxiliary components

Besides silane coupling agent and film-former, sizings often contain other components in smaller amounts. These auxiliary ingredients might include lubricants, anti-static agents, emulsifiers, chopping aids, wetting agents, and antioxidants. Lubricants are included in sizings to minimize the abrasion between fibres. Anti-static agents prevent the accumulation of static electricity on the non-conductive fibres during high-speed production and processing. Emulsifiers which are typically part of the film former are used to facilitate polymer dispersion in water and to enhance the distribution of other sizing ingredients that are not water-soluble. Chopping aids ease the cutting of fibre strands in the manufacturing stage. Wetting agents lower the sizing's surface tension to enhance its ability to coat the fibre surface. Antioxidants are added to slow down the degradation of the sizing, thereby extending its lifespan.

2.5. Glass fibre-reinforced thermoplastic composites

Thermoset and thermoplastic polymers have distinct properties that define their specific applications, as shown in Figure 2.12. Thermoset polymers, once cured through a chemical reaction, become infusible and insoluble. Their molecular chains cross-link during the curing process, resulting in a material that is exceptionally heat resistant and structurally stable, but cannot be remoulded or reshaped once set. This makes them ideal for high-heat applications such as electrical insulation and auto parts. In contrast, thermoplastics do not undergo such cross-linking, allowing them to be repeatedly melted and reshaped. This recyclability and flexibility make thermoplastics widely used in consumer products, packaging, and in situations where material reuse is a priority. While thermosets offer superior dimensional stability and heat resistance, thermoplastics provide versatility and ease of processing, leading to their selection based on the specific performance requirements of the application.

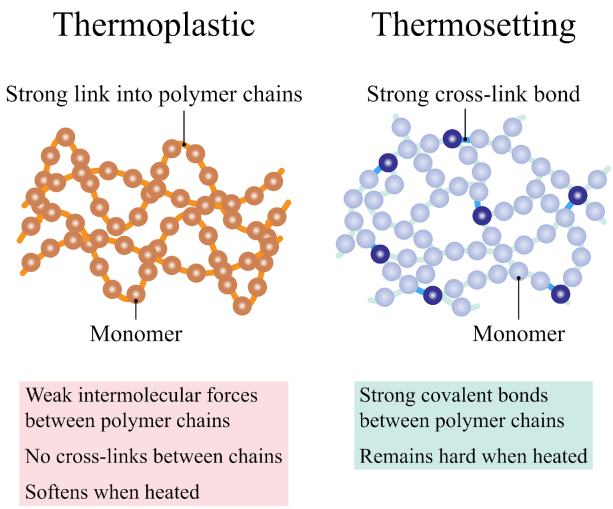

Figure 2.12. Thermoplastics vs. thermoset plastics [34].

Recent studies emphasize the growing importance of thermoplastic polymers over thermosets, primarily due to cost savings due to non-heated tooling, shorter manufacturing cycle times, and recovery of raw materials from the retired part (see Figure 2.13). As composite parts have high embedded energy, recovery of their constituent materials can provide substantial economic benefits. An example of this is seen in wind turbine blades, which are typically made of GFRPs and either balsa or foam core. Discarding these blades in landfills results in a substantial addition of composite materials to the waste stream. One study estimated that each megawatt of installed capacity generates around 9.6 metric tons of composite waste [35]. This not only poses environmental challenges but also equates to a loss of capital that could potentially be recovered. In this context, thermoplastic resins, known for their recyclability [36], emerge as a

more favourable option, especially considering the tightening regulations on landfilling composite waste. The European Union, for instance, has implemented specific laws, such as Directive 1999/31/EC [37], which bans the disposal of large composite parts, including wind turbine blades, in landfills. This regulatory landscape further underscores the advantages of adopting thermoplastic resins in manufacturing.

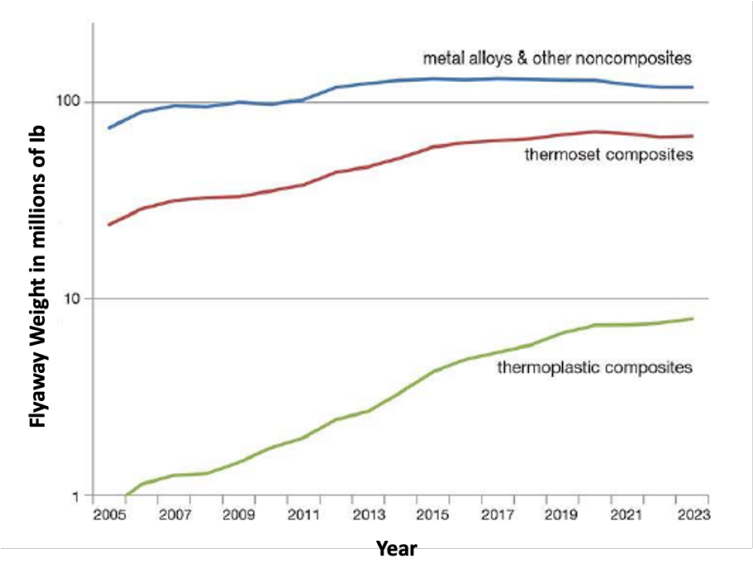

Figure 2.13. Materials trends in aerospace systems flyaway weight requirements [38].

Various types of thermoplastic polymers exist, and in this PhD project, we focus on those frequently utilized in composites with glass fibres. The study investigates the PP, MAPP, PA6 and PBT thermoplastic polymers. A brief description of these polymers is provided below, and the molecular structure of these polymers are shown in Figure 2.14. The main properties of the investigated polymers are summarised in Table 2.2.

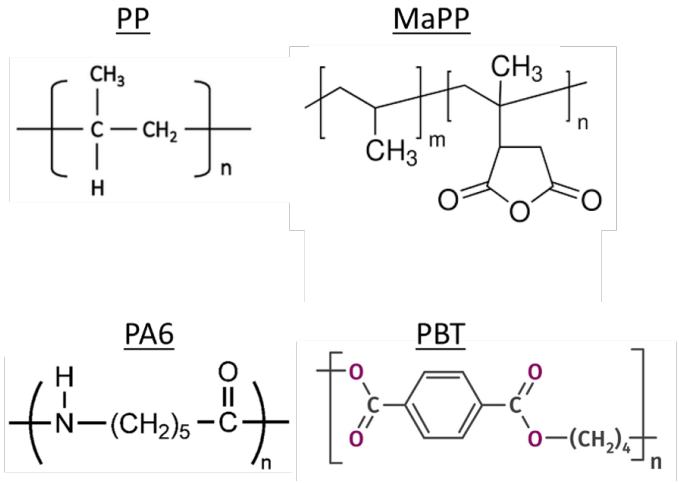

Figure 2.14. Molecular structure of the investigated polymers.

Table 2.3. Properties of the investigated polymers [39]

Polymer	MFI (g/10min)	Density (g/cm^3)	Melting point (°C)
PP	11 (230°C/2.16 kg)	0.90	163
MAPP	115 (190°C/2.16 kg)	0.91	157
PA6	32 (270°C /2.16kg)	1.13	223
PBT	14 (250°C /2.16kg)	1.52	224

PP: PP is a thermoplastic polymer used in a wide array of applications. It is known for its versatility, chemical resistance, and excellent fatigue resistance. Structurally, PP is a linear hydrocarbon polymer expressed as $(C3H6)_n$. It is rugged and unusually resistant to many chemical solvents, bases, and acids. PP is used in packaging, textiles, automotive parts, reusable containers, and laboratory equipment. One of the key characteristics of PP is its ability to function effectively as both a plastic material and as a fibre [39].

MAPP: MAPP is a modified form of PP. The addition of maleic anhydride introduces polar groups to the polymer, enhancing its compatibility with other polar substrates. This modification is achieved through a grafting process, where maleic anhydride is chemically attached to the PP backbone. The resulting MAPP exhibits improved adhesion properties, making it an excellent choice for composite materials, where it acts as a coupling agent between hydrophobic polymer matrices and hydrophilic fillers. It is also used in automotive parts and the modification of bitumen for road construction [40] .

PA6: Polyamide 6, also known as Nylon 6, is a semi-crystalline polyamide. It is known for its high mechanical strength, stiffness, and good wear resistance. PA6 is synthesized by ring-opening polymerization of caprolactam. Its chemical resistance, particularly to oils and greases, makes it suitable for use in automotive components, industrial parts, electrical and electronic applications, and consumer goods. PA6 also possesses good thermal stability and is widely used in textiles, particularly in the manufacturing of carpets [41].

PBT: Polybutylene Terephthalate is a thermoplastic engineering polymer that is part of the polyester family. PBT is valued for its balance of properties and processability. It exhibits high strength and stiffness, good resistance to solvents, excellent dimensional stability, and it is easy to mould. PBT is often used in electrical components due to its insulating properties, in automotive parts for its durability and stability under high-temperature conditions, and consumer electronics for its blend of strength and aesthetic qualities [42].

CHAPTER 3: EXPERIMENTAL METHODS

This chapter presents a comprehensive examination of the characterization methods employed in this project, concentrating on the evaluation and analysis of the performance of the newly developed spin-coating sizing technique and the interfacial characterization of fibres with various sizes in thermoplastic and thermoset matrices. The selected methods, including microbond, hot stage microscopy, TGA, SEM, AFM, and FTIR are explained in detail. Additionally, the reasoning behind the selection of these specific methods is discussed, highlighting their relevance and effectiveness in achieving the project's objectives.

3.1. Microbond test

Many researchers have focused on understanding the interaction between glass fibres and polymer matrices, with methodologies for assessing stress-transfer abilities of fibre and matrix in composites falling into two main categories based on the nature of the sample and the testing scale [7, 43, 44] . Macromechanical testing, which evaluates bulk composite samples for inter-/intralaminar shear strength or transverse tensile strength, provides insights into interfacial properties but with limited control over microscopic loading conditions or failure modes. This testing includes interlaminar and short beam shear tests, inducing interfacial failure in shear mode, and 0°/90° tensile tests that link IFSS to transverse cracking in the central 90° plies [45]. While these techniques mainly concern continuous fibre reinforced laminate, other studies have been reported to evaluate short fibre thermoplastic moulding using derived values for the IFSS and a fibre orientation factor from a simple combination of the composite tensile stress-strain curve and the fibre length distribution [46, 47].

On the other hand, micromechanical testing, primarily involving single-fibre microcomposite sample [43] and includes methods like pull-out, microbond, fragmentation, indentation, and push-out tests, each exploring the fibre/matrix adhesion behaviour. These single fibre methods are cost-effective and efficient, ideal for initial evaluation of fibre sizings and evaluating composite processing parameters without upscaling to fabric production or macromechanical testing. However, each of the mentioned micromechanical testing methods has its benefits and challenges, which are defined in detail in chapter 5, Section 5.2.2.

Among the mentioned various micromechanical techniques, the microbond test was chosen to be the most compatible test, due to the diverse fibres and matrices involved in this research. The microbond test was used for apparent IFSS measurements. The microbond test was first

introduced by Miller in 1987 [48]. This was followed by a sequence of publications detailing the refinement and methodology of the technique [48-52]. The microbond test has been widely applied in research to evaluate the bond strength at the interface across diverse fibre types such as glass [53] carbon [54], polyethylene [55], aramid [56], cellulose [57], silk [58], and polyamide [59], with the spectrum of thermoset and thermoplastic polymer matrices like epoxy [60], polypropylene [61], vinyl ester [62] and polyester [63].

Many researchers focused on modifications to the microbond testing method to enhance its utility and extend its application range. Innovations include the use of adjustable shearing blades [64], fixed [65], circular loading schemes [66], and adaptations to the testing equipment for assessing the IFSS's sensitivity to different test parameters like temperature [67] and moisture [68]. In a most recently study, Thomason [69] has shed light on potential scaling issues within various polymer systems in microbond test. It has been observed that certain phenomena may significantly influence the test outcomes. In thermosetting resins, some factors such as the level of homogeneity in the resin mix, and the cure cycle of microdroplet samples [70, 71] were identified as influences on the test results. In thermoplastics polymer, degradation due to high viscosity and consequently higher temperature required for droplet formation [72], the number of spherulite in droplet [72, 73], droplet morphology [69] and moisture absorption [68, 74] were named as the effective factors on IFSS results. Thomason [69] concluded that the microstructure and characteristics of polymers in microdroplet form might not accurately represent those of the same polymers when prepared on a larger scale.

The microbond test involves a microdroplet of matrix material cured on a single fibre and is tested by applying tensile force to the fibre until debonding of fibre and matrix occurs. This process involves careful measurement of the force at debonding, the fibre’s diameter and embedded length. The force and measured embedded area are the used to calculate IFSS.

The effectiveness of the microbond test is largely determined by the embedded fibre length, stress distribution, and the interaction at the fibre/matrix interface. To achieve accurate results, the embedded length should be kept short enough to induce shear failure at the interface, rather than fibre breakage. When the embedded length is too long, the bond strength in the interphase may exceed the fibre’s strength, causing the fibre to fail instead of the desired interfacial debonding. With shorter embedded lengths, stress distribution is more uniform, ensuring the embedded portion fully contributes to bond strength. In contrast, longer embedded lengths result in stress being concentrated near the ends of the embedded fibre, leading to increased

variability in test outcomes [75, 76]. Preparation of thermoset and thermoplastic microbond samples are described in the following sections.

3.1.1. Thermoplastic droplet sample preparation

Sample preparation for the microbond testing of the thermoplastic samples was carried out following the procedure described by Nagel et al [77]. Figure 3.1 shows a schematic of the thermoplastic sample preparation process. As shown in Figure 3.2a steel washers were employed as the sample holders for the microbond test. Individual fibres were removed from bundles using tweezers taking care not to touch the fibre along the short length where the polymer microdroplet was to be applied. The sample fibre was first fixed to the steel washer with double-sided tape and then secured with a drop of cyanoacrylate superglue. Long polymer fibres were pulled from thermoplastics pellets and then 5 cm of it used to make a knot around the fixed glass fibre on the washer.

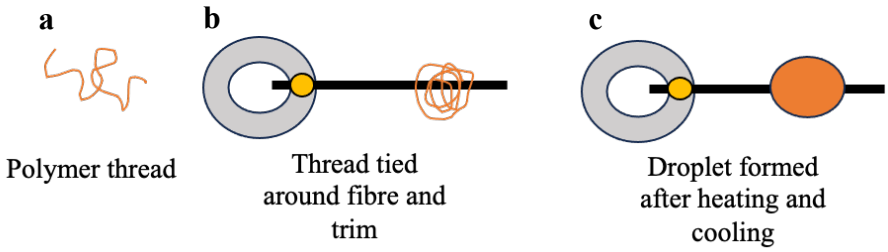

Figure 3.1. Schematic of thermoplastic droplet sample preparation. a) thermoplastic fibre. b) knot around the fibre with thermoplastic fibre. c) Droplet formed after processing

The prepared specimens were placed on the steel hooks (Figure 3.2b) and placed in the oven as shown in Figure 3.2c to be proceed at 220 °C for PP and 200 °C for MAPP and 260 °C for PA6 and PBT, as suggested in their technical data sheet, in a vacuum oven (the heating ramp were measured to be around 2.5 °C/min) under nitrogen flow and then cooled to ambient temperature still under nitrogen flow for about 4-5 hours.

a b c

Figure 3.2. Thermoplastic sample preparation process. a) Fibre mounted on the steel washer and polymer thread tied around fibre. b) Specimens placed on the steel hooks to be placed in the vacuum oven. c) Specimens in the vacuum oven

3.1.2. Thermoset droplet sample preparation

Glass fibre bundles, each approximately 10 cm in length, were extracted from their larger groupings. The individual fibres were then detached from the bundle and orderly positioned along the vertical axis of a card mounting template. The fibres were affixed in place with double-sided adhesive tape and further secured using Loctite gel super glue, which was given a full day to cure prior to the application of droplets.

For the epoxy mixture, resin (MGS^{TM} RIMR 135) and hardener (MGS^{TM} RIMH 134- RIMH 137) from Hexion were combined in stoichiometric proportions (100:30 parts by weight). Roughly 2 g of resin were dispensed into a small plastic vessel via a 1 ml syringe, while the hardener was added with a pipette, with each addition being meticulously weighed on a microbalance. The blend was stirred vigorously to ensure even consistency and then subjected to a 10-minute vacuum degassing to eliminate any trapped air and to enhance the homogeneity of the mixture. The resin droplets were then transferred to the fibres using a slender steel wire, which had a diameter of 125 μm. The wire's tip, bearing a small bead of resin, was gently brought into contact with the fibre on both sides of the alignment markers, which were situated 5 mm from the card tab's edge. Each touch of the wire to the fibre generates multiple droplets, a notable difference when compared to manufacturing thermoplastic microbond samples. A single droplet of resin was used to prepare six specimens, after which a fresh droplet was gathered for subsequent samples. The curing process involved an initial stage at 23 °C for 24 hours, followed by a secondary stage at 80 °C for 15 hours, with a consistent temperature increase of 2 °C per minute maintained throughout the process. The samples were then left to cool down within the oven over the course of the night before being taken out. The sample preparation process is depicted schematically in Figure 3.3.

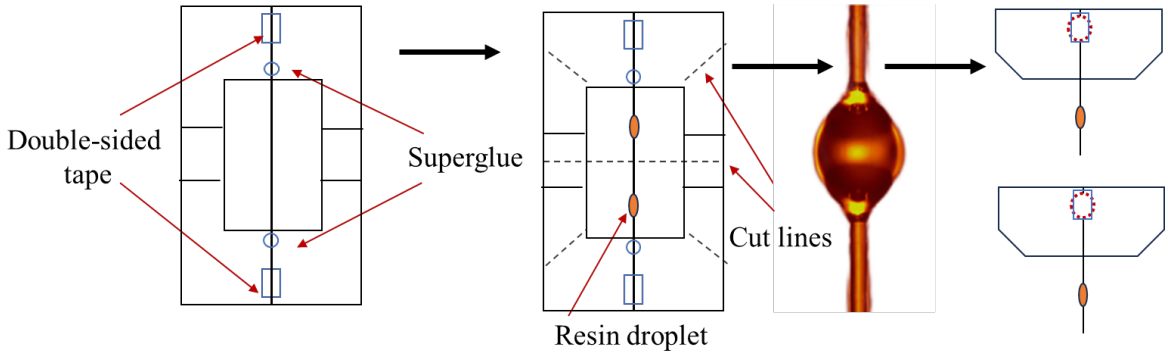

Figure 3.3. Thermoset droplet sample preparation.

3.1.3 Microbond test procedure

Prior to performing the test, the droplets were examined under a Leitz Ergolux microscope (200x) and only axisymmetric droplets were chosen for the test. Figure 3.4 shows an example of a fine PP droplet that is prepared for the test. The fibre diameter, length of the droplet (embedded length) and droplet diameter were measured using the image processing software package ImageJ. An average total of 40 samples were prepared for each batch and were subjected to microbond test using an Instron 3342 universal tensile testing machine as shown in Figure 3.5. The droplet was brought to just below the blades and the blades were closed until touching the fibre. The details of the sample were then input into the Instron software, and the test run at a rate of 0.1 mm/min using a 10 N load cell. The sample IFSS was calculated using the standard equation.

$$\tau = \frac{F_{max}}{\pi D_f L_e} \qquad (1)$$

Where τ is the IFSS, F_{max} is the maximum debonding load, D_f is the diameter of the fibre and L_e is the embedded length. The results are calculated from about 30 successfully conducted microbond tests for each specified case.

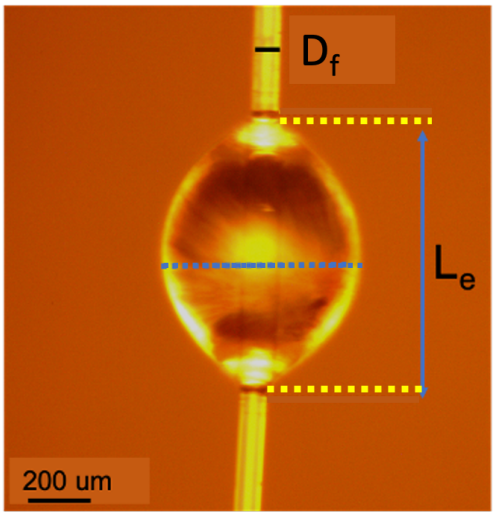

Figure 3.4. An example of a PP droplet and measurements.

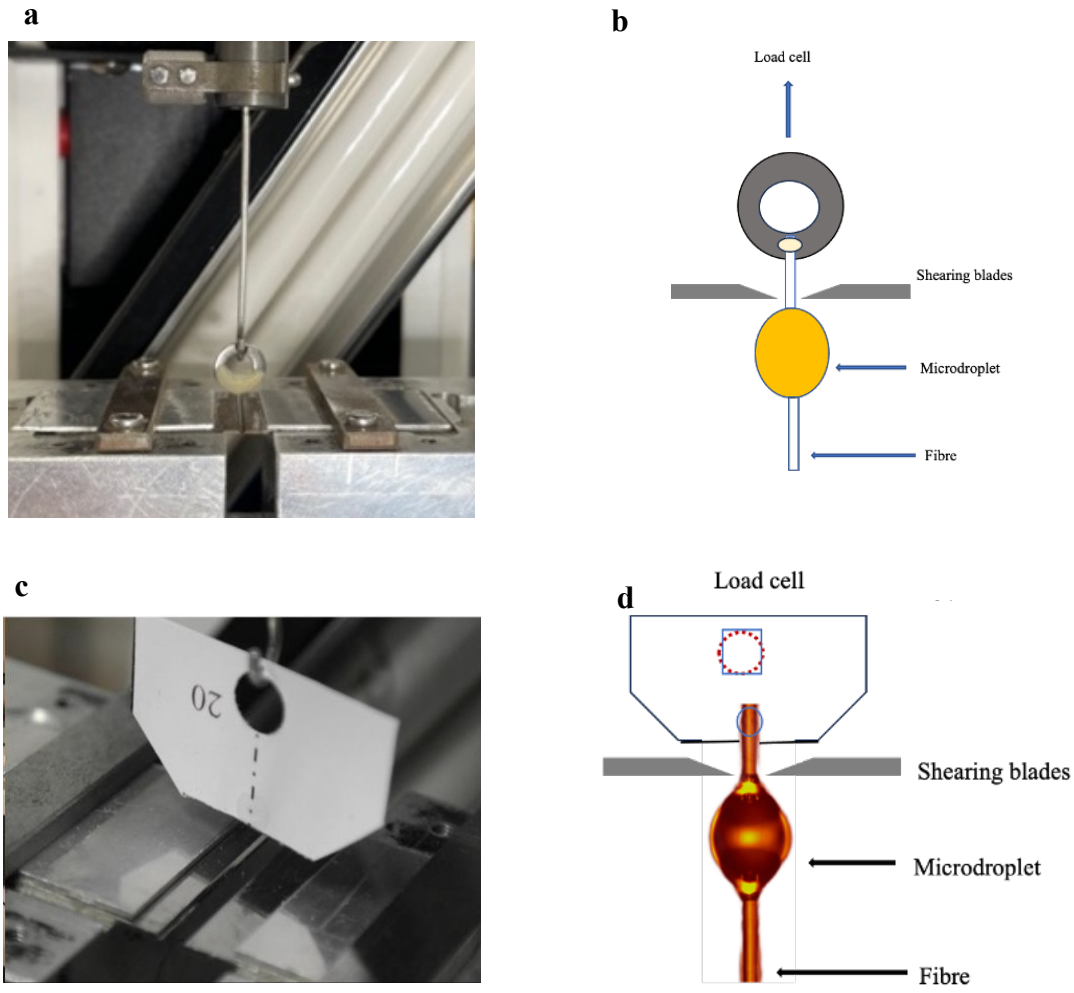

Figure 3.5. a) Thermoplastic microbond sample b) thermoplastic microbond test set up and c) thermoset microbond sample d) thermoset microbond test set up.

The process of fibre/matrix debonding is crucial for understanding the interface dynamics in composite materials. By closely monitoring the loading of microdroplets and analysing the resulting load versus displacement data, one can determine the success or failure of the debonding process. Successful debonding is confirmed when it is visually observed that the fibre remains intact after the test, and the load versus displacement plot displays a frictional component, i.e. the fibre and matrix are not fully separated, indicating the microdroplet's continued movement along the fibre. In contrast, premature fibre fracture is identified when the fibre breaks before debonding can occur, which is reflected in the plot as an abrupt termination of the load curve. Figure 3.6 shows an example of both successful debonding and premature fibre fracture. In the case of debonding, there is still some remaining load capacity in the test sample.

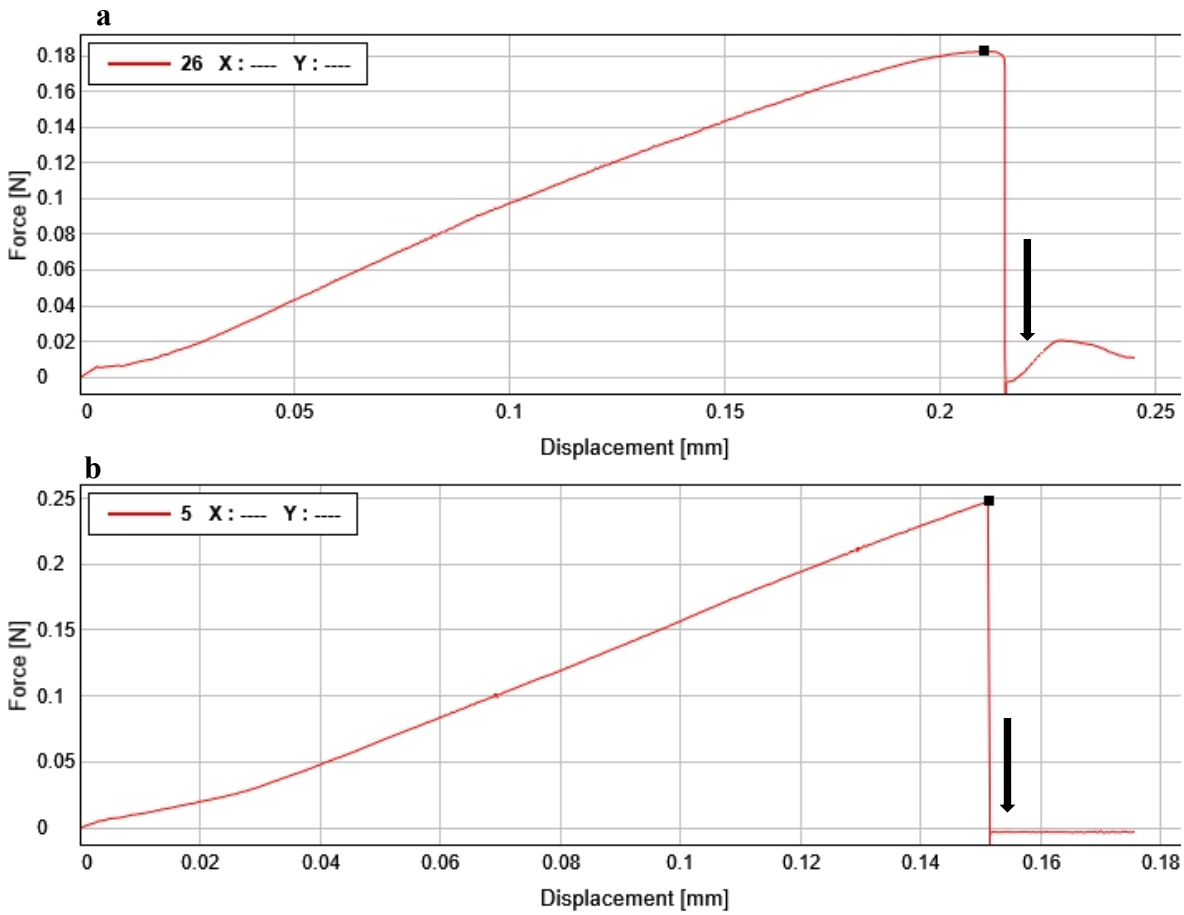

Figure 3.6. Microbond load versus displacement plot showing a) successful debonding and b) premature fibre fracture.

3.2. Hot stage microscopy set up

Hot stage microscopy combines thermal analysis with microscopic observation, enabling the study of material properties in response to temperature variations over time. This technique

merges conventional thermal analysis methods with a visual technology, including high-resolution optical microscopes and digital cameras, coupled with advanced software for analysing transformations captured in images during thermal experiments [78]. Introduced by Mettler in 1967, the first modern hot stage microscope quickly became a favoured instrument for its user-friendliness and precise measurements, as noted by McCrone and colleagues in 1984 [79] and Vitez et al. [80]. Hot stage microscopy was also used to monitor the microdroplet formation for microbond test. For example, Yang et al. [72] used hot stage microscopy to establish a profile for dimensional loss of molten PP microdroplets during heat treatment. Minty et al [81] employed hot stage microscopy to analysed the curing process and resultant shrinkage of epoxy resins. Bryce [16] conducted a similar study utilizing this technique for observation of volumetric shrinkage during the curing of a few epoxy microdroplets.

The hot stage microscopy setup and preparation were performed following the same process as described in Yang et al. [72] and Minty et al. [81] work. Hot-stage microscopy was performed using a Mettler Toledo FP90 hot-stage combined with an Olympus BX51 optical microscope (200x magnification) and a Nikon Coolpix P5100 digital camera. The inclusion of a hot-stage allowed a controlled temperature schedule matching that of the microbond specimen curing schedule to be programmed. A representative schematic and a picture of the hot-stage microscope setup used for the samples is depicted in Figure 3.7. The position of the hot-stage pinhole was initially marked on 1 mm rectangular glass microscope slides. Single bare glass filaments were then suspended above the slides using slow setting cement. The assembly was allowed to stand for 24 h to ensure full setting of the cement. Care was taken to ensure that glass fibres did not contact the surface of the glass cover slip in order to prevent contamination and ensure the droplet remained suspended once applied. The height of the cement was controlled in order to avoid contact with the hot-stage heating element and sample damage during set-up. Each sample consisted of a thermoplastic thread securely tied around a glass fibre and placed on a microscope slide. The samples underwent a controlled heating process in the hot-stage, with temperatures set specific to the polymer type: PP at 220 °C, MAPP at 200 °C, and both PA6 and PBT at 260 °C. Consistent with the oven protocol used during microbond sample preparation, a temperature ramp of 2.5 °C/min was applied. After the heating cycle, the samples were immediately allowed to cool naturally without any controlled ramping, as the equipment did not support setting cooling rates until reaching room temperature.

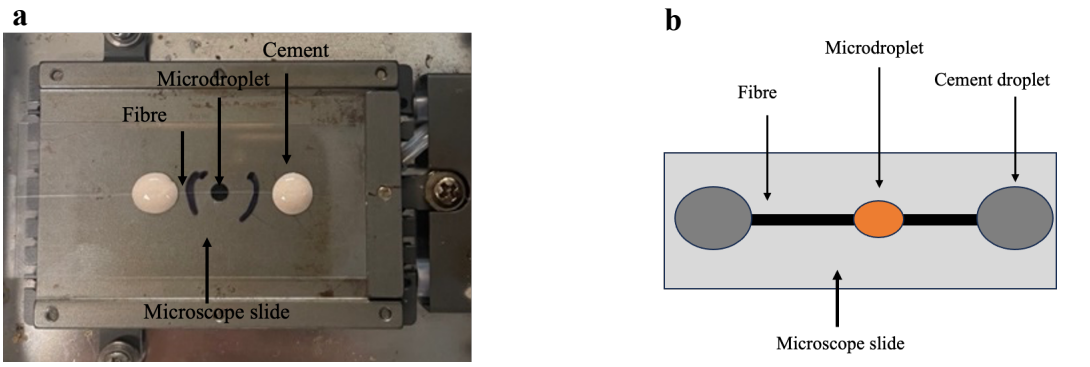

Figure 3.7 a) Hot stage microscopy setup with sample in place, b) Schematic of hot-stage microscopy sample with microdroplet shown

3.3. TGA

TGA measures the percent weight loss of a test sample while the sample is heated at a uniform rate in an appropriate environment. The loss in weight over specific temperature ranges provides an indication of the composition of the sample, including volatiles and inert filler, as well as indications of thermal stability [82]. A critical characteristic of the organic compounds utilized in sizing formulations is their resilience to the elevated temperatures typically encountered during the manufacturing of advanced composite materials. Additionally, the LOI% of the glass fibre, which is an important factor in glass fibre industry can be measured using TGA on a small sample mass between 10 to 15 mg. There have been some studies on sizing thermal stability and LOI% evaluation using TGA. Thomason et al. [83] conducted a thermal stability study using TGA across a variety of commercial glass fibres. They found that sizings compatible with PP degraded between 200 and 250 °C, compromising adhesion. Similarly, Jenkins et al. [84, 85] confirmed the thermal instability of aminosilane sizings within that temperature range on both glass and basalt fibres, potentially affecting the reinforcement efficiency in composites. Rudzinski et al. [86] explored the thermal degradation of E-glass fibre sizings using TGA-FTIR and Pyrolysis-GC/MS. They examined four sizings common in polyamide-compatible glass fibre reinforcements, achieving industry-standard LOI of 0.5 wt%. They found sizing degradation on fibres could begin up to 100 °C lower than in cast films. Gao et al. [87] similarly assessed the thermal stability of silane sizings on glass fabrics. They compared sizings with APS and an undefined amino-functional silane, TG790, noting TG790's superior temperature stability.

In this thesis LOI% values and sizing thermal stability were determined by thermogravimetric analysis performed at 25–700 °C with a heating rate of 10 °C/min using a TA Instruments Q50

TGA. The flow rates were 40 mL/min and 60 mL/min for the balance and sample, respectively. The sample's LOI was taken as the sample weight loss recorded at 500 °C under the air atmosphere. The air atmosphere was preferred over nitrogen because the presence of oxygen can lead to different thermal decomposition pathways. In nitrogen, these pathways may result in less degradation and lower mass loss. A study by Fei et al. [88] found that TGA comparisons using both nitrogen and air showed a small but measurable difference, with less mass lost above 300 °C in the nitrogen atmosphere.

A platinum TGA pan was used for the dedicated TGA analysis. As shown in Figure 3.8, usually 7 mm of the fibre bundle is carefully placed in the pan to cover the entire surface area, ensuring sufficient amount of fibre material (around 5-15 mg) and proper contact with the pan. A minimum of three samples were tested for each type of fibre in the investigations.

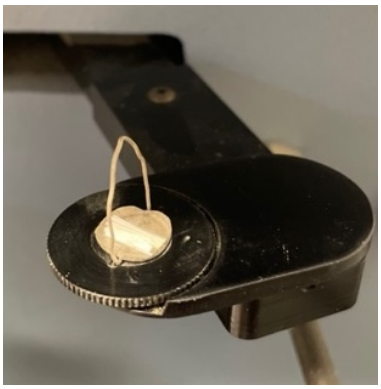

Figure 3.8 Fibre bundle in TGA pan.

3.4. SEM

SEM functions analogously to optical microscopy but uses electrons instead of light to form an image. In an SEM, electrons are emitted from a cathode and are then accelerated toward a positively charged anode. These electrons are then deflected and focused by electromagnetic lenses, similar to the way glass lenses focus light inside optical microscopes. This technology enables the generation of highly detailed images with superior magnification capabilities. The imaging process involves detecting the electrons that are backscattered or released as secondary electrons by the sample in response to the electron beam. These electrons are converted into a signal by the microscope's detectors and processed by software to create a visual representation on a monitor. As the emission of secondary electrons varies across different areas of the sample, so does the intensity of the received signal. An increase in emitted electrons results in a stronger signal. It is this variance in the signal that constructs an image with distinct contrasts, distinguishing areas of the sample based on their differing levels of secondary electron

emissions [89]. SEM observations were used by many researchers to characterise the sizing in glass fibres. Some relevant examples to this thesis are given below.

Berg and Jones [11] used SEM and XPS to estimate the thickness and uniformity of the sizing layer on these fibres. Bledzki et al. [90] studied the uniformity of the sizing layer using field-emission scanning electron microscopy (FE-SEM). Findings revealed a complete encapsulation of glass fibre surfaces by sizings that contained either polyethylene film formers or cationic silanes. In contrast, sizings with APS and coupled with either polyurethane or epoxy film formers resulted in only a partial coverage of the glass fibre surfaces. Le-Huy et al. [91] conducted a study on how silane concentration influences the adsorption of sizings on E-glass fibres, employing SEM, XPS DRIFT, and LOI as part of their analytical methods. The study reported that minor increases in silane concentration seemed to have an impact on the volume of sizing that bonded with the E-glass fibres. This is because the silane appears to increase surface coverage on the fibres. Bryce [16] used SEM to characterise epoxy sized fibre bundles and individual sized fibre uniformity. He reported that the distribution of epoxy coating was suboptimal in fibres treated with 0.1 wt.% and 1 wt.% emulsion. For single fibres treated with 3 wt.%, the distribution remained poor, lacking the node-like structures seen in the fibre bundles. At higher concentrations of 5 wt.% and 10 wt.%, the coating appeared more even.

In this thesis, SEM was employed to scrutinize the glass fibre bundles, individual fibre surfaces, and regions where microdroplets debond. Copper tape secured lengths of glass fibre roving, preserving the integrity of approximately 10 mm bundles during both preparation and SEM analysis. Bundles were then placed on carbon tape affixed to specimen stubs, with each stub accommodating three bundles. For the assessment of single fibres, particularly those involved in microbond testing, a dozen samples were arranged on carbon-taped stubs. These assemblies, still attached to their card tabs, were precisely positioned before being trimmed with a scalpel to remove any excess material. The analysis was conducted using a Hitachi TM3000 scanning electron microscope with an accelerating voltage of 15.0 kV. All SEM samples were sputter gold coated using an Agar sputter coater. Sputter coating was performed under Argon atmosphere with an operating pressure of 0.08 mbar, 30 mA current, and a 40 s coating time. The fibre bundles and microbond droplet samples, which are not easily visible in the image, are illustrated in Figure 3.9.

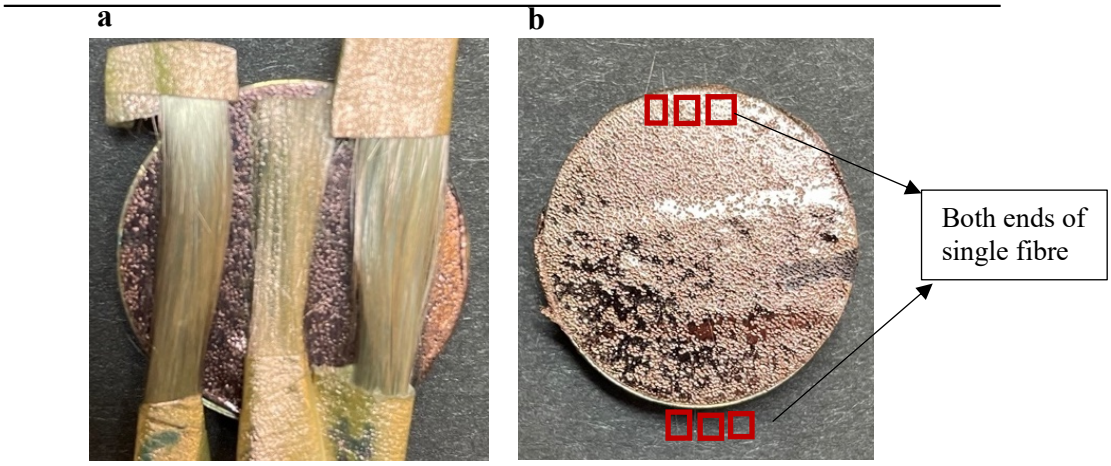

Figure 3.9. a) Gold coated Fibre bundle SEM specimen. b) gold coated single fibre with microbond droplet SEM specimens.

3.5. AFM

AFM serves to detect surface defects and changes in the overall surface topology after different treatments such as polishing, cleaning, aging and corroding [92]. An AFM uses a cantilever with a very sharp tip to scan over a sample surface. As the tip approaches the surface, the close-range, attractive force between the surface and the tip cause the cantilever to deflect towards the surface. AFM is normally used for characterizing flat surface specimens. In addition it has been used in analysing glass fibre surface and effect of sizings on morphology and surface roughness of fibre by number of researchers. Raedlein and Friscat [93] outlined the optimal instrumental and sample preparations for using AFM on glass materials. Achari et al. [94] conducted a topographical analysis of untreated and variously sized glass fibres, noting differences in surface smoothness and structure. Sized fibres exhibited a more uniform topography compared to the rougher surfaces of unsized fibres. Turrion et al. [95] integrated AFM with fluorescence to study aminosilane sizings on heat-cleaned glass fibres, revealing uniformly distributed silane "islands" affected differently by solvent treatments. Behary et al. [96] employed AFM for friction force analysis of fibres sized with starch or epoxy, discovering significant variations in frictional forces indicative of chemical heterogeneity and processing effects. Gupta et al. [97] compared the roughness of silica and E-glass fibres, linking the surface characteristics to the melt surface tension and the inherent structural inhomogeneities of the glass. Mai et al. [98] visualized the roughness of sized and unsized glass fibres with AFM. Sizing with APS led to rougher surfaces, while the addition of a polyurethane film former resulted in complete coverage but increased roughness. They also used AFM to detect interphase variations in fibre/matrix combinations, suggesting differing mechanical behaviours compared to the bulk matrix.

In this work, a Bruker Innova atomic force microscope was employed to analyze the surface roughness of bare and sized fibres . Tapping mode was utilized with a Silicon tip visibly pointed at the apex, possessing an average resonance frequency of 70 kHz and a spring constant suitable for fibrous samples at 2 N/m. AFM images were captured at a resolution of 128 x 128 pixels with a low scan rate of 0.1 Hz. For each fibre sample three fibres were chosen at random and affixed to a metal plate using carbon double-sided tape as depicted in the schematic in Figure 3.10. Two distinct areas on each fibre were examined over a 3 x 3 µm square.

Height and tapping phase images underwent a flattening process to correct curvature. This was done using the 'Flatten' feature in NanoScope Analysis software at a second-order level, an illustration of which is presented in Figure 3.11.

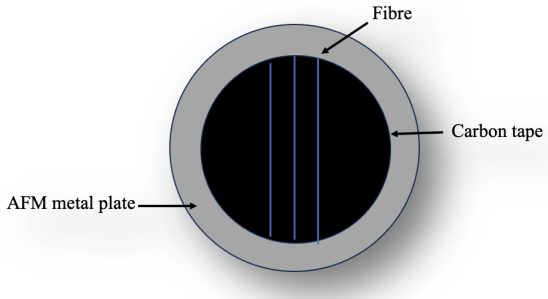

Figure 3.10. Schematic of an AFM plate with mounted fibres

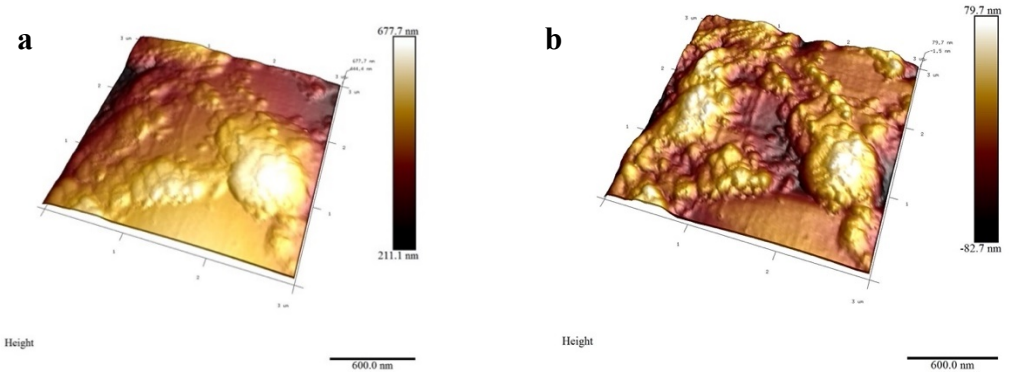

Figure 3.11. AFM 3-D height image of Industrial fuuly sized fibre, a) before flattering and b) after flattering to remove curvature.

3.6. FTIR

FTIR is a technique used to obtain an infrared spectrum of absorption or emission of a solid, liquid or gas. An FTIR spectrometer simultaneously collects high-resolution spectral data, over a wide spectral range. The adsorption and adhesion of sizing components to glass fibre surface,

hydrolytic stability of silane layer, when exposed to moisture, and sizing decomposition can be obtained through design of experiment and FTIR data interpretation.

Researchers have used FTIR for different analysis like chemical identification of sizing, sizing decomposition (thermal), adsorption and adhesion of sizing components to glass fibre surface layer after hot water extraction. For example Chiang et al. [99] employed FTIR spectroscopy to investigate the organization of APS in solution and its interaction with E-glass fibre surfaces, postulating that APS forms multiple layers where amino groups create intramolecular rings, influencing the coupling agent's interaction with resin matrices in composites. Naviroj et al. [100] also utilized FTIR to examine how APS's structure and adsorption on E-glass fibres are affected by solution pH, finding maximal adsorption at a natural pH of 10–11 and noting the structure's susceptibility to atmospheric CO_2 between pH 6 and 12. Dibenedetto and Lex [9] used FTIR Spectroscopy to detect the presence of silane on the surface of E-glass fibres post-treatment with boiling water. Bikiaris et al. [101] explored the use of silane coupling agents with modified PP for glass fibre-PP composites, discovering that APS-coated fibres outperformed APS in composite properties, where one of the sizing characterisation method was FTIR.

In this thesis, a 4100 ExoScan FTIR equipped with a spherical diamond ATR interface and an adjustable probe, was employed for surface analysis of as received glass fibre bundles and for assessing the chemical composition of sizings. For optimal contact, the fibres were placed on a stage, and the probe was precisely lowered onto the fibre bundle. Spectra were acquired at ten distinct points along 15 cm lengths of fibre, with background signals measured after each spectral acquisition and the crystal cleansed with acetone in between. The analysis spanned a spectral range of 4000 to 650 cm^{-1}, with a resolution of 8 cm^{-1} and 64 scans for each sample. Each type of fibre was tested with five repetitions. Spectral data processing and the plotting of normalized average spectra were conducted using OriginPro, while SpectraGryph facilitated peak identification and quantitative analysis. Increased spectral resolution did not significantly impact the sensitivity of the spectra; scans at 4 cm^{-1} resolution revealed no notable differences from those at 8 cm^{-1}.

CHAPTER 4: A NEW LABORATORY-SCALE APPROACH TO GLASS FIBRE SIZING USING A SPIN COATING METHOD

4.1. Introduction

As mentioned in chapter 2 sizings are essential processing aids for both the fibre manufacturing process and the manufacture of polymer composites. Moreover, due to its initial location on the fibre surface, the size layer is a critical component in the formation and properties of the fibre-polymer interphase [4]. Obtaining an optimised composite interphase in the final composite is known to be essential in achieving the required short-term and long-term mechanical performance from a composite.

Despite the critical need of the composite industry to fully understand and control all aspects of the materials it uses; commercial glass fibres are often supplied with only two sizing related details [1]. The first is an indication of the chemical compatibility of the sizing with a general class of matrix polymer. The second is normally a value for the LOI% which gives a measurement of the amount of organic sizing present on the glass fibre product [1, 6, 102]. LOI% is determined by the weight loss of a sample after heat treatment at elevated temperature (in the 500–600 °C range) [103]. This lack of information on the physical and chemical nature of the sizing on a glass fibre product is an issue for many users of glass fibres, be they interested in quality control for manufacturing or the fundamentals of the fibre/matrix interphase.

From the above discussion it should be clear that those involved with polymer composites research and development have a need for practical tools which can assist with the understanding of the nature and role of sizings on the glass fibres which reinforce their composites. However, most researchers working in this field know that there has been a lack of systematic research and development published on analysis and characterization of sizings. Two factors contribute significantly to the challenge of developing a more useful (to those downstream from glass fibre production) fundamental understanding of the complex role of sizings in chain of composite producers and users. The first is the well-known confidentiality around the chemical formulation of the sizings used on commercial glass fibre products. The second is the fact that fundamental systematic research of the role of sizings requires the ability to formulate and apply sizings to glass fibres under conditions which are relevant to real-world glass fibre production. In reality this means having access to a knowledgably built, operated, and maintain (pilot) glass fibre forming facility. The financial, engineering and resource

challenges of operating such a facility is the reason that there are so very few of these available to researchers outside of the glass fibre manufacturing industry.

Researchers outside of glass fibre production often use dip-coating with lab-made sizings for study, but this method does not replicate the industrial sizing application's speed and shear [8-12, 104]. This casts doubt on the relevance of such studies. An example of common dip coating proses is presented in Figure 4.1. Dip-coating typically results in a higher LOI% and thicker sizing layer (~1280 nm) and makes glass fibre more brittle. To achieve a more controlled and realistic layer thickness, researchers often have to adjust the concentration of the sizing solutions or emulsions [13-17]. This adjustment is necessary because the sizing layer's thickness directly influences the mechanical and interfacial properties of the resulting composite materials. The other challenge when sizing fibres in laboratories without a bushing and sizing applicator is the drying method. Typically, drying is done by laying the sized fibre in a tray, as depicted in Figure 4.1b, or suspending the fibres bundle, either horizontally or vertically, as shown in Figure 4.2. The drying techniques for dip coated fibres have certain issues. For example, excess sizing on and around the fibres can cause the fibre bundle to adhere to the tray. Removing the fibres then requires pulling them from the tray (Figure 4.1c), which is not ideal and may result in fibre damage. While hanging the fibres avoids the sticking issue after drying, it can result in most of the sizing migrating to the lower part of the bundle, which brings inconsistency in the fibre bundle and is undesirable.

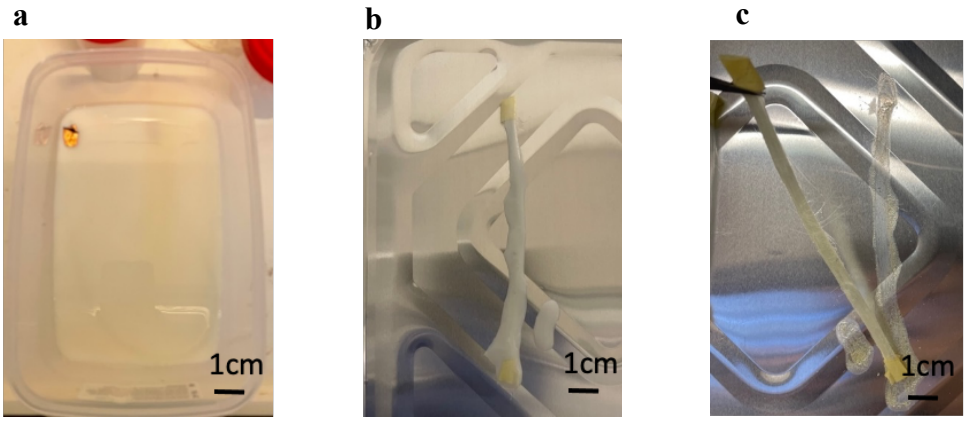

Figure 4.1. An example of the dip coating and drying process of a glass fibre bundle. a) Dip coating of glass fibre bundle, usually for 15 min. b) Placed in an aluminium tray for drying in a conventional oven usually at 110 C. c) Dried fibre.

Figure 4.2. An example of the dip coated fibre bundles hanged for drying.

Overall, the literature suggests a lack of an appropriate laboratory sizing processing technique to replicate industrial sizing conditions, and the current techniques may result in sized fibres with different properties than industrial sized fibres. This situation can clearly hinder optimal research and development of the fundamental role of sizing. There is therefore a pressing need to generate a lab-scale sizing process that more closely mirrors the industrial sizing process.

This chapter introduces a novel spin coating-based sizing process for better replicating some of the factors associated with the high-speed, dynamic industrial glass-fibre sizing process. Although spin coating methods have been widely used for film formation in various sectors [105], it is believed that this is the first reported use of this method for glass fibre sizing. To assess the effectiveness of the proposed method, two distinct types of sizing were prepared in-house: one that is compatible with PP and another that is compatible with epoxy. While this thesis primarily focuses on sizings that are compatible with thermoplastics, an epoxy-based sizing was also created to thoroughly evaluate the spin coating method. TGA has been used to analyse the LoI and thermal stability of spin coated, and conventional dip coated fibres. The microstructure of the applied coatings on the fibre surfaces in both the spin coated and conventionally dip coated samples was examined through SEM and AFM for comparative analysis. In addition, both coating techniques were applied to microscope slides to evaluate their effectiveness on different glass substrates and to gather additional data for comparing the methods. Furthermore, the effectiveness of the sizing process on IFSS has been evaluated using

the microbond test utilising a number of in-house sized fibres and one industrial sized glass fibre combined with two different types of thermoplastic matrices.

4.2. Literature review

4.2.1. Glass fibre sizing techniques

The common industrial sizing process of the glass fibre is shown schematically in Figure 4.3 [4]. The sizing applicator is typically positioned around 1–2 m below the bushing plate, and it is responsible for delivering the size onto the freshly formed glass fibres. Figure 4.4 shows a typical recirculating sizing applicator [1] including a roller partially submerged in a sizing reservoir. The sizing emulsion is usually constantly recirculated, and it is often cooled, and the rotating roller picks up a layer of the size of controlled thickness on its surface. The thickness of the layer on the roller is proportional to the rotation speed of the roller, and it is related to the amount of size picked up by the fibres.

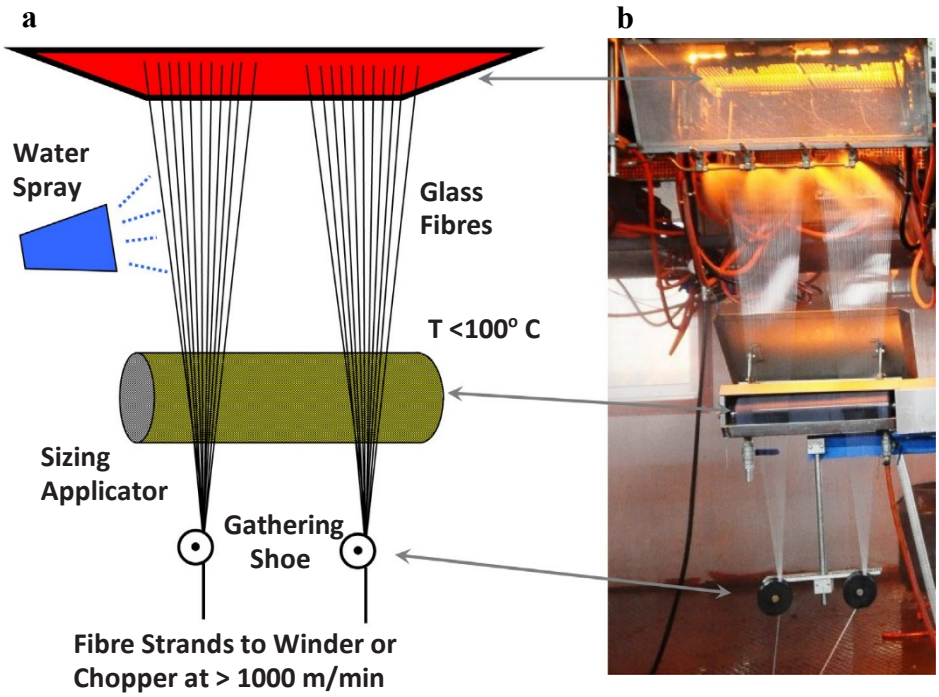

Figure 4.3.a) Schematic and b) picture of a glass fibre forming position [4].

Figure 4.4. A picture of a sizing applicator in glass fibre production [1].

Most researchers, outside of the glass fibre manufacturing companies, who attempt to work in this field choose dip-coating of glass fibre samples with small scale laboratory produced sizing emulsions [8-12, 101]. Some investigations were done by dip coating the fibre only with silane, for example Bikiaris et al. [101] reported on E-glass fibres heat cleaned and then dip coated with silane solutions to produce injection-moulded glass fibre-PP composites. They investigated silane sizings with PP to affect adhesion levels in glass fibre-PP composites, noting differences between APTMS and APTES coated fibres. Naviroj et al. [100] investigated APS on E-glass fibres, dip coated in pH-adjusted APS solutions, affecting the structure of the aminosilane layer on the fibres. They used FTIR to study APS structure and adsorption on E-glass fibres, showing pH-dependent layer structure and adsorption peaks. Berg and Jones [11] studied the formation of the interphase region in glass fibre-epoxy composites, focusing on the effects of different sizing formulations. They used bare E-glass fibres dip coated with a range of coatings based on APS and epoxy resin sizing emulsions with varying molecular weights i.e., low, medium, and high. Additionally, a commercial epoxy sized fibre was employed as a control in their experiments. The researchers used XPS and SEM to estimate the thickness and uniformity of the sizing layer on these fibres. In an effort to simulate the potential properties of a sizing interphase, they created blends of two film formers and the matrix resin. These blends were shown to significantly affect the modulus, strength, and glass transition temperature of the matrix. However, when IFSS was evaluated using single fibre fragmentation tests, it was found that all sized fibres exhibited lower interfacial strength compared to bare. They suggested that this may be due to the sizing reducing the adhesion quality between the fibre and matrix. These results were attributed to varying degrees of sizing resin plasticization

in the interphase region. It is possible that the formulation used was not fully compatible with the resin in their study. Dong et al. [106] described the making of an aqueous sizing based on APS, epoxy resin film former, and silica particles, with sizings dip coated onto thermally desized glass fibre roving. They reported the sample coated with the sizing containing the silica gave a 50% higher level of IFSS compared to the desized glass fibre. It was noted that the IFSS base value for the desized fibre was significantly low, whereas the glass fibre-epoxy system is typically expected to have a much higher IFSS value based on commonly observed results. Gao et al. [12] studied the effects of silane blends on water-sized E-glass fibres by applying TES/GPTMS blended sizings through dip coating. Dwight et al. [107] examined how Lewis acid-base interactions function at the interface between the fibre and matrix in composite materials, where E-glass fibres were sized with silane coupling agents through dip coating.

Although the dip coating technique enables the investigation of similar chemistries that might use for sizing formulations, this process lacks any real connection with the high speed, high shear, application and distribution of real-world sizing application. Frey and Brunner [108] emphasized the challenge associated with the creation and assessment of glass fibre sizing in the absence of glass fibre bushing and advanced sizing technologies. They investigated the resizing of glass fibres using a dip coating process with glass fibres that had undergone either solvent extraction or thermal treatment at 600 °C to remove sizing. Although the chemical extraction process produced fibres that could be relatively easily resized and evaluated, uncertainty persists regarding the role of the non-extractable portion of the original sizing, complicating the analysis of the resizing materials. Thomason's [8] study found that E-glass fibres dip coated in 1% silane solutions had higher tensile strength than water-sized fibres, but still lower than fibres sized with APS in standard industrial condition. Consequently, this cast serious doubts on the usefulness of any results obtained from dip coated samples. The dip coating method generally results in a thick layer of sizing and a higher LoI due to the exposure of the fibres to a high volume of sizing. Usually, the thickness of the applied sizing layer must consequently be controlled by creating different (lower) concentrations of sizing solutions or emulsions [13-17] which are often significantly different from those used in fibre manufacturing. These studies varied the concentration of silane or other sizing components to assess their effects on the properties of glass fibres and their composites. The sizing layer thickness and its uniform distribution has a significant effect on interfacial and mechanical performance of the resultant composite materials. Vazquez et al. [14] reported that as the sizing thickness increases, the tensile, compressive, and shear strength decrease for composites with

monofunctional epoxy-coated fibres. They discussed how applying an epoxy coating to glass fibres affected the flexural performance of unidirectional glass-fibre epoxy composites, using commercial E-glass fibres with an APS and urethane film former mixture for sizing. It was found that increased coating thickness led to lower mechanical strengths, likely because thinner sizing allows for better adhesion by promoting stronger fibre/matrix interaction and more efficient load transfer. In contrast, excessively thick sizing acts as a lubricant, reducing shear strength and weakening the bond due to incomplete reactions or uneven distribution, compromising the composite's mechanical properties. Yue and Quek [17] identified an optimum silane thickness (about 3.2 pm) for the silane coating applied to the surface E-glass fibres dip coated in aminosilane solutions to generate a maximum IFSS with a PP matrix.

4.2.2. Spin coating

Spin coating as detailed in Tonya's review [109] is a fabrication process widely used in different industries such as semiconductor industry, pharmaceutical, solar energy and so on, and the aim is creating or applying uniform thin films to flat substrates. The solution to be coated is dispensed onto the centre of a substrate, and then the substrate is rotated at high speed. This process results in the spreading of the solution due to centrifugal force, which, after solvent evaporation, leaves a uniform thin film on the substrate. The thickness and uniformity of the film can be controlled by the spin speed, viscosity of the solution, solvent type, and the duration of spinning. Typically, faster spin speeds and lower viscosities result in thinner films. As illustrated in Figure 4.5, the processes are dynamic, and the final film properties depend on the interplay between centrifugal force, viscous force, and solvent evaporation rate. Higher speeds and forces, results in a lower thickness film. The technique is praised for its simplicity, repeatability, and ability to produce high-quality films. It has been adapted for a wide range of materials, including polymers, sol-gel precursors, and nanoparticle suspensions [110-112]. However, care must be taken to avoid defects such as striations, which can be caused by variations in spin speed or solution concentration.

Figure 4.5. A picture of a sizing applicator in glass fibre production [113].

4.2.3. Sizing characterization

As stated in introduction, typically, manufacturers only disclose two key pieces of information related to sizing. The first piece of information concerns the sizing's chemical compatibility with a wide range of matrix polymers [1] . The second piece of information is the LOI% , which quantifies the amount of organic sizing present on the glass fibre [1, 6, 102]. There are a few studies on the glass fibre LOI% and sizing thermal stability. Zinck and Gerard [114] analysed different E-glass fibre sizings, including an antistatic agent, a 1 wt% APS solution, and an industrial sizing. The LOI values were measured using TGA and the numbers were 0.17% for APS, 0.77% for the full sizing, but they couldn’t reach the LOI value of antistatic agent. Thomason et al. [83] used TGA to investigate the thermal stability of a wide range of commercial glass fibre products, noting complete degradation of PP compatible sizings at 200-250 °C. In a related study, Jenkins et al. [84] conducted TGA to examine the thermal stability of sizings compatible with epoxy on both glass and basalt fibres. They also verified that the degradation of aminosilanes occurs within the 200–300 °C temperature range.

4.2.4. Literature conclusion

In conclusion, the comprehensive review of sizing techniques, their characterization, and an introduction of the spin coating method were discussed. The research community's understanding of the critical role of sizings in forming and enhancing the properties of fibre-polymer interfaces was highlighted in the introduction chapter. However, commercial glass fibre manufacturers provide limited information on sizing formulations. While the dip coating technique allows for investigation into similar chemistries used in sizing formulations, it does not simulate the high-speed, high-shear application and distribution typical of real-world sizing processes. The absence of a standardized laboratory technique to replicate industrial sizing conditions has posed longstanding challenges for researchers and manufacturers alike.

4.3. Experimental procedures

4.3.1. Materials

The available details of the sizing components used in this study are given in Table 1. APS and GPS were purchased from Sigma-Aldrich. The PP and epoxy film former aqueous emulsions were supplied by Sisecam who had sourced the emulsions from two different suppliers. The fibre coating experiments were conducted using bare (water-sized) E-glass fibres taken from a large roving supplied by Sisecam. To create 100 grams of PP compatible sizing with a solids concentration of 10 wt% after drying, which is the most common solid percentage of thermoplastic compatible sizing[1] , the process involved the following steps (See Figure 4.6): initially, 1.6 grams of APS were mixed with 50 gr deionised water and agitated for 10 minutes. Subsequently, 24.2 grams of film former emulsion were added to the mixture along with deionised water, resulting in a total of 100 grams of sizing with a solids concentration of 10 wt%. The solid content of the sizing for the spin coated and dip coated fibres was measured and maintained at 10%, which is also common for industrial sized fibres. To create 100 grams of epoxy compatible sizing, with a solids concentration of 5 wt% after drying, which is the common solid percentage of thermoplastic compatible sizing [1], the process involved the following steps: initially, 1.0 grams of GPS were mixed with 50 gr deionised water and agitated for 10 minutes. Subsequently, 7.8 grams of film former emulsion were added to the mixture along with deionised water, resulting in a total of 100 grams of sizing with a solids concentration of 5 wt%. Th solid content of the sizing for the spin coated and dip coated fibres was measured and maintained at 5%, which is also common for industrial sized fibres [1] . Furthermore, for the dip coated S1A a sizing dispersion with a concentration of ~2.6 wt% was prepared. This was accomplished by diluting the sizing concentration and solid content by a factor of 10. The purpose of this step was to evaluate the impact of the dip coating solution's concentration on the LOI% of the sized fibres. The investigated fibres are summarized in Table 1. The PP (PETOPLEN EH102) and MAPP (Polybond® 3200) used for the microbond testing were supplied by Petkim and Addivant respectively. The resin used for the microbond testing was MGS™ RIMR 135 with the curing agent MGS™ RIMH 134–RIMH 137 at a stoichiometric ratio of 30 phr as per the manufacturer’s recommendation. Both resin and

hardener were supplied by the project industrial partner Sisecam.

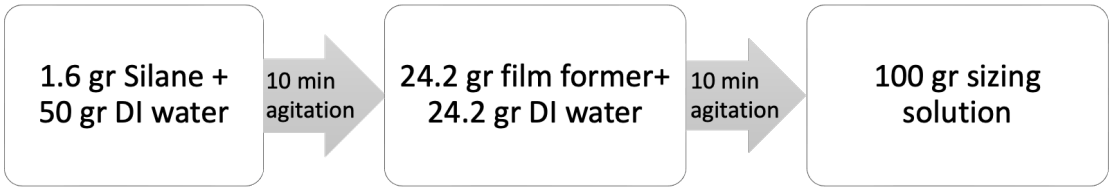

Figure 4.6. PP compatible sizing process steps

Table 4.1. Commercial and in house PP compatible sized fibres

Designation	Film former	Silane	Sizing concentration (wt%)	Sizing Solids (wt%)	Mean fibre diameter (μm)
BF	Bare (water size)	Bare (water size)	_	_	17.0
IS	Industry sized PP compatible	Confidential	_	_	17.5
S1A	Copolymer PP with medium percentage of Maleic Anhydride	APS	25.8%, 2.6%	10%, 1%	17.0
ISE	Industry sized Epoxy compatible	Confidential	_	_	17.0
S3A	Epoxy film former	GPS			17.0

4.3.2. Sizing techniques

As briefly summarised in Figure 4.7, dip coating and spin coating techniques were used for applying the in-house prepared sizes on the BF. For the dip coating, Figure 4.5a, the 10 cm BF bundles were completely immersed in the size emulsions, for 10 minutes, then removed and dried in an oven for 120 minutes at 110 °C. Spin coating utilizes centrifugal force and the surface tension of the liquid to achieve a uniform coverage by rapidly spinning a fibre bundle with a droplet of sizing applied all over the bundle, which was the same amount |(0.2 ml) for all the samples. The initial inquiry addressed the optimal method for applying sizing to a fibre bundle: whether to confine the sizing to the middle section or to cover the entire bundle. To

investigate this, microscope slides were utilized to examine the distribution of sizing under centrifugal force.

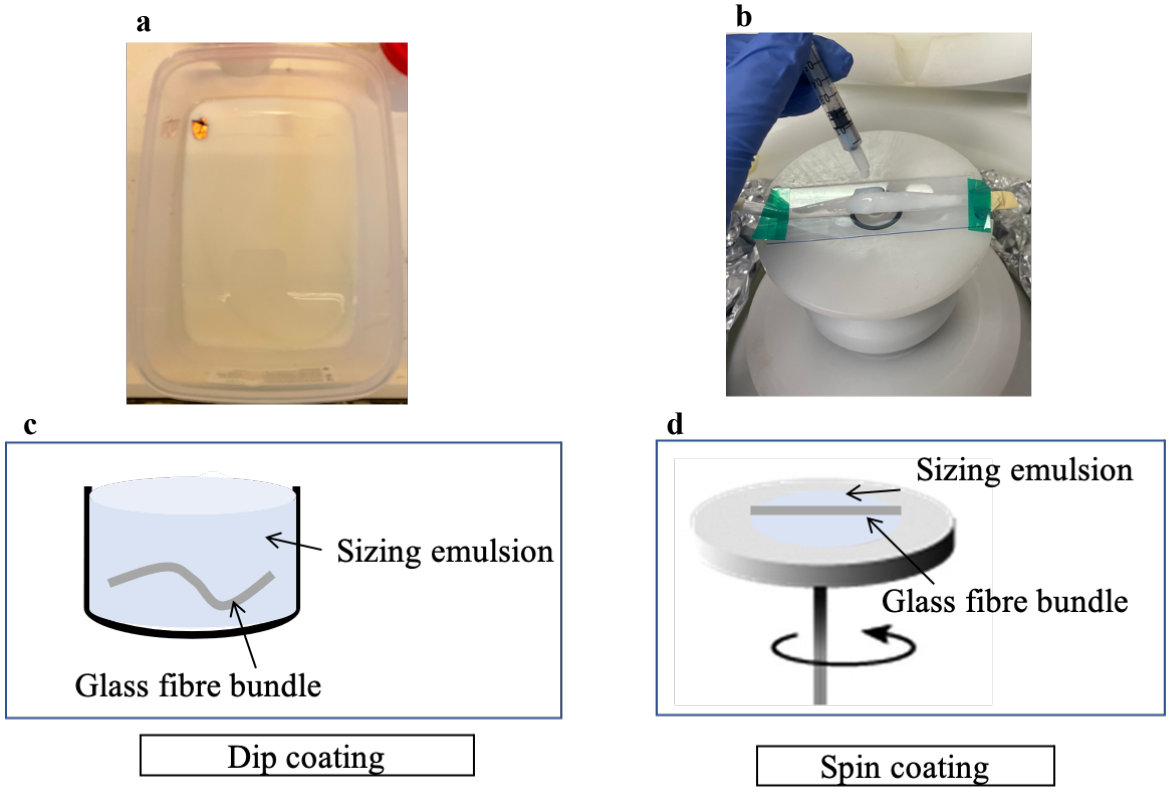

Figure 4.7. Schematic of the a,c) dip coating and b,d) spin coating methods.

To determine the optimal application of sizing to the fibre bundle, an evaluation was conducted. Sizing was applied at the centre (Figure 4.8a) and across the entire slide to mimic the fibre bundle (Figure 4.8b). The results were observed after spinning, the findings indicated that a more uniform distribution of sizing is achieved by coating the entire slide or fibre bundle. Consequently, for the purposes of this thesis, all fibres prepared with spin coating were covered with sizing prior to the initiation of spinning. By subjecting the emulsion to high speeds, the spinning action effectively distributes the coating onto the fibre surface.

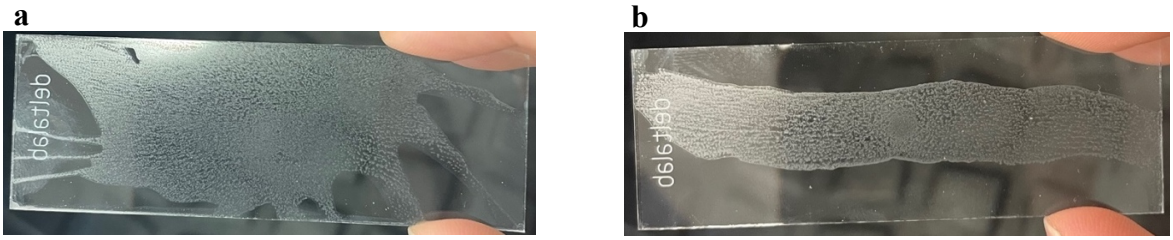

Figure 4.8. a) Sizing was placed at the middle of the slide right b) sizing was placed all over the slide as placed on the fibre bundle.

To perform the sizing spin coating a 10 cm BF bundle was placed onto a plastic microscope slide. To ensure stability and prevent any separation during the process, both the bundle and

the slide were securely attached to the spin coater using a tape, see Figure 4.5b. A total of 0.2 ml of sizing, which proved sufficient to cover the entire bundle, was applied all along the BF sample. The same 0.2 ml was used for all the spin coated fibres to ensure consistent sizing application across the study. Once the machine was sealed, various spin speeds (rpm) were investigated for their influence on the final LOI. After spinning for 10 seconds, the sized fibres were carefully detached from the microscope slide and dried in an air circulating oven for 120 minutes at a temperature of 110 °C.

Figure 4.9 shows drying process of both spin coated fibre bundle at 10000 rpm and dip coated fibre bundles. The spin coated fibre bundle at 10000 rpm did not adhere to the surface of the aluminium tray as it does with dip coating. Additionally, it was observed that there was some stickiness with the spin-coated fibre at lower speeds such as 500 and 1000 rpm. As the spinning speed increased, less sizing remained on the fibre, resulting in reduced adherence to the drying tray.

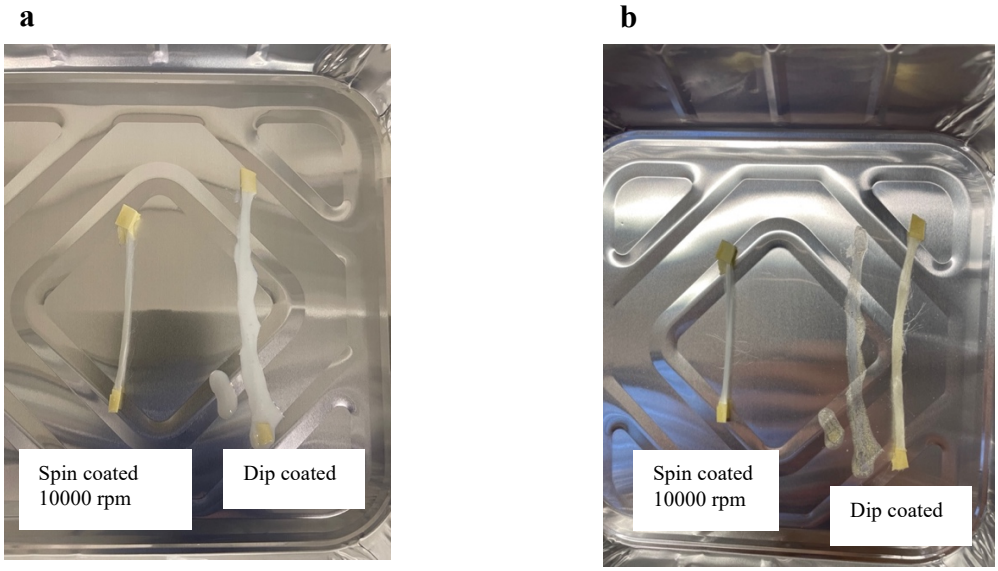

Figure 4.9. a) Spin coated and dip coted bundle in an aluminium tray before placed in the oven b) Spin coted and dip coated fibre bundles after 120 min drying.

4.3.3. TGA of sizing layer

TGA process was done as described in section 3.3, with the temperature scans of a heating rate of 10 °C/min. The weight loss of the sized glass fibres was recorded as a function of the temperature under the air atmosphere. The sample's LOI was taken as the sample weight loss recorded at 500 °C. The average thickness of the glass fibre sizing layer was calculated assuming a uniform distribution on the surface of all the coated fibres using the TGA LOI data

as formulated in Equations 4.1 [115]. The dimensionless fraction W_S (LOI) uniformly coated on the surface of a fibre sample can be calculated using Equation 4.1:

$$W_S = \frac{\pi(R^2-r^2)\rho_{sizing}}{\pi[(R^2-r^2)\rho_{sizing}+r^2\rho_{fibre}} \quad (4.1)$$

Where ρ_s is the sizing layer density and ρ_f is the density of the glass fibre. The sized fibre radius is R and unsized fibre radius is r. The sizing layer thickness (t) can therefore be calculated using Equations 4.2.

$$t = R - r = r\left[-1 + \sqrt{\frac{W_S}{1-W_S}\frac{\rho_{fibre}}{\rho_{sizing}} + 1}\right] \quad (4.2)$$

A typical TGA thermogram of sized glass fibre is shown in Figure 4.10 showing the relevant parameters used in the equations. The glass fibre and sizing layer are assumed to be perfectly cylindrical, with the sizing layer uniformly distributed. The density of unsized glass fibres, as reported by the manufacturer, is 2.62 g/cm³. The density of the sizing is assumed to be approximately 1 g/cm³, which is close to the density of water, given that the majority of the sizing composition consists of water [116].

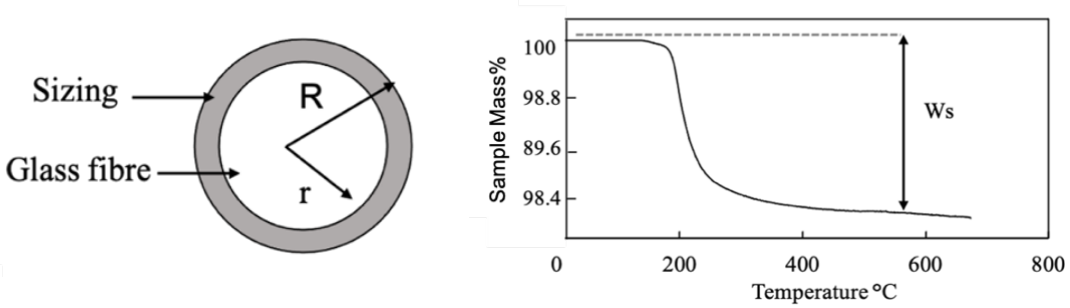

Figure 4.10. Glass fibre sizing layer model graph.

4.3.4. Morphological analysis using SEM and AFM

The structure and morphology of sized glass fibre bundles (Dip coated S1A, 10 wt%, Dip coated S1A 1wt%, Spin coated S1A 10%, and IS) as well as microscope slides dip and spin coated fibre using S1A sizing were examined through SEM, as described in section 3.5, with an accelerating voltage of 15.0 kV. All SEM fibre samples were sputter gold coated using an Agar sputter coater under Argon atmosphere with an operating pressure of 0.08 mbar, 30 mA

current, and a 40 s coating time. The microscope slides were not gold coated as the images without gold coating were clearer. AFM images were captured to analyse the surface topography of fibres as outlined in chapter 3. The BF, IS fibres, fibres sized with dip coating and spin coating techniques, specifically sample S1A, were subjected to analysis at a spinning speed of 10,000 rpm.

4.3.5. Microbond test

The preparation of the microbond test samples followed the procedures outlined in Section 3.1. The study utilized both thermoplastic and thermoset compatible fibres, which were sized using two distinct techniques: spin coating and dip coating, to assess the effect of sizing application methods on the IFSS. For comprehensive analysis, each batch consisted of forty meticulously prepared samples. The IFSS results presented in the results section are derived from a statistically robust dataset, with the values representing the mean of around 30 successful microbond tests for each sample set, with a 95% confidence level.

4.4. Results and discussion

4.4.1. TGA study

Figure 4.11 presents results for weight loss (TGA) and differential weight loss (DTG) of the dip coated and spin coated glass fibres when heated in an air atmosphere in the range 30–500 °C with a temperature ramp of 10 °C per minute. Two completely different sizings were investigated: S1A, which is PP-compatible with 10 wt% solids, and S3A, which is epoxy-compatible with 5 wt% solids.

There are major differences in the TGA results depending on the sizing technique and the rotation speed in the case of the spin coated fibres in both sizing systems. Given that E-glass is thermally stable in this temperature region, it is reasonable to assume that the weight changes are caused primarily by the degradation of the organic materials in the fibre sizing layer. Upon examining the TGA and DTG graphs of PP compatible sizing, a distinct disparity becomes evident beyond 500 rpm, suggesting a notable alteration in the graph patterns between the dip, no spin (0.2 ml of sizing applied without spinning) and 500 rpm configurations and the graphs at higher rpm values.

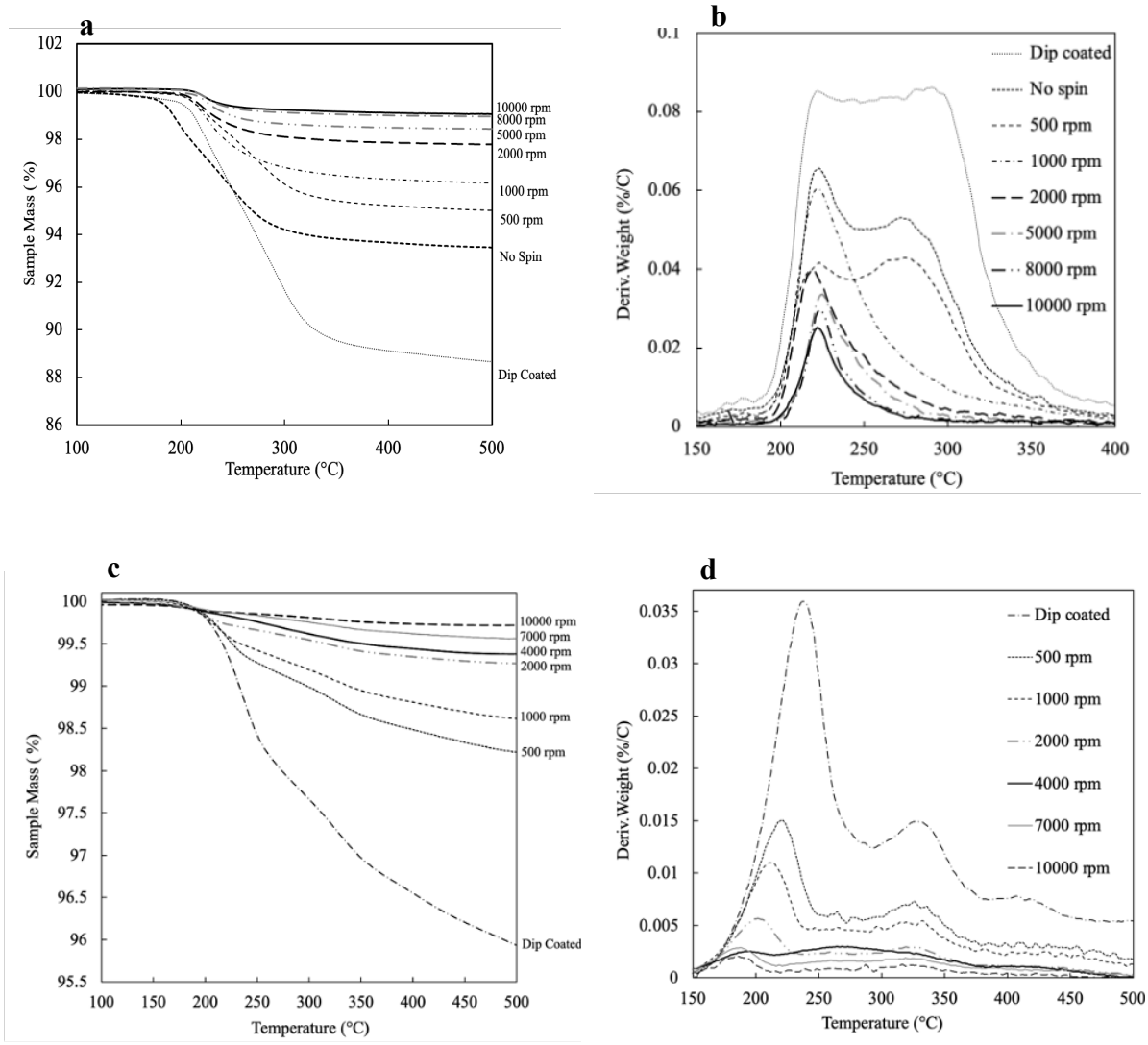

Figure 4.11. Comparison of a) TGA and b) DTG graphs, of the S1A samples with the coating method of dip coated, spin coated, No spin (0.2 ml of sizing applied without spinning), Comparison of c) TGA and d) DTG graphs, of the S3A samples with the coating method of dip coated, spin coated and S3A fibre samples.

In the TGA graph of PP compatible sizing (see Figure 4.9a), for the dip coated, no spin and 500 rpm coated fibre, the weight loss is observed in the temperature range of 200–350 °C. For fibre spin coated at higher speeds the width of the degradation temperature range appears to be smaller. This can be seen more clearly in the DTG curves (Figure 4.9b) which appear to exhibit two overlapping thermal degradation events, a “low temperature” event peaking around 225 °C and a “high temperature” event peaking around 280 °C. The lack of available information regarding the formulation of the commercial film former emulsions precludes any detailed discussion of what component may be preferentially lost during the higher speed spin coating. However, further investigation such as Fourier transform infrared or X-ray photoelectron spectroscopy may assist in identifying the lost component. The graph from the epoxy sized

fibres in Figure 4.9c exhibits the two-stage weight loss which were observed in the temperature ranges of 200–360 °C and 260–355 °C in dip coated fibre. For the spin coated fibres the width of the degradation temperature range appears to be smaller. The first stage of degradation is around between 200-240 °C and second stage between 240-335 °C. Figure 4.9d shows the DTG graph with a major peak at 240 °C and a second peak at 330 °C in dip coated fibre. For the spin coated fibres the first peak appears to shift from 224 for the 500 rpm to 190 for the 10000-rpm fibre. The first peak could correspond to a film former as an epoxy resin. The second peak can be assigned to organosilanes with higher thermal stability, which is GPS in our formulation. Petersen et al. [116] used the thermogravimetric analysis-mass spectrometry (TGA-MS) to examine Soxhlet-extracted glass fibre with epoxy compatible sizings and revealed a degradation sequence occurring in three stages. The primary decomposition was observed with a significant mass loss peaking at 372 °C. Subsequent to this, a secondary peak manifested at 409 °C, interpreted as a shoulder peak, and a final peak was discerned at 551 °C. The initial peak is believed to represent the disintegration of the polymeric film former, which could either be polyurethane or an uncured form of epoxy resin. The shoulder peak suggested the breakdown of a film former as well, possibly due to the presence of a variety of polymeric elements within the sizing mixture. The last peak indicated the decomposition of organosilanes, which are known to possess a thermal stability. The study noted that the mass loss data closely aligned with the distribution of sizing components.

Figure 4.12 compares TGA and DTG results for both industrial sized fibre IS and fibre S1A spin coated at 10000 rpm. Both these fibre samples exhibit a single major weight loss event in the temperature range 200–300 °C, and the graphs follow a very similar pattern. The peak in the differential mass change data occurs at 225 °C, signifying the maximum rate of weight change. Thomason et al reported similar TGA degradation results from a range of industrial coated PP compatible glass fibre products and suggested that the majority of the weight loss between 200-300 °C appears to be due to degradation of the MAPP film former and the aminosilane coupling agent [83].

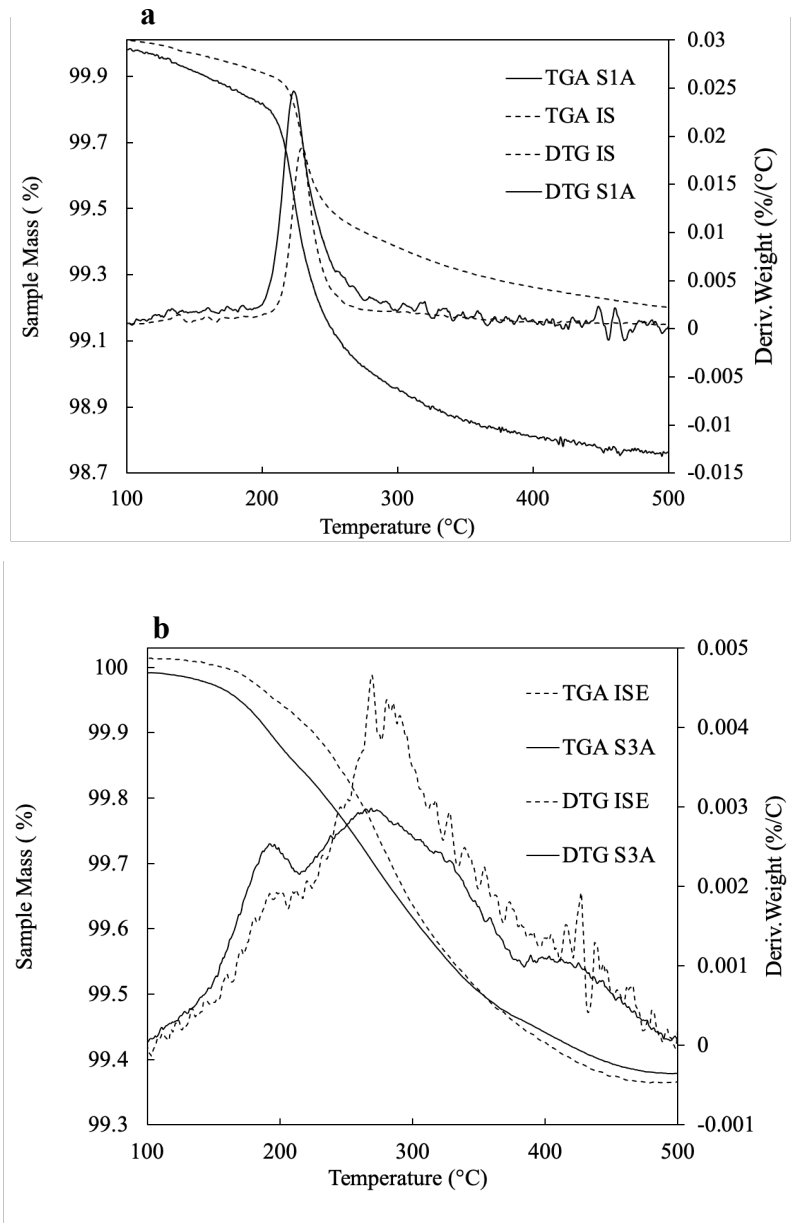

Figure 4.12. a) Comparison of TGA and DGT graphs of the IS and spin coated S1A at 10000 rpm. b) Comparison of TGA and DTG graphs of the ISE and spin coated S3A (4000 rpm).

Given that the exact formulation of the sizing on IS is unknown and that the exact composition of the film former emulsions used in this work are also unknown due to industrial confidentiality, then the similarity in these results is notable. Thomason has published a review of industrial sizing formulation patents and has also noted that the same two principal constituents of most PP compatible sizings (from different fibre manufacturers) does consistently appear to be MAPP and APS [1]. The same comparison (Figure 4.10b) was made with the epoxy compatible sized fibres, TGA of the in-house sized epoxy-compatible glass fibres (S3A) indicated that the majority of the mass loss occurred in the 200–400 °C range and was attributable to the decomposition of the polymeric film former component of the sizing. It

was noted that 4000 rpm spinning rotation speed could give almost 0.5 LOI%, which could be compared with the industrial coated fibre. As for the TGA and DTG graphs of the industrial and in house sized fibre with epoxy compatible sizing i.e., ISE and S3A. The graph in Fig. 4.10b exhibits a major peak at 270 °C with a shoulder peak at 190 °C and a peak at 415 °C. The first peak could correspond to a film former as epoxy resin. The shoulder peak can be of a similar polymer type since film formers are often a mixture of different polymers. The third peak can be assigned to organosilanes with higher thermal stability.

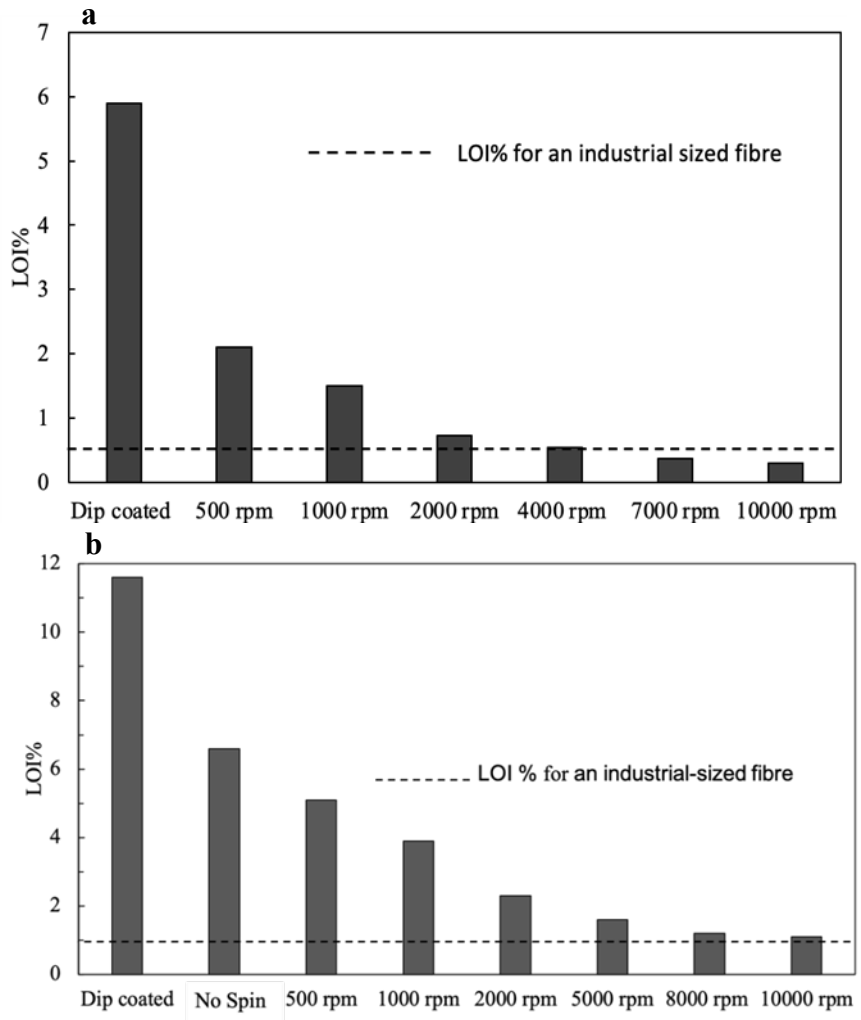

Figure 4.13. Comparison of average LOI% of a) PP compatible industrial sized fibre (IS), spin coated (S1A). b) Epoxy compatible industrial sized fibre (ISE) and spin coated (S3A).

Figure 4.13 summarises the TGA obtained LOI values for both systems i.e., PP and epoxy compatible sized fibres that were spin coated at different speeds along with values for the dip coated fibres and the industrial sized fibres IS and ISE respectively. The LOI% of PP compatible industrial sized fibre is 0.8%, while for epoxy compatible sizing, it is 0.5%, which aligns with the reported LOI% range for commercial sized fibres between 0.5%-1.5% [1].

Depending on the fibre's application, the sizing and LOI% are adjusted accordingly. One possible reason for the higher LOI% in PP compatible sizing could be the less reactive nature of PP compared to epoxy, requiring more sizing components, especially silane, in the formulation. In both systems the spin coated fibres exhibit a much lower LOI compared with the dip coated fibres, and the LOI approaches that of the industry sized fibres when the rotation speed is increased[4]. As shown in Figure 4.11b, in epoxy compatible sizing, it is even possible to achieve lower LOI% than 0.5%, for example the 10000-rpm speed gave the LOI% value of almost 0.3%.

In order to evaluate the consistency of the sizing along the fibre bundle produced using the spin coating method, three different 7 mm lengths of fibre were sampled (approximately the middle and both ends) from a 10 cm fibre bundle of S1A spin coated at 10000 rpm and S3A spin coated at 4000 rpm and tested using TGA. Figure 4.14 shows the TGA and DTG of the ends and middle of the S1A fibre bundle. The curves for all three sample appear very similar. The sizing material on all samples exhibit a similar thermal degradation process within the temperature range of 200-300 °C. The final LOI of all three samples can also be considered equal within acceptable experimental error.

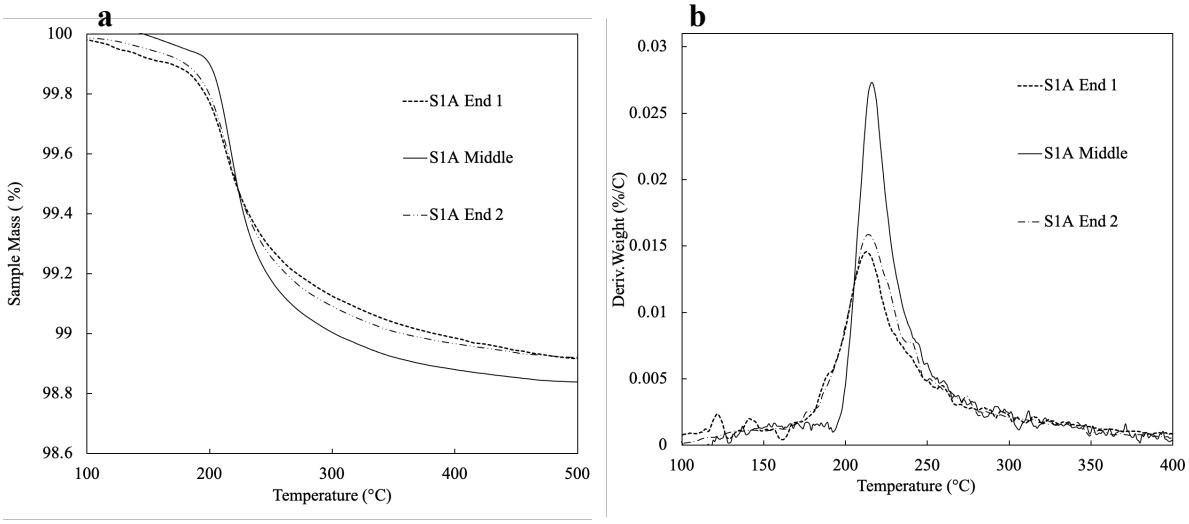

Figure 4.14. Comparison of TGA analysis different parts of spin coated S1A at 10000 rpm a) TGA and LOI%, b) DGT

The same evaluation of consistency of the sizing along the fibre bundle was done with the S3A spin coated at 4000 rpm (see Figure 4.15). The curves for all three sample appear very similar. The sizing material on all samples exhibit a similar thermal degradation process within the temperature range of 190-380 °C. The final LOI of all three samples can also be considered equal within acceptable experimental error. Therefore, the spin coating method appears to

produce a relatively consistent sizing layer along the full length of the 10 cm fibre bundle sample. Consequently, selecting single fibre samples for microbond testing from different points on the spin-coated bundle should not adversely affect the experimental variability in the obtained IFSS results.

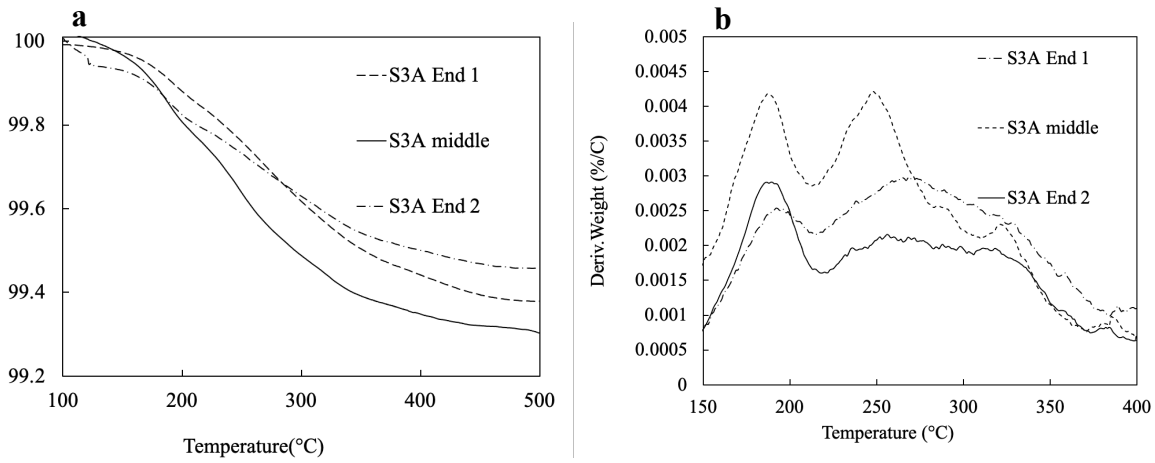

Figure 4.15. Comparison of TGA analysis different parts of spin coated S3A at 4000 rpm a) TGA and LOI%, b) DTG.

Figure 4.16, compares the TGA and DTG graphs of S1A dip coated with 1% solids, S1A spin coated with 10% solids (10000 rpm) and the commercially sized fibre sample IS. The LOI of the 1 wt% dip coated fibre is around 2.3%, which is now significantly less than for the 10 wt% dip coated fibre which had an LOI of 11.2% in Figure 4.13a. However, even by diluting the sizing solids concentration by a factor of 10 it was still not possible to reach the lower LOI levels which are typical of industrial sized fibres (e.g., 0.8% for IS). On the other hand, the spin coated S1A at 10000 rpm exhibits an LOI much closer to the industrial sized IS fibres and also exhibits almost similar degradation behaviour in the temperature range from 200 °C to 300 °C in both the TGA and DTG plots.

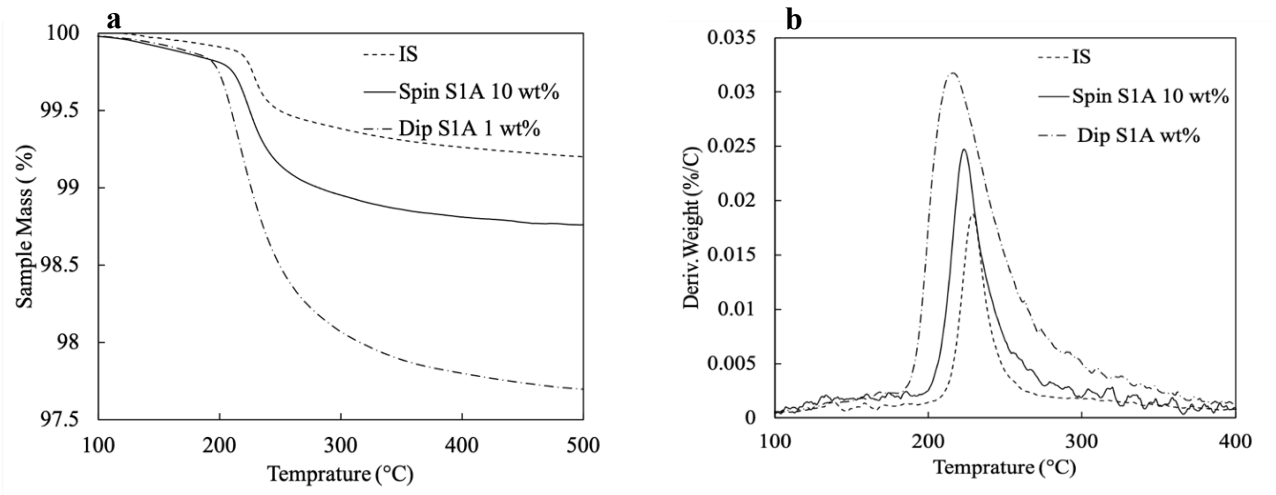

Figure 4.16. Comparison of TGA results of S1A (1%) dip coated, S1A (10%) spin coated and IS a) TGA weight change b) DGT differential weight change.

These results show that lowering the concentration of sizing in the dip coated fibre bundle, in an attempt to approach a typical industrial value of LOI, results in a higher LOI and a larger temperature range as evidenced by the different thermal degradation pattern in Figure 4.14 Hence even though dip coating using a very low solids concentration sizing does result in a sample LOI approaching that of the industrial level, the properties of that dip coated sizing layer are significantly different from the sizing layer on an industrial sized sample. On the other hand, a sample which has been spin coated using a sizing with a normal solid appears to perform in a TGA experiment in a very similar manner to the industrial sized sample.

Table 4.2 summarizes the LOI values and calculated sizing layer thickness (using equation 4.2) which are average of three measurements. From the data presented in Table 4.2 it can be seen that the thickness of the sizing layer varies from hundreds of nanometres for the spin coated sizes to micrometres for the dip coated one. Comparing LOI between dip coated S1A with 10 wt% solids and 1 wt% solids sizing and spin coated S1A with 10 wt% solids sizing in Figure 10a, it is evident that the LOI of spin coated S1A samples are all lower than the dip coated sample and approaches the LOI value of the industrial sized fibre at higher spin speeds.

Table 4.2. LOI% and sizing layer thickness.

	LOI%				
Fibre	**1**	**2**	**3**	**Mean**	**Sizing thickness (nm)**
Dip coated	11.3	12	10.5	11.2	1280
No spin	6.5	6.2	5.8	6.1	685
500 rpm	4.9	4.9	6.8	5.5	618
1000 rpm	3.8	3.5	2.9	3.4	376
2000 rpm	2.2	3.4	2.6	2.7	302
5000 rpm	1.5	1.4	1.4	1.4	156
8000 rpm	1.1	1.1	1.2	1.15	125
10000 rpm	1	1.2	1	1.0	116
IS	0.9	0.8	0.7	0.8	86

4.4.2. SEM observation

Figure 4.17 presents SEM images of the PP-compatible sized fibre bundles. The effects on the sizing structure on the fibre surface of the different methods of dip coating, spin coating, and industrial coating are compared. In Figure 4.17a, the fibre bundle is heavily covered with sizing, rendering the fibres almost invisible as they are fully coated with a high thickness of PP sizings. More fibres are visible in the dip coated bundle with 1 wt% sizing solid (Figure 4.15b) than in the 10 wt%, which is related to the lower thickness of the 1 wt% sizing. However, there is still a thick sizing coverage visible on some parts of the bundle. The micrographs in Figures 4.15c and 4.15d show that the spin coated, and industrial-sized fibre bundles exhibit a similar sizing distribution pattern, with less sizing coverage in the bundle and little sign of any thick areas of sizing connecting the fibres.

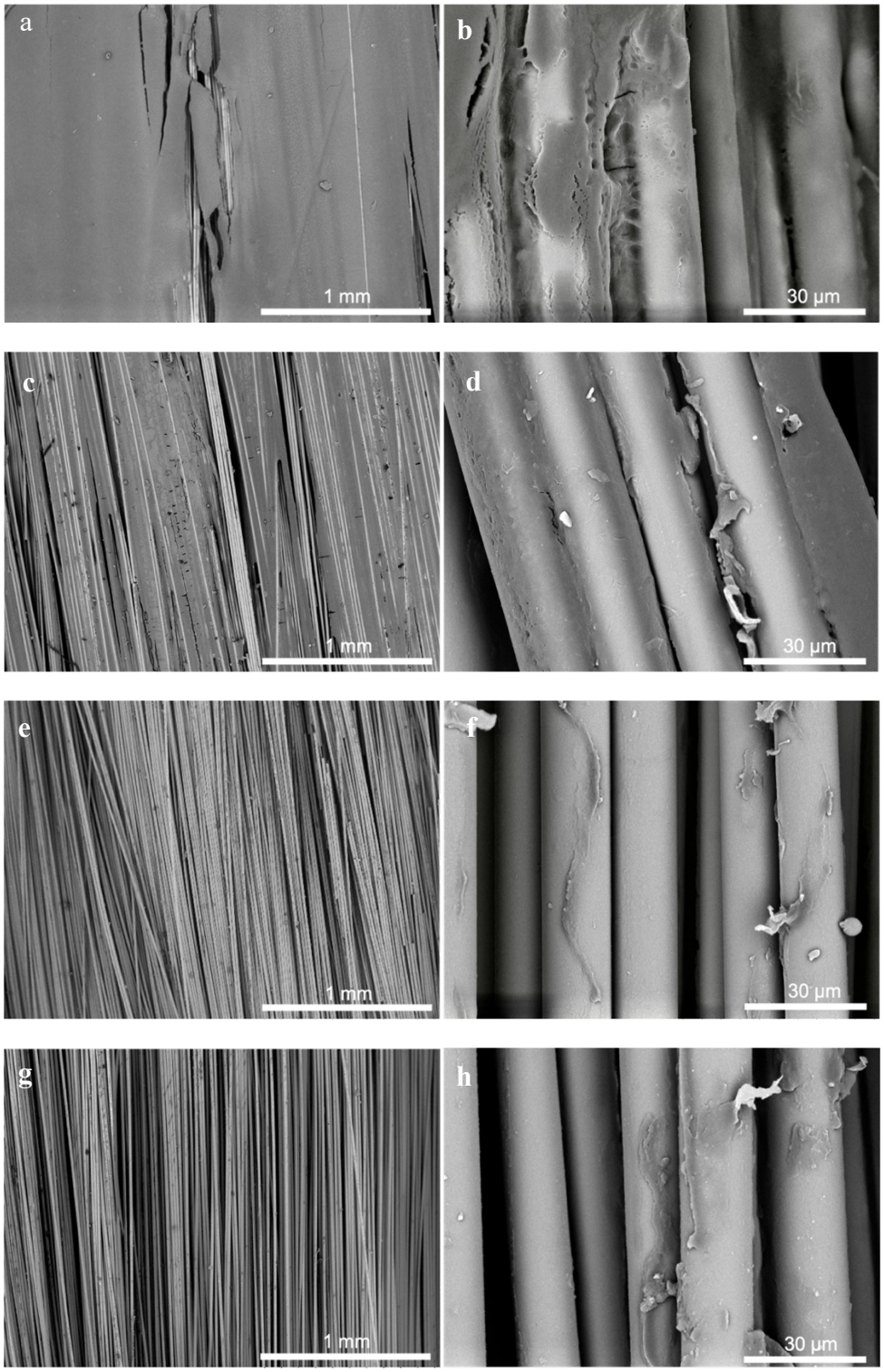

Figure 4.17. SEM images of fibre bundles i.e., a,b) Dip coated S1A 10 wt%, c,d) Dip coated S1A 1wt%, e,f Spin coated S1A 10 wt%, and g,h) Industrial-sized

Figure 4.18 showcases SEM images that compare the structures and distribution patterns of PP-compatible sizing applied to microscope slides via different methods: dip coating and spin coating at 10,000 rpm. The dip coated slides exhibit a coverage of sizing (still gaps can be seen

between the dried sizing particles in some areas), with a noticeably higher distribution of particles on the surface, in contrast to the more thinly coated spin coated slides.

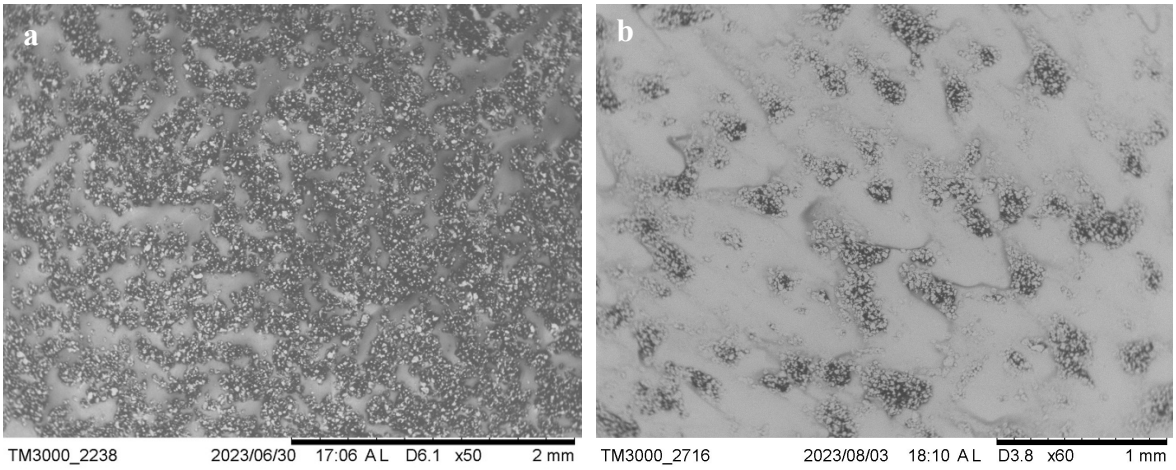

Figure 4.18. SEM images of microscope slide, a) Dip coated S1A 10 wt%, b) Spin coated (10000rpm) S1A 10 wt%

Figure 4.19 provides a detailed examination of the particle distribution across various sections of a slide that has undergone spin coating, specifically focusing on the middle and both ends of the slide. This analysis is crucial to comprehend how sizing deposition varies across different areas post-spin coating, which might have a closer distribution than a dip coating technique on a fibre bundle. Observations indicate that the variance in particle distribution across different areas of the slide is minimal.

This relatively uniform distribution can be attributed to the centrifugal forces at play during spin coating, which tend to spread the sizing evenly across the surface. However, factors such as the viscosity of the sizing, spin speed, and drying time can influence the final distribution.

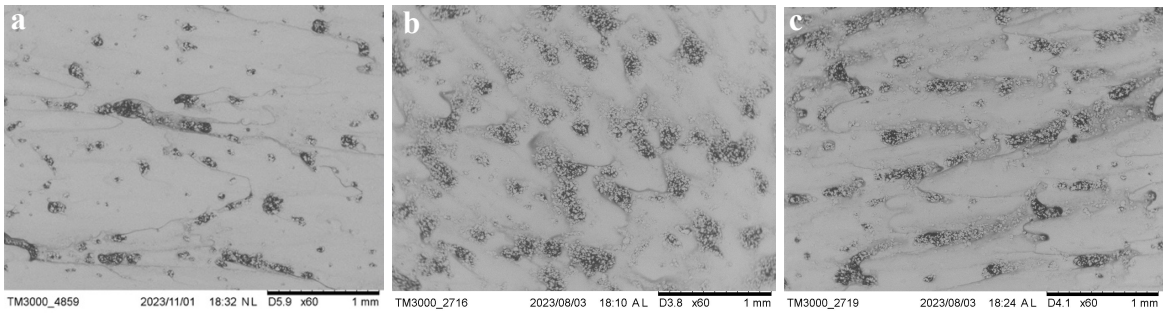

Figure 4.19. SEM images of different part of the spin coated 10000 rpm microscope slide with S1A 10% wt% sizing, a) End1 b) Middle c) End2

4.4.3. AFM results

AFM images were captured to analyse the surface topography of fibres treated with different coating processes: BF, IS and fibres that were dip coated and spin coated (S1A) at a velocity of 10,000 rpm. We measured the average surface root mean square (RMS), or R_q, to evaluate roughness. Figure 4.20 presents a comparison of the surface textures of these fibres. The RMS roughness of the BF was found to be around 7.1 nm, indicating a smoother surface relative to the others.

Upon examining the dip coated fibres, it was apparent that there was a significant accumulation of sizing material, forming a thicker, more compliant layer on the surface, which may account for the increased roughness measurements. This cushion-like layer, while increasing the RMS value to approximately 23.6 nm, suggests a thicker layer of sizing agent was deposited during the dip-coating process. However, it was observed that both the IS and spin coated fibres exhibited higher roughness compared to the dip coated fibres, with RMS values of approximately 25.8 nm for IS fibres and 25.3 nm for spin coated fibres.

These higher values suggest that the processes used for IS and spin coated fibres, while more precise, resulted in a surface that retains more particulate matter, increasing the roughness. This observation is consistent with the SEM analyses, which showed smaller particles present on the surfaces of the IS and spin coated fibres, yet contributing to a higher overall roughness due to the nature of the coating process.

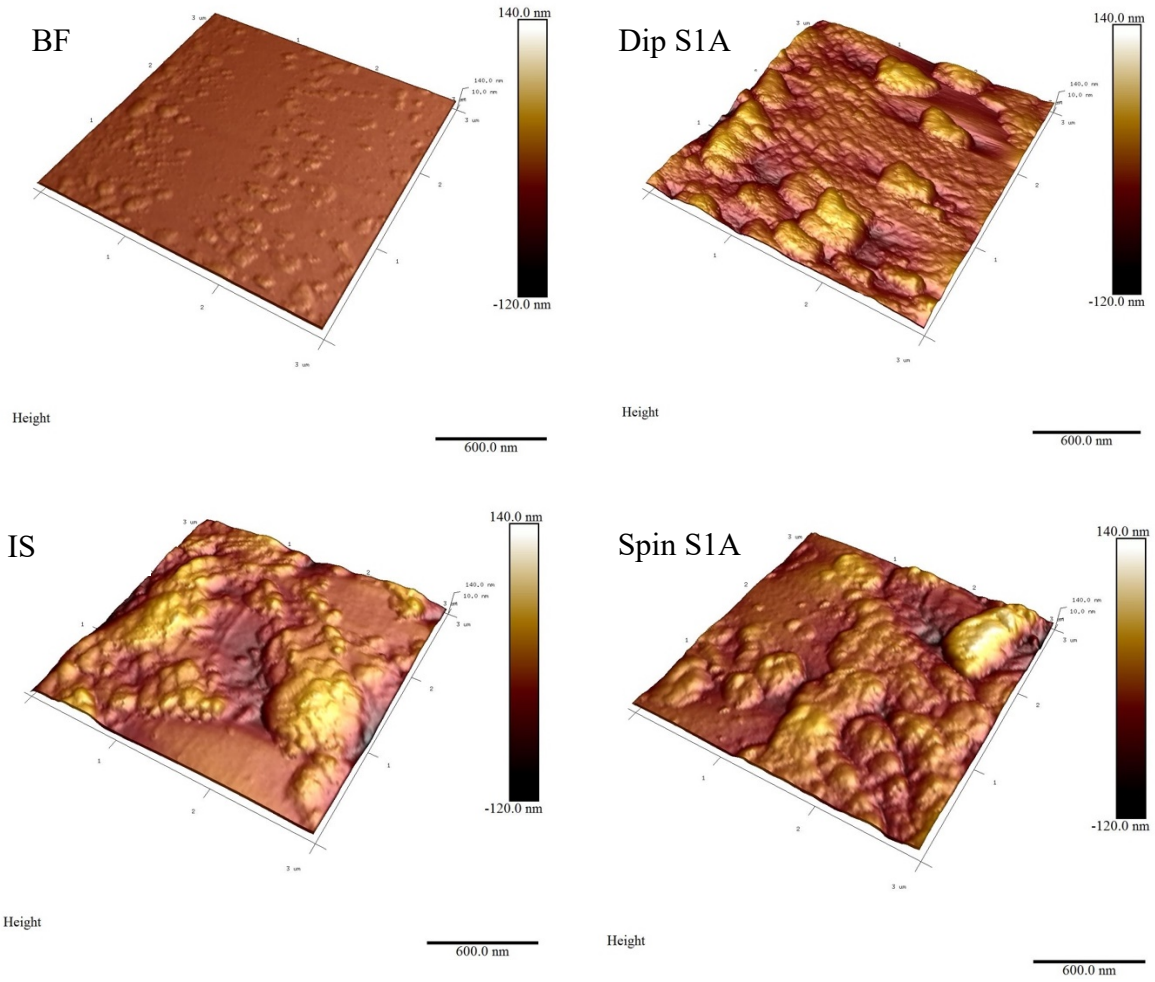

Figure 4.20. AFM images of BF, IS, dip and spin coated S1A.

4.4.4. Microbond test results

Given the fact that fibre sizing plays a significant role in determining the level of apparent adhesion in composites, microbond tests were performed to provide a direct measure of the IFSS between the sized glass fibres and the thermoplastic matrices of HomoPP and MAPP. The effect of sizing concentration on IFSS in the dip coated fibres (S1A) was evaluated for 1% and 10 wt% sizing, and the results are compared with the spin coated S1A fibres with 10 wt% sizing in Figure 4.21. The data shows that the sizing concentration change influenced the IFSS values differently in the different matrix systems. When examining the HomoPP systems, it is evident that reducing the sizing concentration to 1 wt% resulted in lower values of apparent IFSS. The spin coated S1A (10 wt%) fibres demonstrated a slightly higher value of apparent IFSS compared to the dip coated fibres S1A at 1 wt%, with a 95% confidence limit. Similarly, in the MAPP system, the spin coated S1A (10 wt%) fibres and the dip coated S1A fibres at 1 wt% exhibited a similar trend. However, there was no statistically significant difference

between the dip coated S1A fibres (1 wt%) and the spin coated S1A fibres (10 wt%) in this case.

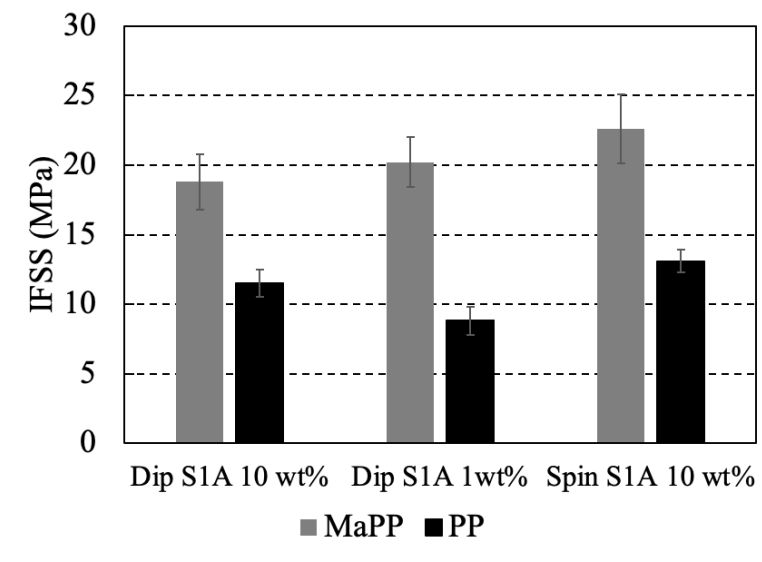

Figure 4.21. IFSS results for the dip coated fibres with varying sizing concentrations (10%, 1%) and the spin coated fibres (10%).

The IFSS results for BF, S1A dip and spin coated and IS are shown in Figure 4.22 In all the MAPP matrix systems, excluding S2A, it was observed that spin coated fibres exhibited a relatively higher average IFSS compared to the dip coated samples. At a 95% confidence level, no significant difference was found between the IFSS of spin coated fibres and IS, which had an IFSS value of 21.3 MPa.

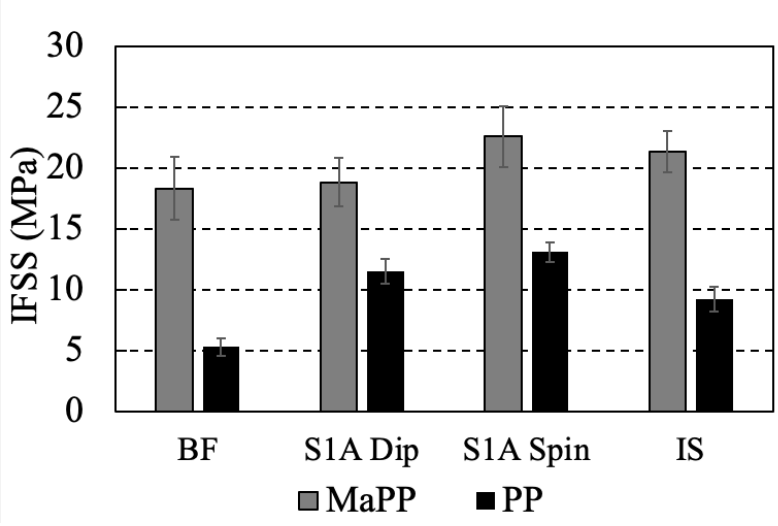

Figure 4.22. IFSS results for the dip coated, spin coated and Industrial PP sizing compatible coated fibre.

When analysing the IFSS results of the PP matrix systems statistically, it was noted that spin coated S1A displayed a significantly (at 95% confidence level) higher IFSS compared to dip

coated S1A. The IFSS value for IS, approximately 10.5 MPa, was closer to the IFSS of dip coated S1A and lower than that of spin coated fibres. The IFSS improvement in some systems might be due to the decrease in the thickness of the sizing layer. This aligns with previously published research [17], which found that in the case of a thin sizing layer, a few random lumps of matrix on the treated fibre surface increase friction, leading to higher IFSS. Conversely, when the sizing layer is thicker, it acts as a cushion around the matrix lumps on the fibre, which reduces the frictional stresses and lowers the IFSS. The thicker sizing layer absorbs more of the mechanical interaction between the fibre and matrix, preventing direct contact that would otherwise enhance interfacial bonding through friction, thus resulting in decreased adhesion strength.

Figure 4.23 presents the IFSS results for the epoxy resin systems, showing a trend similar to that observed in the previous PP system. Comparing the IFSS values of the sized fibres with BF having a value of 43.6 MPa, dip coating the fibres did not significantly improve the IFSS value, with a measured value of 45.46 MPa. In contrast, there was a significant difference between the IFSS values of BF and both spin-coated S3A and ISE fibres. The results indicate a significant difference between the IFSS values of dip coated S3A (45.46 MPa) and spin coated S3A (53.5 MPa). However, the IFSS value for spin coated S3A (53.5 MPa) is comparable to that of ISE (55.4 MPa), which is not statistically significant.

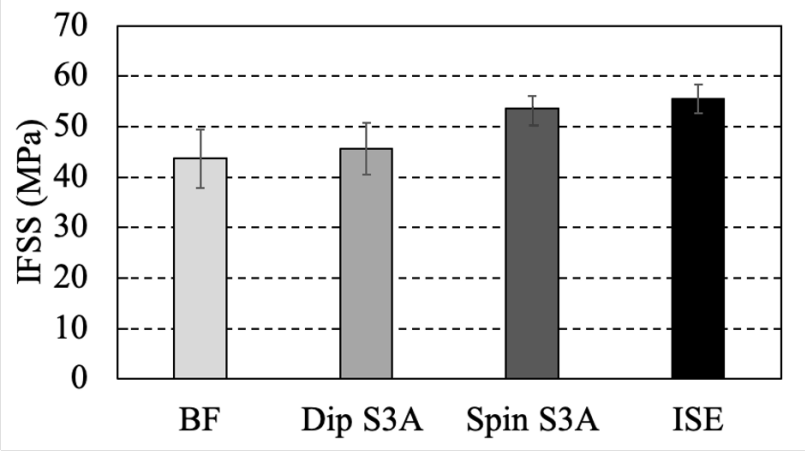

Figure 4.23. IFSS results for the dip coated, spin coated and Industrial epoxy compatible sized fibre.

4.5. Conclusions

The experimental evidence gathered through the various mentioned analyses paints a clear picture of the advantages of spin coating over dip coating. The ability to precisely control the thickness and uniformity of the sizing layer with spin coating leads to an optimized sizing layer, which is crucial for the adhesion between fibre and matrix and final mechanical performance of composites. The research presented in this chapter addresses the challenges posed by the lack of detailed information on commercial sizings and the lack of suitable laboratory-scale methods that emulate industrial processes. The spin coating process, with its ability to mimic the dynamic conditions of industrial sizing applications, has shown to produce fibres with comparable interfacial properties to those sized industrially. This indicates a promising path forward for researchers and manufacturers in the pursuit of high-quality composite materials.

The chapter concludes the need for improved laboratory-scale sizing methods for replicating the industrial sizing condition. The novel findings presented here lay the groundwork for future innovations in development of glass fibre sizing for better representation of industrial sized fibres. This improvement could lead to better understanding of the sizing process and therefore composites with superior performance characteristics.

CHAPTER 5: CHARACTERIZATION AND ADHESION PERFORMANCE OF SILANE-SIZED GLASS FIBRES IN THERMOPLASTIC COMPOSITES

5.1. Introduction

As described in chapter 2, sizing is applied to bare glass fibres in order to improve their adhesion properties and to protect the fibres from damage. Sizing is well recognised as a key component in determining the effectiveness of the reinforcements in composites. In addition to functioning as an essential processing aid during fibre and composite manufacturing, sizing is a critical component in the formation and properties of the fibre/matrix interface. Accordingly, any investigation of the interfacial properties must involve an examination of the contribution of sizing. Optimisation of the stress-transfer capabilities of the interface is well recognised as being essential in achieving the desired performance in composite materials. Silane coupling agents, with their unique ability to bond dissimilar materials, are pivotal in improving the mechanical strength and environmental resistance of composite materials [117]. A substantial portion of the sizing formulation in patents, reviewed by Thomason [1], involved one of the three commonly used silanes: APS, GPS and MPS. APS is the most prevalent, frequently cited in the patents of leading glass fibre manufacturers and widely accepted as a coupling agent for sizings compatible with thermoplastics. It is often utilized as a secondary agent in polyester-compatible sizings and is increasingly being incorporated into new formulations for epoxy-compatible sizings. MPS is predominantly used for polyester-compatible sizings, while GPS is favoured for epoxy and multi-compatible sizings. This highlights that, despite the vast array of organosilane molecules available, the glass fibre industry's sizing formulations rely heavily on a narrow selection of silanes, i.e. APS, GPS and MPS. That’s why in this chapter these three silanes are characterised, with the special focus on APS. The focus on APS is attributed to its enhanced compatibility with thermoplastic matrices [4]. This compatibility could arise from the presence of the amine group in APS, which could react with reactive groups in matrix.

This study conducts an in-depth analysis on the effects of different silane coupling agents, APS, GPS and MPS on the IFSS of glass fibre thermoplastic composites. The microbond test was used to measure the IFSS between the glass fibres and various thermoplastics, including PP, MAPP, PA6, and PBT. Furthermore, this research explores the chemistry behind the silane coupling agents and their interaction with the thermoplastic polymers. While it is understood

that these agents form chemical bonds with thermoset polymers, the nature of their interaction with these high molecular weight thermoplastics is less clear in the literature and it is examined in this chapter. Additionally, the research aims to address the gap in knowledge regarding the influence of the pH of silane solutions on the quality of fibre/matrix adhesion. With APS as a case study, this investigation probes into how its concentration and pH adjustment during the hydrolysis and condensation steps influences the silane effectiveness, an area that has been underexplored despite its practical relevance in the sizing process. The findings of this chapter are expected to offer a deeper understanding of the effects of silane coupling agents on interfacial properties of fibre/thermoplastic matrices. This can help to optimise the key parameters to enhance the performance of glass fibre-reinforced thermoplastics.

5.2. Literature review:

5.2.1. Silane coupling agent and its role in composite material

The pivotal role of silane coupling agents in enhancing the interfacial bond between glass fibres and polymer matrices has been extensively documented. Plueddemann [117] pioneered the understanding of silane agents, articulating their dual functionality. [X-Si $(OR)_3$] is the general structure of silane coupling agents, where the organofunctional group 'X' reacts with the polymer matrix while the alkoxy group 'OR' form siloxane bonds with the glass fibre surface. Ishida [118] carried an expansive overview of the molecular and microstructure aspects of silane coupling agents, providing valuable insights into silane and aminosilane chemistry.

5.2.2. Adhesion between glass fibre and matrix

The critical role of the fibre/matrix interface in influencing the mechanical characteristics of composite materials is well established [119]. Research efforts have extensively analysed how glass fibres interact with polymer matrices. Macromechanical and micromechanical approaches are employed to assess the stress-transfer in composites. Macromechanical testing, encompassing interlaminar and short beam shear tests, assesses bulk composite properties but may not precisely determine fibre/matrix interactions. Micromechanical testing, including techniques like the microbond test, the fragmentation test, the indentation test, and the push-out test, targets these interactions, specifically measuring IFSS. This microscopic focus is crucial for a granular understanding of composite behaviour, revealing how changes at the interface affect overall strength. These methods are cost-effective and less material-intensive

[120], making them suitable for sizing development and process parameter assessment, allowing for preliminary optimizations before scaling up.

In the subsequent sections, the thesis elaborates on different micromechanical methods utilised in investigation of micromechanical properties and characterization of the interphase between glass fibre and matrix. Additionally, the advantages and disadvantages of these methods are discussed.

5.2.2.1. The fragmentation test

The single-fibre fragmentation test is based on embedding a fibre within a matrix and carrying tensile test for determining IFSS. Moulded in a silicone mould, the matrix's ductility is crucial for energy absorption during fibre breakage. Observations can be made under polarized light if the matrix is transparent, allowing visualization of fibre debonding. The critical fibre length, found when fibres can no longer fragment, is used to calculate IFSS [40, 41]. Figure 5.1 presents a simple illustration of the test. This method provides extensive data and replicates composite behaviour; however, its limitations include the matrix's strain capacity and oversimplified stress assumptions. Dai and Piggott [121], and others criticized the method for its unrealistic extrapolation of fibre strength and assumptions about constant interfacial stress. Similarly, Nairn et al. [122] suggested that assuming IFSS was constant was simply unrealistic for many interfaces. Therefore, they introduced a three-dimensional axisymmetric analysis of the single-fibre fragmentation test using Bessel- Fourier series stress functions. Tripathi and Jones [123] highlighted the lack of a data reduction methods for the interfacial factors, that can be correlated to changes in the fibre surface chemistry.

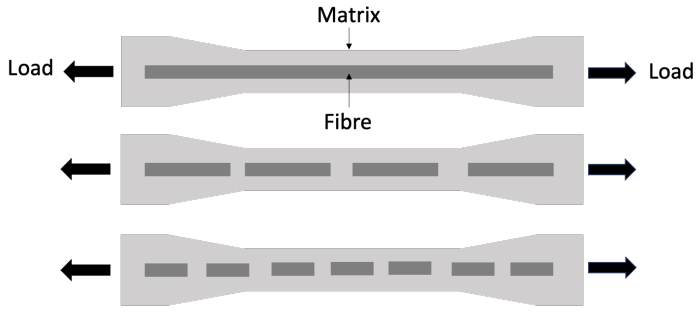

Figure 5.1. Single-fibre fragmentation test.

5.2.2.2. The single-fibre pull-out test

The single fibre pull-out test is a foundational technique for interfacial strength assessment, originating from early interfacial testing methods [124]. This test partially embeds a single

fibre in a liquid resin, setting it perpendicular to the resin surface before it cures in thermoset resins[11], whereas in thermoplastics a single fibre embeds in between two thermoplastic films. As shown in Figure 5.2, the fibre is pulled from the cured matrix using a tensile test, and it is assumed that the force recorded reflects a uniform shear force across the interface

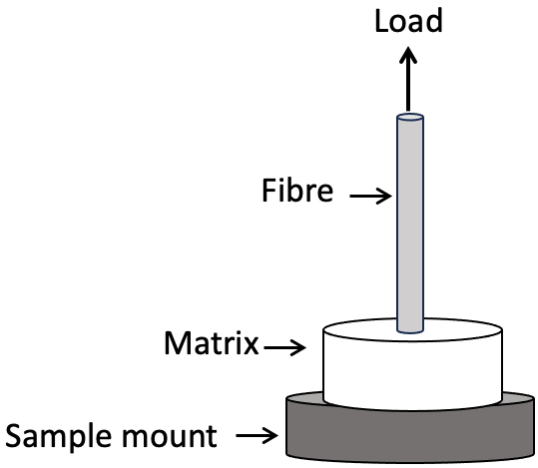

Figure 5.2. Single-fibre pull-out test.

However, this method has a significant limitation when applied to fibres commonly used in composite materials like carbon, glass, or aramid. If the pull-out force exceeds the fibre's tensile strength, the fibre may break before debonding, making the measurement of interfacial strength impossible. The test's effectiveness is further constrained by the meniscus formed when fibres are partially immersed. If the matrix isn't sufficiently dense, the meniscus height can reach up to 1 mm, complicating the maintenance of the necessary short embedded lengths. Moreover, utilizing thin fibres demands an extremely thin matrix layer, around 0.05 mm, to prevent premature fibre breakage. Despite these challenges, under optimal conditions, the pull-out test can yield valuable data on interfacial yielding stress and work of fracture, as observed by Piggott and Xiong [125] without needing to account for friction.

5.2.2.3. The indentation test

The indentation test [90], [96], is a contemporary technique for assessing IFSS. This test uses an actual composite specimen [96], contrary to its designation as a single-fibre method. It begins by sectioning a unidirectional composite perpendicular to the fibre orientation, followed by careful polishing. The prepared sample is then placed under a specialized optical microscope equipped with a precision microprobe. This probe, cantered over an individual fibre, applies a

compressive force until the fibre debonds from the matrix at the surface, allowing for the calculation of interfacial stresses upon failure.

Figure 5.3, illustrates the setup for the indentation test [90]. This method's strengths lie in its ability to perform in-situ measurements and evaluate the interface within real sample conditions, providing rapid, automated data collection conducive to industrial application and yielding multiple data points. It offers a more accurate simulation of in-service conditions, accounting for thermal stresses and the impact of adjacent fibres.

However, the indentation test has limitations: the failure modes are not visually traceable, surface preparation can introduce damage, therefore, the assumptions made during IFSS calculation may not be valid. Moreover, certain fibre types may be susceptible to crushing under the test conditions. A variant of this test, the single-fibre push-out test, uses a thinner composite section, in the range of 20–40 µm [126, 127]. The principal distinction lies in the fibre being completely pushed out rather than merely indented. Employing a microprobe with a tip diameter of about 5 µm, the IFSS is calculated based on the force required to dislodge the fibre divided by the bond area.

Both tests, the indentation and push-out, provide valuable insights into the composite's performance by more closely mirroring real-world conditions. They allow for the exploration of fatigue and environmental effects on the material [128], despite the complexity of sample preparation and the influence of neighbouring fibres on stress calculations.]

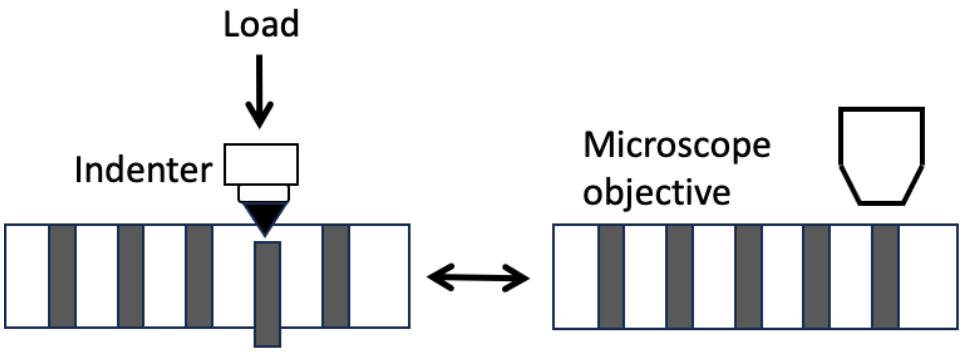

Figure 5.3. Schematic diagram of the indentation test.

5.2.2.4. The microbond test

The microbond test, refined since its inception by Miller et al. [48], serves to measure the interfacial strength between fibre and matrix. The setup involves adhering a resin microdroplet

to a single fibre; the droplet is then sheared off, and the force required to debond the fibre is measured. This process, demonstrated in Figure 5.4, is more straightforward than producing resin blocks for pull-out tests, allowing for the use of microdroplets ranging from 40 to 100 μm in diameter [90].

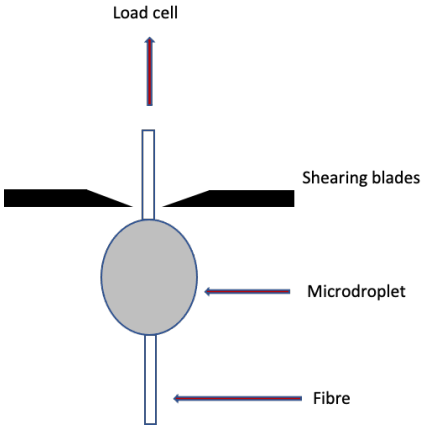

Figure 5.4. Schematic diagram of the microbond test.

The microbond test's advantage lies in its precision in measuring the debonding force and its versatility in testing various fibre and matrix combinations. However, this method's precision can be compromised by the meniscus effect on the polymer droplet, which impacts the stress distribution along the embedded fibre length. This uneven distribution can lead to inaccuracies in measuring IFSS. Afrizal et al. [129] studied the impact of the meniscus effect on fibre/matrix interactions by evaluating the influence of variations in the meniscus angle on the maximum von Mises stress and IFSS (interfacial shear strength) in a typical fibre-epoxy matrix, using the finite element method. The simulation results revealed differences in maximum stress across each model, while the IFSS values remained largely unaffected by the variations in the meniscus angle. This suggests that the meniscus angle significantly influences the maximum von Mises stress, but has a minimal effect on the IFSS between the fibre and epoxy matrix. Figure 5.5 illustrates an example of how different meniscus angles affect stress distribution across the fibre.

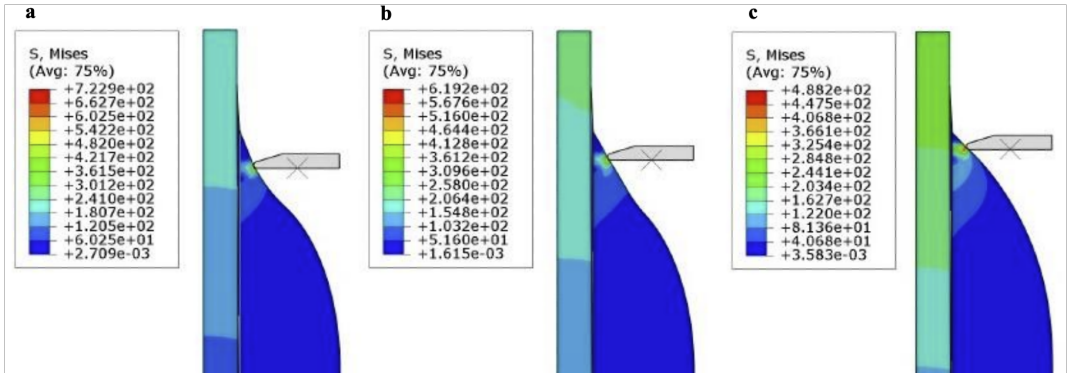

Figure 5.5 Illustration of how different meniscus angles affect stress distribution across the fibre [129].

To ensure accurate results, it is crucial that the fibre does not fracture before the debonding event occurs. This requires maintaining an embedded length in the range of approximately 0.05 to 1.0 mm. This range was established through trial and error experiment and typically varied depending on type of matrix and diameter of fibre [69]. A longer embedded length can result in premature fibre failure due to excessive stress concentration at the ends, while too short a length can lead to insufficient load transfer, compromising the accuracy of the test. Additionally, ensuring an optimal embedded length helps in distributing the stress more evenly along the fibre/matrix interface, which reduces the risk of localized failure and allows a better assessment of the true bonding properties between the fibre and matrix. The other issue relates to processing conditions due to scaling effects; while the matrix cures or processes effectively at the plaque level, it may not necessarily cure or process properly at the microbond level. While the microdroplet's small size can make observing the failure process challenging, adjustments to blade positioning and droplet handling can mitigate these issues. The microbond test has evolved to include variations like fixed or movable shearing blades and different loading configurations. This test has been extensively applied across fibre types such as glass [130], carbon [11], aramid [126], and various polymers like epoxy [126], polyester [106], PP [26]. It has been proven valuable in material science research, praised for its simplicity and minimal sample preparation [120]. Despite its limitations, such as potential damage during fibre handling or the influence of the fibre's variable nature along its length, the microbond test remains a critical tool for interface characterization in composites.

5.2.2.5. Micromechanical test selection

Given the drawbacks of various techniques, the microbond method was the chosen micromechanical test for this study. The fragmentation test was ruled out for evaluating the sizings on glass fibres with different matrices, primarily due to the absence of an established data reduction method to link an interfacial parameter with alterations in fibre surface chemistry [123]. Further, concerns about the reliability of Weibull statistical approaches [121], the impractical assumptions in determining IFSS [122], and the stringent compatibility demands for fibre/matrix interfaces emphasized its unsuitability [131]. Other micromechanical tests that involve actual composite components, like indentation and pull-out, were also dismissed because of the costly, laborious nature of producing large-scale composite parts and the intricate sample preparation and polishing they necessitate. Despite the mentioned inherent limitations, the microbond test was considered the most compatible with the diverse fibres and matrices involved in this research.

5.2.3. Silane effect on glass fibre/matrix interphase

The common belief is that the silanes present in the glass fibre sizing undergo condensation and polymerization, resulting in a crosslinked coating on the glass fibre surface. This coating is thought to remain within the composite material, forming an interphase that potentially incorporates certain elements of the matrix [117, 132-134]. It is hypothesized that the capacity of the interphase to transmit stress is affected by the silane's proficiency in establishing bonds with the fibre surface, improving the adhesion of the coated fibre when in contact with liquid or molten resin, and creating connections with the matrix [4]. Previous research efforts have been directed toward characterizing the interphase of silane-sized fibres with various thermoplastic and thermoset matrices as summarised below.

5.2.3.1 Thermoset composites

The reactive groups in silane are known to chemically bond with reactive groups in both the resin and the hardener [135]. Some investigations demonstrated that the use of a silane coupling agent can notably boost the interfacial properties of glass fibre/epoxy composites [48], even without a film former [136-138]. This enhancement is influenced by the concentration [48, 139] and silane type [140, 141]. The most commonly used silanes in thermoset systems, are GPS and APS. The nature of the bond formed is likely to be either covalent or acid-base in nature [1, 135]. Hamada et al. [10] investigated how a silane interphase affects the interfacial

strength in composites made of glass fibre and epoxy. E-glass fibres, once cleaned by heat, underwent a dip-coating process in a mixture of single and combined aminosilanes. To measure the interfacial strength, a specialized single-filament test was employed. From their findings, the researchers deduced that the process of siloxane cross-linking within the silane interphase actually diminished the strength at the interface. This is because the crosslinked structure depresses the penetration of the resin into the interphase and avoid reaction between the resin and silane organofunctional groups. Gomez and Kilgour [142] also assessed the IFSS in epoxy resin samples. Modifications to the silane structure using a two-step combination of liquid-phase oxidation and grafting of silane coupling agent, were found to enhance the infiltration and intertwining of the matrix, observed by AFM images, with the polysiloxane interphase, which in turn elevated the IFSS. Feresenbet et al. [143] The study examined how mixed silane sizings affect the surface morphology of fibres and IFSS between glass fibres and epoxy resin. E-glass fibres provided by Owens Corning, without previous sizing, were treated with a blend of hydrolysed propyltrimethoxysilane (PTMS) and APS. The use of AFM and ellipsometry demonstrated that the sizing films laid down were of multilayer thickness. DRIFT spectroscopy revealed that below a concentration of 45 mmol/L (about 1% by volume), the E-glass fibres were only partly coated with the silane solution. The increased APS content in the sizing formulation led to a greater polarity on the fibre surface, as shown by contact angle tests. Furthermore, the fragmentation tests on single fibres indicated that the IFSS was greater when there was a higher proportion of APS in the sizing mixture. It was concluded by the authors that both the silane type and the silane blend composition in the sizing notably affected the adhesion between the glass fibres and the epoxy matrix.

Modified microbond test results for both silane and air plasma surface treatments by Liu et al. [59] analysed the interphase in vinyl ester composites reinforced with glass, utilizing E-glass fibres that were sized solely with silane. The fibres were obtained from Nitto Boseki Co. as a plain-woven fabric and underwent dip coating in silane solutions prepared in water. Two different silane coupling agents, MPS and GPS, were employed at varying concentrations, with the solutions acidified to a pH of 4.0 using acetic acid. The interface that developed between the glass fibres and the resin matrix was examined through nanoindentation and nano scratch tests. It was noted that higher concentrations of the silane coupling agent led to the formation of a thicker interphase. Gao et al. [12] investigated the effect of fibre surface texture created from silane blends on the strength of the glass fibre/epoxy interface. GPS and tetraethoxysilane (TEOS) were applied to glass fibres in various concentrations and blends. AFM was used to

characterise the fibre surface and interfacial adhesion was determined by microbond testing. The authors reported that IFSS was increased by the application of GPS, attributable to the silane acting as a bridge and facilitating chemical reaction with both the glass fibre and the epoxy/amine matrix resin. Further increases were observed when a blend of the two silanes was used, though interfacial adhesion diminished with increasing TEOS content. Reduced adhesion in these cases was likely due to either insufficient change in fibre surface roughness by the excessive amount of TEOS, or the high molar fraction of TEOS, which formed weak and brittle aggregates that could shear easily. The high concentrations of TEOS can form clusters or aggregates that are structurally fragile. These brittle clusters are prone to breaking or shearing under stress, further weakening the bond between the fibre and matrix.

Olmos et al. [144] research explored the effect of silane-based sizings on the moisture uptake in glass-fibre-reinforced epoxy composites. Commercial E-glass fibres were subjected to a cleaning process at 500 °C for an hour, treated with 2% aminosilane solutions, and subsequently dried at 110 °C for an hour. The study focused on three different silanes, i.e., APS; 3-aminopropylmethyldiethoxysilane and 3-aminopropyldimethylmonoethoxysilane. It was observed that the inclusion of silane treated fibres influenced the water absorption dynamics of the epoxy resin, leading to a reduced mass increase when equilibrium was reached. Equilibrium is reached when the matrix's absorption and diffusion of water balance out, with the fibre silane interaction influencing the overall moisture dynamics in the composite. This hinted at the possibility that the glass fibre surface might alter the epoxy matrix's structure compared to the unreinforced polymer. The quantity of water absorbed at the interface was found to be dependent on the specific silane sizing applied to the glass fibre, with a lower uptake of water corresponding to silanes of lesser functionality. The silane functionality plays a key role in moisture absorption dynamics. Silanes with more reactive groups (greater functionality) are likely to form stronger and denser chemical bonds at the fibre surface and fibre/matrix interface, thereby creating a more hydrophobic layer that reduces water uptake. In contrast, silanes with lower functionality (fewer reactive groups) may result in weaker or fewer bonds at the interface, allowing for greater water absorption. Sahin et al. [145] investigated tailoring interfaces in glass fibre-reinforced photopolymer composites. Glass fibres were initially desized by a multiple-step cleaning process involving Soxhlet extraction with acetone, processing in a cellulose extraction thimble, and rinsing in an acidic piranha solution and deionised water. Adhesion was adjusted by applying either MPS or a photoactive silane and silanes were selected based on their ability to facilitate covalent bonding of the modified fibre

surface and acrylic matrix during photoinduced curing. Characterisation of the glass fibre/acrylic interface by single-fibre pull-out indicated that apparent IFSS and frictional strength was lowest for unsized fibres, while surface-modified fibres showed improved adhesion. Frictional strength was generally the same for both the silane-treated fibres. Interfacial strength was highest when the photoactive silane was used due to enhanced covalent bonding between the organosilanes and matrix and greater reactivity of phosphorous radicals facilitating improved cross-linking. Interfacial strength was, however, also highly dependent on the degree of curing of acrylic matrix.

5.2.3.2 Thermoplastic composites

When addressing sizings for reinforcing thermoplastic polymers, the dominance of chemical interactions is less clear than thermosets. It has been observed that aminosilanes are mainly utilized in the development of sizings suitable for thermoplastics [146]. Therefore, enhancing the interphase in thermoplastic composites hinges on a better understanding of the role of silanes, especially the aminosilane molecule. This compatibility could arise from the presence of amine groups (-NH2) in APS, which could form hydrogen bonds with polar groups in certain thermoplastics [147]. Additionally, these amine groups could contribute to increased van der Waals interactions between glass fibres and thermoplastics [148]. Some studies were shown that sizing the fibre with silane improves the interfacial properties of thermoplastic composites. Bikiaris et al. [101] studied how silane coupling agents (APS and 3-aminopropyltrimethoxysilane (APTMS), when used with modified PP, affected the adhesion qualities within glass fibre-PP composites. Chopped E-glass fibres from Cristaleria Espanola underwent a process of heat cleaning before receiving a coating of silane solutions. The solutions were prepared in pure alcohol, constituting 10% of the fibre weight, which is not a method commonly aligned with standard glass fibre production techniques. These treated fibres were then utilized in the fabrication of injection-moulded glass fibre-PP composites. The coatings on the fibres were examined with the help of SEM and FTIR analysis. Fibres that were coated with APTMS) showed an enhancement in the composite material's properties in contrast to those coated with APS. Shokoohi and Azar [149] assessed the impact of a silane-only sizing coating on heat-cleaned chopped E-glass fibres from Cam Elyaf and its effect on the structural integrity of injection-moulded composites containing 30% fibre-reinforced Acrylonitrile Butadiene Styrene (ABS). The silanization process utilized three distinct silanes APS, TCVS, and GPS and extended over an unusually lengthy period of 36 hours at a pH of 3.5, with the

silane constituting 0.1% by weight of the glass fibre. It was observed that glass fibres without treatment exhibited suboptimal composite performance, which was notably enhanced by silane application, despite a decrease in notched impact strength across all samples. Among all of the silanes tested, TCVS resulted in the superior enhancement, likely due to improved adhesion between the fibre and matrix. However, the study overlooked the potential impact of silane treatment and the high-temperature treatment of fibres at 500 °C on fibre strength and the subsequent shortening of fibre length within the composites, which could explain the diminished notched impact performance noted in treated fibres.

Lee and Jang [150] reported on the use of a mixed coupling agent system to improve the performance of PP-based composites reinforced with short glass fibre mat. Application of a N-β(N-vinylbenzylaminoethyl)-γ-aminopropyltrimethoxysilane hydrogen chloride (STS) resulted in an increase in flexural strength and modulus and a reduction in impact absorption energy, while the use of a titanate coupling agent isopropyltriisostearoyl titanate (TTS) showed the inverse effect. In a mixed coupling agent system, however, it was possible to improve the impact absorption properties without the corresponding loss in flexural properties. The improvement of the flexural modulus using STS sized fibres was attributed to a reduced void content and improved interfacial strength as evidenced by shorter fragmented lengths compared to unsized fibres. The higher IFSS was in fact responsible for the reduced impact absorption due to the prevention of debonding and fibre pull-out. TTS sized fibres showed fragmented lengths comparable to that of unsized fibres, thus no improvements to interfacial strength were conferred by its application. The loss in IFSS, combined with a lubricating effect of the silane, was responsible for the reduction in flexural properties while increased ease of pull-out conferred greater energy absorption during impact fracture. The long carbon chain present in TTS also diffused into the PP matrix, acting as a plasticiser and creating a micro-ductile interphase region near the glass fibre surface. Fragmented lengths indicated that treatment with a mixed coupling agent resulted in interfacial properties comparable to that of the STS only fibres. In the composite material, however, regions of high and low interfacial strength occurred depending on the presence of either STS or TTS in those regions. Zykaite et al. [151] report that silane sizing did not result in significant changes in IFSS using both basalt and glass fibres with a PP matrix. Hoecker and Karger-Kocsis [152] have, however, reported that IFSS of a glass fibre/PP was increased substantially by the application of a commercial sizing, though matrix modifications were able to produce similar IFSS in unsized fibre samples. Laura et al. [153] analysed how sizings based on silane affected the mechanical attributes of

injection-moulded, rubber-enhanced PA6 composites reinforced with glass fibre. Owens Corning supplied the E-glass fibres, which were then treated with one of five different silanes featuring anhydride, epoxy, or amine groups. These silanes appeared to exert minimal influence on the mechanical performance of the composites in the absence of maleated ethylene-propylene rubber within the polyamide matrix. In contrast, the presence of the rubber toughener was found to significantly impact the mechanical properties, with composites sized with aminosilane displaying the lowest tensile and Izod impact strengths, while those with anhydride silane sizing exhibited the highest values. Yun et al. [154] study provided a concise overview of various silane coupling agents IFSS of glass fibre-reinforced polyamide 6 (PA6) composites, as gauged by the microbond technique. Four distinct coupling agents were administered to heat-cleaned E-glass fibres supplied by Owens Corning (111A rovings). The research presented average IFSS values derived from microbond testing but did not delve into the potential impact of moisture absorption or the notable variability often associated with this method, which could affect the reliability of the findings. Nevertheless, the researchers observed that the interfacial strength in the glass fibre-PA6 composites tended to increase alongside the silane's chemical reactivity. According to their microbond test outcomes, the effectiveness of the coupling agents was assessed in descending order from chloropropyl to methacrylate and epoxide, with both being comparable, followed by the diamine silane, and finally the commercial sizing.

Jenneskens et al. [155] applied NMR and FTIR techniques to unravel the molecular interactions that enhance adhesion in glass-fibre-reinforced polyamide-6 composites through the use of various aminosilane coupling agents. It was deduced that the amine groups on the surface-anchored coupling agents, the carboxylic ends of PA6, and the amide linkages within PA6 all play roles in improving adhesion. The development of a distinctive interphase layer was governed by a synergy of chemical and physical bonds. The researchers noted that achieving a monolayer of aminopropylsilane on the fibres is conducive to enhanced adhesion with PA6. However, Thomason's research [13] indicated that the amount of APS applied to commercial glass fibre products significantly exceeds what would be required for a monolayer coating on the fibres. His computations revealed that there is about 4–12 mg/m2, which translates to roughly 8–24 monolayers of aminosilane, present on the surface of glass fibre reinforcements. Such findings suggest that instead of a simple single layer, there's a more intricate, multi-layered silane interphase existing on these glass fibre surfaces. Noda et al. [156] focused on the interfacial structure and the dynamics of molecules within short glass fibre-reinforced

polyamide (PA66) composites. The composites for this study were injection-moulded using fibres in three different states: without any sizing, with APS sizing at varying concentrations, and with a dispersion of APS-maleic anhydride film former. These fibres were noted to have undergone commercial treatment processes. Subsequently, the glass fibres were extracted from the composites with phenol. Phenol used to dissolve the polymer matrix in the composites, leaving the fibres intact for extraction. and were subject to extensive analytical examination. The findings indicated a robustly bonded PA66 layer to the aminosilane sized glass fibre surface. Additionally, the glass transition temperature (Tg) of the PA66 on the fully treated glass fibre was found to be greater than the Tg of the PA66 matrix, 117 °C vs 47 °C suggesting a limitation on the thermal movement of the polyamide molecules at the interface. The conclusion drawn was that the sizing facilitated a strong interfacial interaction between the glass fibre surface and the PA66 matrix, primarily through the formation of covalent bonds during the creation of the interphase.

5.2.4. Chemical interactions of silanes with thermoplastics

Chemical bonding typically involves direct formation of covalent bonds between fibres and matrix. While chemical bonding is crucial for most thermosetting polymers, it often contributes weakly or insignificantly to fibre/matrix adhesion in thermoplastic composites [157-159]. In thermoplastics, the primary contributors to the fibre/matrix adhesion are weaker van der Waals and London dispersive forces, along with residual stresses at the interface caused by polymer shrinkage during cooling [160-162]. While the chemical interactions of silanes with thermoset polymers are well-characterized, their interactions with thermoplastics are less understood. Park et al. [163] explored this by investigating the reactivity of different functional groups of silanes with thermoplastic matrices. Their work sheds light on the potential for chemical bonding in thermoplastics, albeit with less specificity than in thermosets. The hydrolysis of silane coupling agents is a pH-sensitive process, which is critical for the agent's performance. Studies by Mittal et al. [164] explored the influence of pH on the hydrolysis of APS and found that deviations from the natural pH could affect the silane's ability to form stable bonds with glass fibres. However, the literature lacks comprehensive studies on the effects of pH variations on adhesion quality in thermoplastic composites, indicating an area requiring further research.

5.2.5. Literature conclusion

In summary, the literature provides a solid foundation for understanding the role of silane coupling agents in glass fibre reinforced composites, while also identifying gaps in knowledge that this study aims to address. It is clear that there are fewer studies on the effect of silane on the interphase of different thermoplastic composites compared to thermosets. While aminosilanes are commonly employed in sizings for thermoplastics, the impacts of other silane coupling agents like MPS and GPS were not researched.

There remains a clear need for targeted research on the interplay between silane chemistry, and thermoplastic polymer matrices, and the influence of factors such as pH on the interfacial bonding. The literature also lacks the comprehensive study considering different types of thermoplastics which is covered in this thesis by investigating PP, MAPP, PA6 and PBT matrices.

5.3. Experimental procedure

5.3.1. Materials

Bare (water-sized) and silane-coated E-glass fibres were sourced from larger rovings provided by Sisecam. These fibres were manufactured using a bushing and wound into continuous rovings with a nominal tex of 1400 g/km and an average fibre diameter of 17.0 μm. During the cooling phase of production, bare fibres were subjected only to water spraying. Following the cooling phase, silanes were promptly applied using a rotating cylinder (kiss roller) applicator. Subsequent to the coating process, all fibre bundles were subjected to a drying period at 105 °C for 24 hours. Several in-house applications of silanes were conducted to cover a broader spectrum of silane chemistries and explore potential distinctions arising from the method of silane application, encompassing dip coating and spin coating. Most of the fibres studied in this chapter were dip-coated to allow for direct comparison with results from the literature. Additionally, spin coating was employed for APS sized fibres to evaluate the effectiveness of the spin coating technique in silane application. A summary of the fibres used in these experiments is provided below.

5.3.2. Silane treatment

The bare fibres were subjected to APS, GPS, and APS sizing. Silanes were acquired from Sigma Aldrich. For in-house silane coatings, a pH meter was calibrated using buffer solutions

of pH 4, 7, and 10. To facilitate the hydrolysis of GPS and MPS in water, a diluted acetic acid solution adjusted the pH of deionised water within the range of pH 5 to 5.5. Although APS is typically prepared at its natural pH, an acidic APS solution was created to examine the pH effect on APS. A 1% silane solution was hydrolysed for 24 hours in a sealed volumetric flask as shown in Figure 5.6. Three unsized glass fibre bundles (15 cm) were fully immersed in the silane solution for 15 minutes and then dried for 2 hours at 110 °C. Fibre bundles (10 cm) were also spin coated using APS 1% solution (natural pH) at the 3000-rpm speed. The spin coated process was exactly the same as chapter 4.

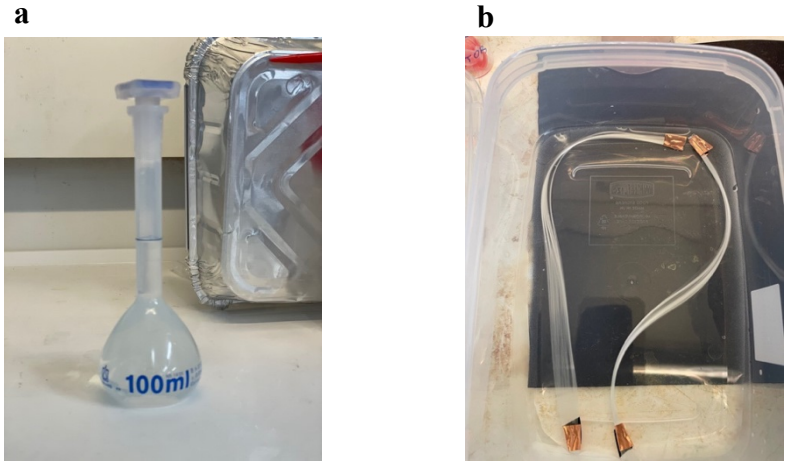

Figure 5.6. a) Silane solution, b) Immersed fibre bundles in the silane solution.

Table 5.1. Summary of the studied fibres, including industrial APS sized fibre with different pH, in house silane sized fibre i.e., different silane types, different APS pH and concentration.

Designation	Sizing	Concentration (%)	Solution pH	Coating technique
BF	Bare (water size)	-	-	-
Sise-APS	Industrial APS sized		10	Industrial
Sise-APS5	Industrial APS sized		5	Industrial
APS	House APS sized	1%, 0.2%	10	Dip & spin
APS5	House APS sized	1%, 0.2%	5	Dip
MPS	House MPS sized	1%	5	Dip
GPS	House GPS sized	1%	5	Dip

APS-sized commercial fibres were taken from larger rovings supplied by Sisecam. In the case of roving bobbins, fibres from the inner section were utilized to avoid potential damage during

packing, storage, and transportation. Flat edges of the roving were also avoided to prevent possible elevated sizing concentrations. The fibres used in the investigation of glass fibre sizing components and their corresponding designations are summarized in Table 5.1

5.3.3. TGA

TGA analysis was performed on BF, dip coated APS, GPS and MPS fibres, as described in Section 3.5.

5.3.4. Spectroscopic characterisation of silane sized glass fibres

FTIR analysis was performed on BF, dip coated APS, GPS and MPS sized fibre, as described in Section 3.7.

5.3.5. Hot stage microscopy

Sample preparation and hot-stage microscopy were conducted following the protocol outlined in Section 3.2 of the thesis. The entire procedure was meticulously documented through video recording, capturing any observable changes. A series of screenshots that illustrate the droplet formation process of each thermoplastic are reported.

5.3.6. Microbond

The microbond test, as outlined in Section 3.1.1, was conducted utilizing both commercially available APS sized fibres at various pH levels and in-house silane sized fibres. The fibres were sized with dip coated GPS, MPS and APS (different pH and concentration) and tested with PP, MAPP, PA6 and PBT. Furthermore, the spin coated APS fibres were tested with the same thermoplastics.

5.4. Results and discussion

5.4.1. TGA results of silane sized glass fibre

Silane coupling agents are commonly recognized for enhancing interfacial adhesion, and their elimination via thermal treatment can markedly affect the interfacial strength of composite materials [86]. Silane coated fibre exhibits minimal mass loss across the majority of tested samples. This phenomenon is likely attributable to the silane coating's mass being negligible relative to the total mass of the fibre. Consequently, the decomposed mass of silane was too minor to permit the application of a baseline subtraction method. Nonetheless, for samples presumed to have a higher silane content, thermograms were produced which provided insights

into the thermal degradation behaviour of silane-coated on to fibres. Figure 5.7 presents the TGA thermograms (Figure 5.7a) and the derivative peak temperatures (Figure 5.7b) of glass fibres treated with APS, GPS, and MPS silanes. It is difficult to determine if the degradation of the fibres sized with the investigated silane has different steps; however, there is a main peak that is obvious in all three silane-sized fibres. APS starts to degrade earlier than the others, with mass loss beginning at approximately 193 °C, peaking at around 245 °C, and most mass loss happening between 150–350 °C. In comparison, GPS has a mass loss onset at 285 °C, derivative peak temperatures at 316 °C, and most mass loss between 230–400 °C. This is in agreement with the findings from Bryce [16] who reported that the thermal decomposition of GPS polysiloxane films showed a primarily two-step degradation process with mass loss onset occurring at approximately 280 °C. MPS shows the greatest thermal stability, with mass loss onset at 328 °C, derivative peak temperatures at 365 °C, and the primary range of mass loss between 277–450 °C.

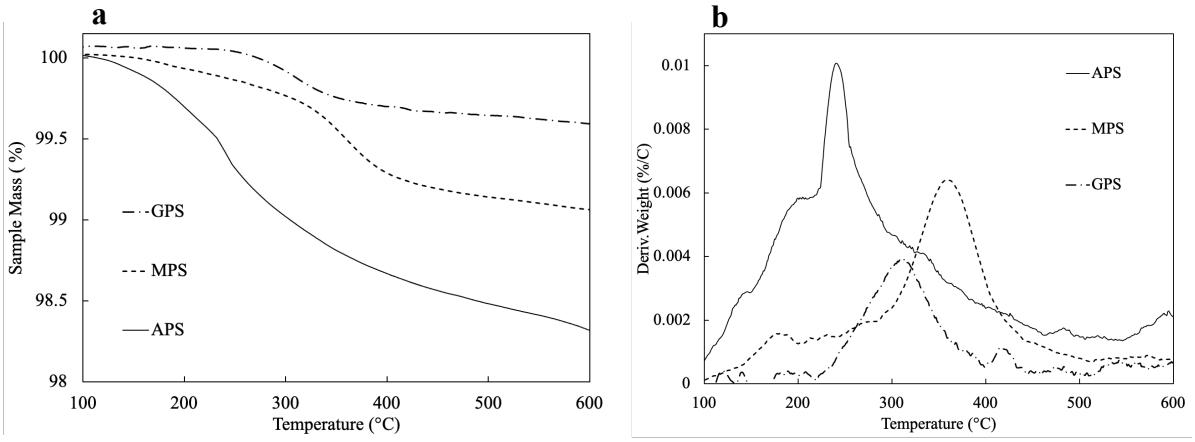

Figure 5.7. a) TGA results of silane coated fibre, b) DTG results of silane coated fibre.

To summarise the TGA results, MPS exhibits the highest thermal stability, followed by GPS and then APS. Different factors such as molecular weight, the presence of other functional groups, and the overall molecular structure can also influence the exact thermal stability of these silanes [117].

5.4.2. Spectroscopic characterisation of silane sized glass fibres

Figure 5.8 illustrates the FTIR spectra of unsized glass fibres, where a significant, high-intensity band is identified in the range of 1200–800 cm^{-1}, signifying the presence of Si-O-Si bonds in the glass fibres. Additionally, the absorption peak at 1400 cm^{-1} corresponds to other oxides like aluminium oxide and boron oxide. It should be noted that the spectral noise occurring between 2650 and 1650 cm^{-1} is due to the inherent absorption of diamond, which is

related to the use of the ATR interface during the spectral analysis. This particular noise is unrelated to the sizing or the surface condition of the glass fibres.

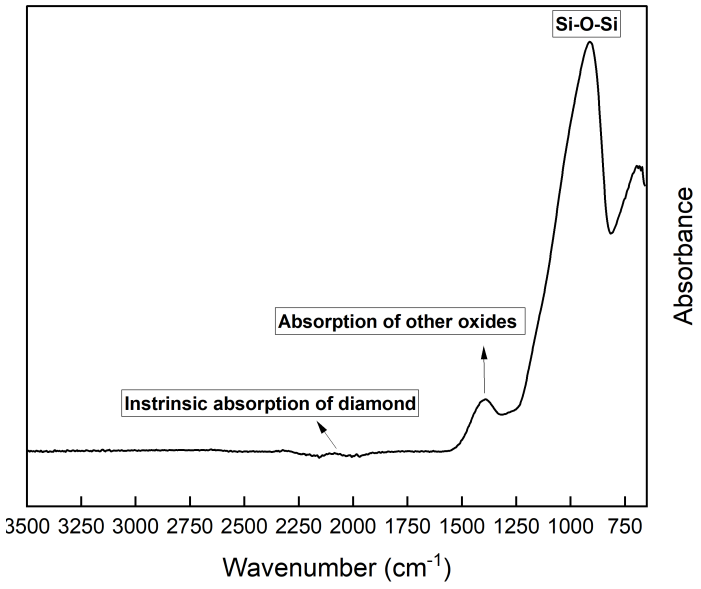

Figure 5.8. presents the FTIR spectra of unsized glass fibres.

In the FTIR spectra of silane-coated glass fibres, shown in Figure 5.9, a broad, high-intensity band within the 1200–800 cm^{-1} range was observed, attributable to Si-O-Si bonds, which significantly masks the characteristic fingerprint region. The prevalent silica signal, due to the ATR-FTIR interface's penetration depth (500–3000 nm), exceeds the sizing layer's estimated thickness of approximately 80 nm. The glass fibre's volume greatly surpasses that of the applied sizing, complicating the identification of bands associated with sizing components. The intense silica signal is dominant, diminishing the weaker signals from components like silanes, polymeric film formers, and lubricants or surfactants. To address this, the FTIR spectra of the glass fibre surfaces are presented with enlarged views of important spectral regions to emphasize the key features.

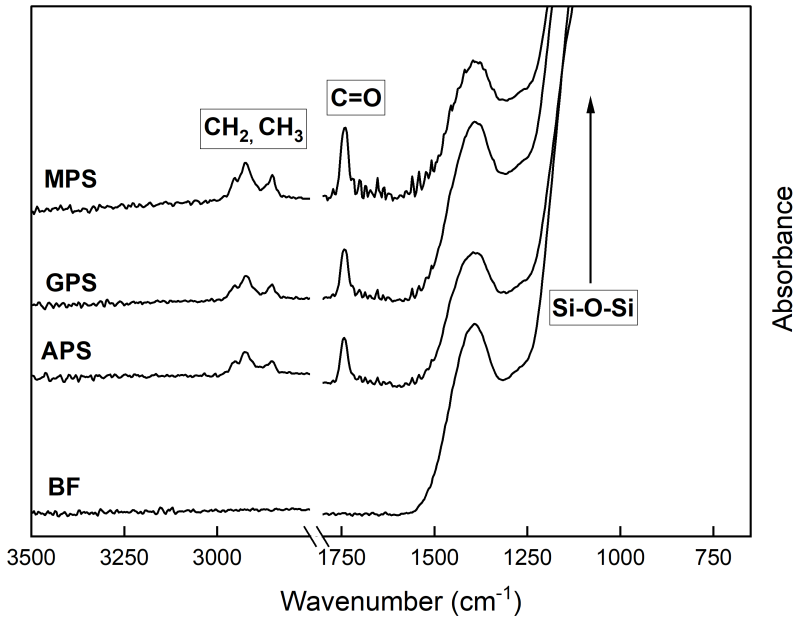

Figure 5.9. Shows the FTIR spectra for silane-coated glass fibres.

In the FTIR spectra of silane-sized glass fibre samples, the distinctive presence of a doublet at 2926 and 2856 cm^{-1} stands out, which is indicative of the propyl chain. This is attributed to the C-H stretching vibrations of CH_2 and CH_3 groups [165], respectively. An additional peak, observed around 1740 cm^{-1}, is related to the C=O stretching vibrations of carbonyls, a feature that is present across all the samples.

The spectra of MPS-sized fibres align closely with the findings reported by Li et al., [166] showcasing characteristic bands at 2942/2850 cm^{-1} and 1720 cm-1, which are typical of a silane such as MPS. Moreover, Guo et al. [167] have observed a pronounced C=O signal in both MPS and MPS-treated alumina nanoparticles. In contrast, Petersen et al. [168] have identified C=O stretching at 1735 cm^{-1} in sizing extracts, but not in fibres coated with GPS or in pure APS and GPS samples. Thomason [169] has reported an unidentified C=O-containing compound in NMR analyses of sizing extracts. While the C=O band is recurrent and documented in the literature, particularly for methacryl silanes [170], its occurrence in GPS samples might be due to contamination, given that epoxy silane typically lacks carbonyl groups. Bashir [171] has proposed that the C=O carbonyl group, appearing around 1750 cm^{-1} in both baseline APS coated and heat-treated fibres. This could result from interactions with organic contaminants and alkali, forming carboxylic species, or it can possibly be due to a halogenated ketone. Given that the analysis was repeated five times for each sample with consistent results, it suggests that this phenomenon could be present across all fibre samples, possibly due to similar interactions or contamination during processing or sample preparation.

5.4.3. Droplet formation observation

Droplet formation of each thermoplastic matrix (PP, MAPP, PA6, and PBT) was observed using the hot stage microscopy before proceeding with the microbond test process. This was done to better understand the droplet shape, size, and consequent wetting ability of each polymer used for the microbond test. This also enabled the assessment of different size of droplets to be possible and how different shapes of the polymer droplets impact the IFSS. Further details on droplet formation are provided in the following sections.

5.4.3.1. PP droplet formation

Figure 5.10 shows a series of micrographs of a glass fibre/PP microbond sample heated from room temperatures until 220 °C in air. As shown in Figure 5.10a, melting started at 163 °C (the same temperature as the melting point reported for PP in the technical datasheet). Droplets formed completely at 170 °C (Figure 5.10b), and as the temperature increased and then cooled, significant shrinkage was observed in the PP droplet. This passage clearly demonstrates a significant decrease in the volume of the PP droplet over time, strongly suggesting that the droplet undergoes substantial shrinkage. This volume reduction is likely due to the evaporation of volatile including water vapor and low-molecular-weight hydrocarbons such as propylene and other oligomers [172]. Yang et al. [72] observed shrinkage when they maintained a PP droplet at 220°C for 30 minutes. They noted that the droplet's width decreases symmetrically around the fibre, whereas the length reduction (along the fibre-embedded length) is more pronounced on the upper part of the droplet than the lower part. In this thesis, to prevent degradation, the PP droplet was immediately cooled upon reaching 220°C.

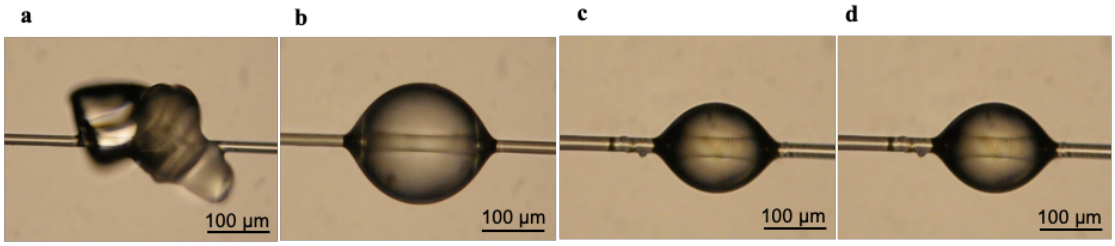

Figure 5.10. HomoPP droplet formation steps under hot-stage microscopy. a) Melt: 163° C, b) Formed: 170°C, c) Max temp: 220°C, d) Cooled: 30°C

5.4.3.2. MAPP droplet formation

The microscopy images in Figure 5.11 illustrates the characteristics of glass fibre-reinforced MAPP. The observed shrinkage pattern is consistent across samples of MAPP, which is more temperature-sensitive due to its chemical composition. As depicted in Figure 5.11, the melting onset for MAPP occurs at approximately 157 °C, which is slightly lower than that of PP. The

formation of the droplet shape is immediate once melting begins within the range of 157-158 °C. Subsequent shrinkage is noted as the temperature reaches 200 °C, followed by cooling as shown in Figure 5.11d.

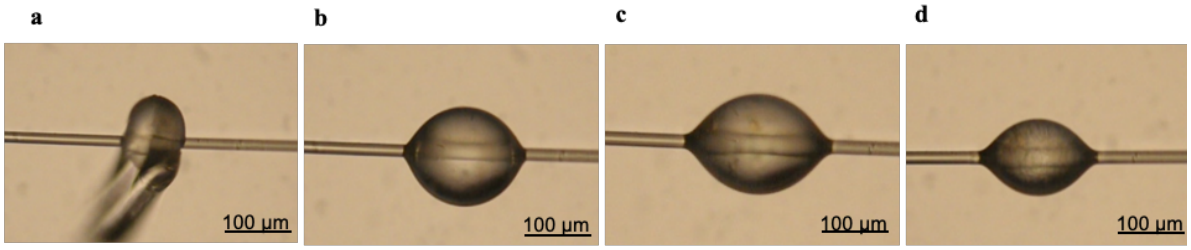

Figure 5.11. MAPP droplet formation steps under hot-stage microscopy. a) Melt: 157° C, b) Formed: 158°C, c) Max temp: 200°C, d) Cooled: 30°C.

5.4.3.3. PA6 droplet formation

PA6 proved to be the most challenging matrix to manipulate due to its inherent chemical properties and higher viscosity relative to other matrices. Figure 5.12 captures a successful droplet formation under a hot-stage microscope. The melting process commenced at 225 °C and was completed at 230 °C, with an increase of just 5 °C. Notably, PA6 experienced negligible shrinkage when heated up to 260 °C and subsequently cooled down. It is hypothesised that this might be due to the high viscosity and molecular tendency of the PA6. Droplets of PA6 tend to be more spherical droplets compared to the other three matrices examined. Due to the smaller size of the droplets formed from this polymer, a larger number of microbond samples (approximately 80) were prepared with PA6 to obtain a reliable dataset, ultimately aiming for 30 data points. Further investigation is needed on the scaling effects of PA6 droplets on IFSS. However, the experimental results were highly repeatable, and no instability was observed during the microbond tests.

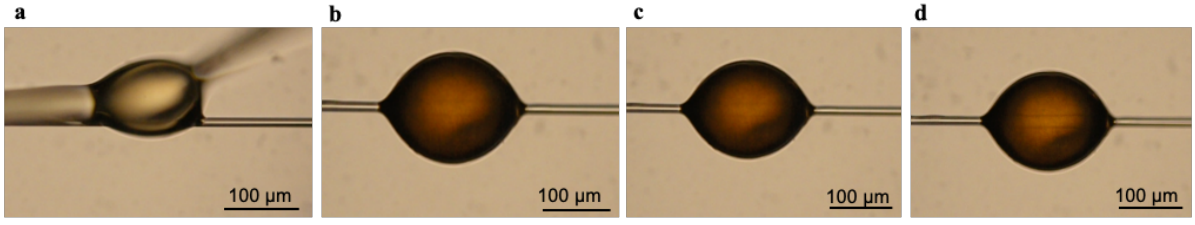

Figure 5.12. PA6 droplet formation. steps under hot-stage microscopy. a) Melt: 225° C, b) Formed: 230°C, c) Max temp: 260°C, d) Cooled: 30°C

5.4.3.4. PBT droplet formation

Figure 5.13 illustrates the process of droplet formation in a PBT matrix. There is no literature on the details of the PBT droplet formation. The melting process began at 223 °C, as shown in Figure 5.13, and the droplet took form at 230 °C. This was followed by heating up to 260 °C, the processing temperature of PBT recommended on the materials technical data sheet, and then cooling down to ambient temperature, which is presented in Figure 5.13. Unlike other thermoplastics, the fibre is not visible through the PBT droplet after cooling, since PBT has a milky white appearance and opaquer compared to the other studied thermoplastics. The shape of the droplet did slightly change when it cooled from the maximum temperature, indicating a minimal shrinkage in PBT. This might be due to PBT having a low coefficient of thermal expansion, which helps it maintain dimensional stability during temperature changes [173].

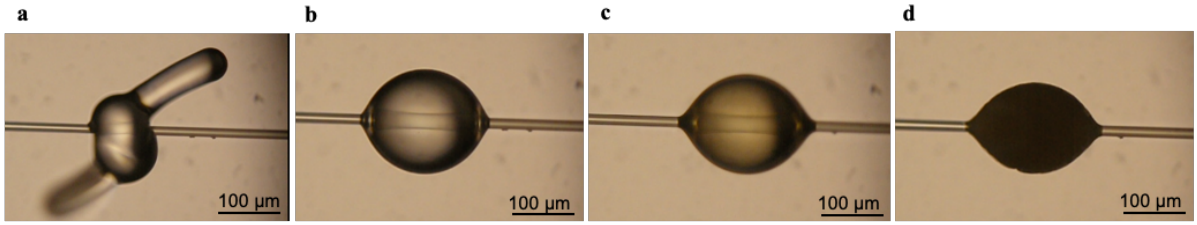

Figure 5.13. PBT droplet formation. steps under hot-stage microscopy. a) Melt: 223° C, b) Formed: 230°C, c) Max temp: 260°C, d) Cooled: 30°C

5.4.3.5. Testable droplet characteristics

It's highly advised to form microbond samples in an inert atmosphere, like nitrogen, to prevent degradation, as previously reported by Yang et al. on PP samples [72]. This is because both microbond and macroscopic samples indicate that changes in their thermo-mechanical properties, especially the modulus, significantly contribute to the reduction of the measured IFSS. This is primarily due to a decrease in the compressive radial residual stress at the interface. A similar observation was made by Minty[174] in an epoxy based system, where factors such as glass transition temperature, storage modulus, gel point, linear coefficient of thermal expansion and the degree of chemical shrinkage during the curing process influenced the residual stress levels and consequently, the IFSS. Hence, in this thesis the droplets were formed under nitrogen flow to minimise the risk of polymer degradation affecting the IFSS results. Figure 5.14 presents examples of four thermoplastic droplets that meet the criteria for effective adhesion testing. The initial assessment of microbond droplets is conducted through visual inspection utilizing a microscope. This examination reveals that the fine microbond droplets, employed to evaluate the adhesion properties of fibre-reinforced composites, are

symmetrical and exhibit no signs of material degradation. As can be seen from Figure 5.14, the droplets' clarity allows the embedded fibre to be distinctly observed, with an exception for PBT due to its white appearance. The other evaluation is during testing, these droplets must demonstrate a resistance to deformation, maintaining their rigidity and not becoming soft. This is an important factor for the droplet quality check, assuring appropriate thermal process of the droplet in the oven.

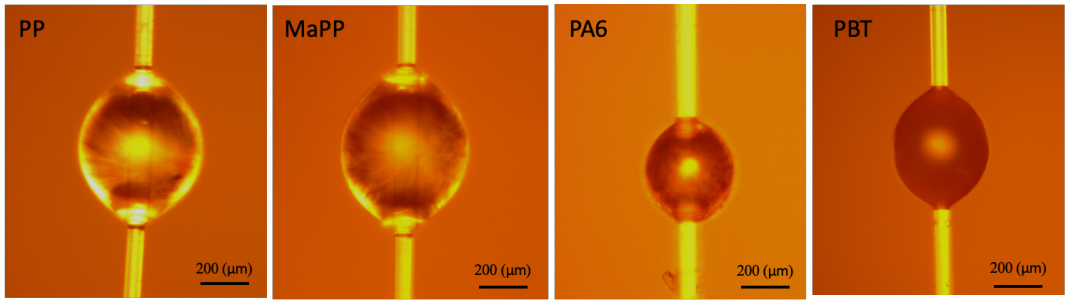

Figure 5.14. Examples of PP, MAPP, PA6 and PBT droplets.

Table 5.2 summarized each thermoplastic droplet dimension and aspect ratio (Figure 5.15 and Equation 1) of the 100 successfully tested samples. The aim was to compare the size of the droplets from each thermoplastic. As expected PA6 had the lowest aspect ratio of 1.1 among all the polymers, and the average droplet embedded length was measured to be around 127.2± 35 (µm). It was also mentioned in section 5.4.1.3 that only small droplets could be made with PA6 and the shape of the droplets were observed to be more circular. This may be due to the significant contact angle, indicating poor wetting on the glass fibre surface. Although it is a polar polymer, which typically enhances wettability, its high viscosity and molecular structure could be contributing factors to this issue. The aspect ratio of the remaining polymers was close to each other with the values of 1.4 for PP and PBT, and 1.5 for MAPP. However, PP had the largest droplet with the average embedded length of 198.0±45 (µm). The MAPP and PBT had a droplet embedded length of 145.1±31 (µm) and 128.7±30.2 (µm), respectively. In this thesis, the goal was to achieve varied embedded lengths to create a robust dataset for analysis. The diameter of the PA6 droplets is different from other polymers, as it was not possible to form larger droplets with this material. This is likely due to PA6's high viscosity and the molecular tendency of this polymer, which makes it difficult to produce larger droplets compared to other polymers used in the study.

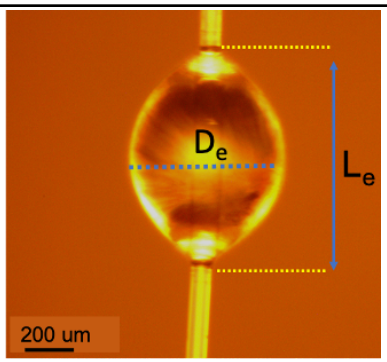

Figure 5.15. Embedded length (Le) and diameter (De).

$$Aspect\ ratio = L_e / D_e \quad (1)$$

Table 5.2. Droplets dimension and aspect ratio.

Polymer	Droplet embedded length (µm)	Droplet diameter (µm)	Aspect ratio
PP	198.0 ±45.0	144.4±36.2	1.4
MAPP	145.1±31.0	98.2±25.7	1.5
PBT	128.7±30.2	93.1±25.4	1.4
PA6	127.2± 35.0	112.6±36.2	1.1

5.4.4. Successful debonding

Figure 5.16 presents SEM images that capture the micro-droplets of PP, MAPP, PA6, and PBT after undergoing the microbond test. These images are helpful in verifying the microbond test's efficacy, as they clearly show the areas where debonding has occurred. The force displacement curves show a successful debonding pattern, as briefly discussed in chapter 3, section 3.1.3. For PP and PA6, the droplets do not experience significant damage during the debonding, which can be due to the lower interfacial strength in PP and a more circular droplet shape in PA6 causing a larger contact area for the blade. The MAPP droplets exhibit noticeable damage, which shows a stronger interfacial bonding compared to its bearing strength. This results from the enhanced bond strength that leads to the blade inflicting some bearing damage to the MAPP matrix during the test, as the interface resists clean debonding. This observation highlights the relative toughness and adhesion properties of MAPP, which, while beneficial for certain applications, presents a challenge for the microbond test, requiring careful consideration when interpreting the results. The PBT droplets do not experience significant damage during

debonding, and a clear fibre/matrix debonding can be observed, indicating the validity of the microbond test.

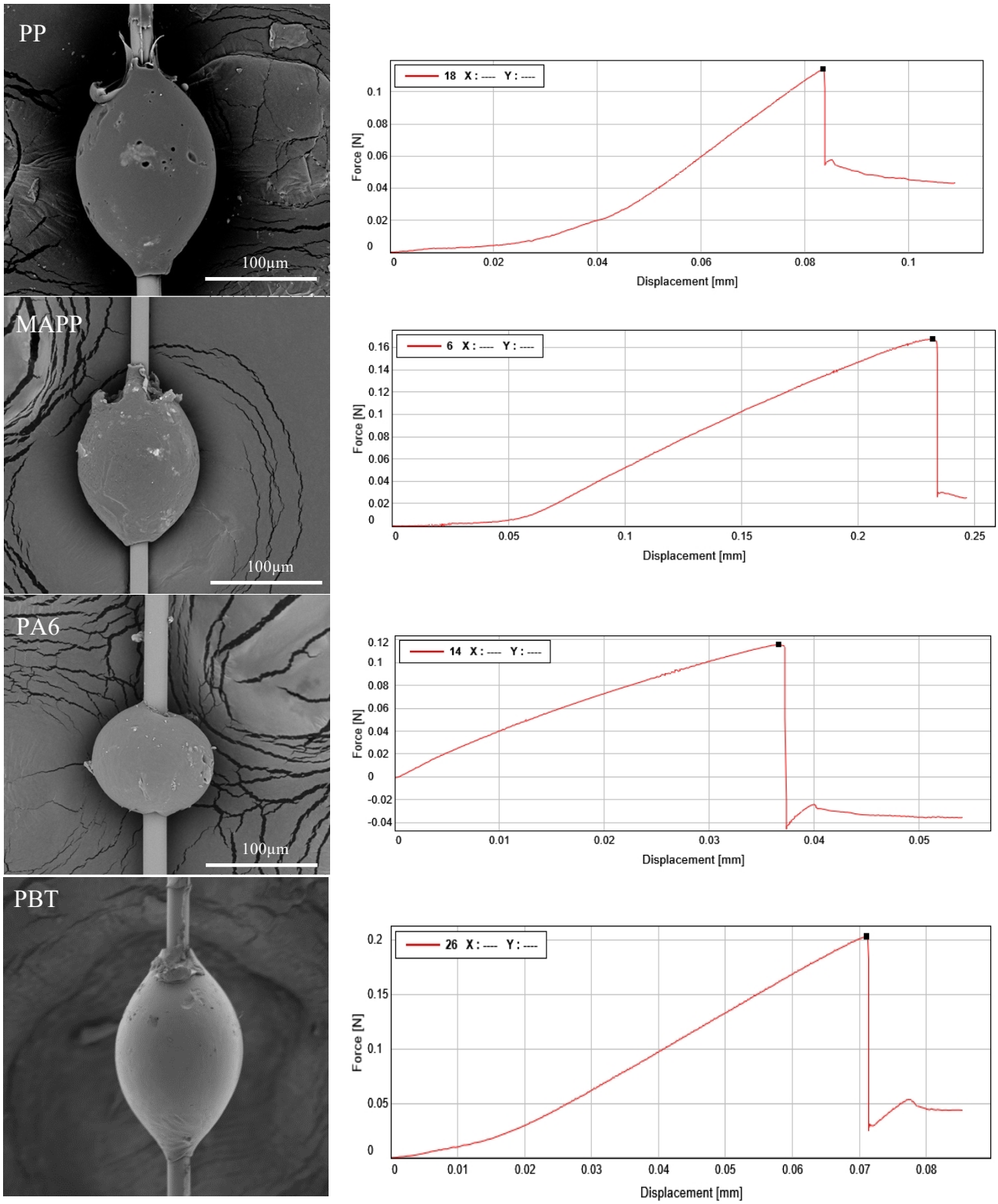

Figure 5.16. Examples of PP, MAPP, PA6 and PBT droplets, and the associated force displacement graphs.

5.4.5. Microbond results

5.4.5.1. Effect of different dip coated silanes on IFSS

The microbond testing results were based around bare and three different dip coated silane fibres (APS, GPS, MPS) with four different thermoplastics (PP, MAPP, PA6 and PBT) as illustrated in Figure 5.17. The IFSS and t.test results are also summarized in Tables 5.3 and 5.4. Looking at the IFSS values of the investigated fibre/matrix systems, the PBT system exhibits the highest IFSS values. The MAPP ranks second in IFSS, followed by PA6 and PP. Pearson et al. [175] assessed the IFSS of PBT and PA6 via pull-out tests. Their results showed that the average IFSS for PA6 was 28.6 MPa, higher than PBT's average of 24.5 MPa.

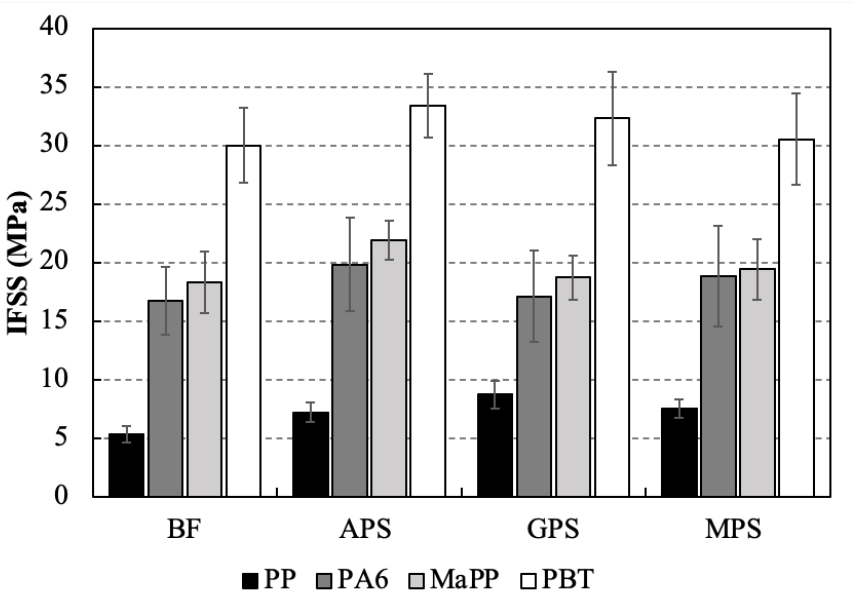

Figure 5.17. IFSS results for the investigated systems.

The lower IFSS value of PA6, compared to PBT and MAPP, could be attributed to a more circular PA6 droplet and possibly a large contact angle, which are the signs for a poor wetting on glass fibre surface. Furthermore PA6's tendency and ability to absorb moisture could be another reason [176], which can adversely affect adhesion within composite materials. An additional consideration is the challenge in creating larger droplets with PA6, which could affect the measured IFSS values due to the influence of droplet size.

For PP systems, the application of any form of silane contributed to an improved IFSS compared to a BF. The silane sized fibres generally exhibited IFSS in the region of around 8 MPa, which shows the improvement in IFSS compared to BF. The p values obtained from the two-tailed t.test, see Table 5.3, between BF and silane sized fibres show that the difference in

average apparent IFSS values for these systems are significant at the 95% confidence level, while there is a small difference when comparing the silane sized fibres with each other.

Table 5.3. Summary of IFSS values for in-house silane sized fibre.

	IFSS (MPa)			
Designation	PP	MAPP	PA6	PBT
BF	5.1±0.6	18.3±2.6	16.7±2.9	30.0±3.5
APS	7.2±0.8	21.9±1.7	19.8±4.2	31.9±3.9
GPS	8.7±1.2	18.7±1.9	17.1±4.3	32.3±4.5
MPS	7.5±0.8	19.4±2.6	18.8±4.9	30.5±3.7

This can be attributed to the inherent chemical structure of PP [177]. As a non-polar polymer, PP consists of a saturated hydrocarbon backbone that lacks polar functional groups. This results in a hydrophobic material with a degree of chemical inertness. Contrastingly, it has been observed that the IFSS values in PP system can be enhanced through the silane treatments to the fibres. Silanes are introducing polar functional groups which in turn increase the surface energy and polarity. This modification facilitates better wetting and chemical bonding between the fibres and the PP matrix, leading to an improved adhesion. The increase in surface polarity due to silane sizing is likely the mechanism responsible for the observed enhancement in the IFSS values, as it contrasts with the unmodified non-polar PP matrix. Petersen et al. [29] reported that the glass surface was more polar after the coating with different silanes, e.g. APS and GPS, implying that the presence of an organosilane results in a change in surface energy. Consequently, a more polar surface could increase the wetting of the glass surface by the matrix. Feresenbet et al. [143] investigated the influence of blended silane sizings on both fibre surface morphology and glass fibre/epoxy IFSS. The contact angle measurements showed an increase in polarity corresponding to increased APS content in the mixture. Apparent IFSS, determined by fragmentation test, increased with increasing APS concentration in the silane mixture. It can be seen that IFSS for MAPP systems are much higher than PP systems for BF and silane sized fibre, this is in agreement with previous observation by Nygård et al. [178]. The results show that APS had the highest IFSS value of 21.9 MPa among all the samples in the MAPP system, and there is a little difference between the MPS and GPS. The t.test results in Table 5.4 also certifies these results. The IFSS results for PA6 systems show that APS has the highest IFSS value of 19.8 MPa, whereas BF and GPS have the lowest value 16.7 MPa and

17.1 MPa, respectively. However, the Student's t.test results indicate that the differences in average apparent IFSS values for these batches are not significant. Microbond results for PBT systems stand as the highest value (approximately 30 MPa for BF and MPS, and 32 MPa for APS and GPS) among all the systems. However, there is only a small improvement in silane sized fibres compared to BF. From the results, the application of silane has some improvement in the IFSS of the thermoplastic composites. Given that there is not a significant difference between the IFSS results using different silane sizing, it is reasonable to suggest that the improvement might be due to the morphological physical bond in interface. Additionally, FTIR results showed some surface chemistry change on the fibre surface, which might be potential chemical bonds in the interface. This requires further investigation to identify the interfacial bonding nature in thermoplastic composites.

Table 5.4. Two-tailed Student's t.test between BF and silane sized fibres

Paired samples	p value in different thermoplastic systems.			
	PP	MAPP	PA6	PBT
BF/APS	0.003*	0.02*	0.30	0.29
BF/GPS	0.0002*	0.82	0.82	0.28
BF/MPS	0.0006*	0.29	0.43	0.60
APS/GPS	0.07	0.005*	0.27	0.89
APS/MPS	0.62	0.14	0.74	0.59
GPS/MPS	0.12	0.16	0.51	0.53

* Significant at 0.05 level, 95% confidence limit

5.4.5.2. Effect of APS pH and concentration

Microbond testing results for bare, industrial and in house dip coated APS sized fibres at different pH levels with four different thermoplastics are reported in Figure 5.18 and Table 5.5. The results show that the PBT system has the highest IFSS values of all the investigated fibre/matrix systems. The second highest IFSS value is for MAPP, followed by PA6 and PP systems. Microbond results for PBT systems stand as the highest value (approximately 30 MPa for BF and MPS, and 32 MPa for Sise-APS5) among all the systems. However, the improvement is small in APS sized fibres compared to BF, and the differences between the different APS pH solutions is not considerable. It can be observed that IFSS for MAPP systems are much higher than PP systems for BF and APS sized fibre. The results show that the APS

sized fibre at their natural pH, either industrial or in house sized fibre, had the highest IFSS value of around 21 MPa among all the samples in the MAPP system.

The IFSS results for PA6 systems show improvement in APS with the IFSS value of 19.9 MPa, but it's not statically significant, whereas Sise-APS has the lowest value 15.7 MPa. For PP systems, the application of all the APS sized fibres (around 6.7-8 MPa) except Sise-APS contributed to a significant improved of IFSS compared to the BF.

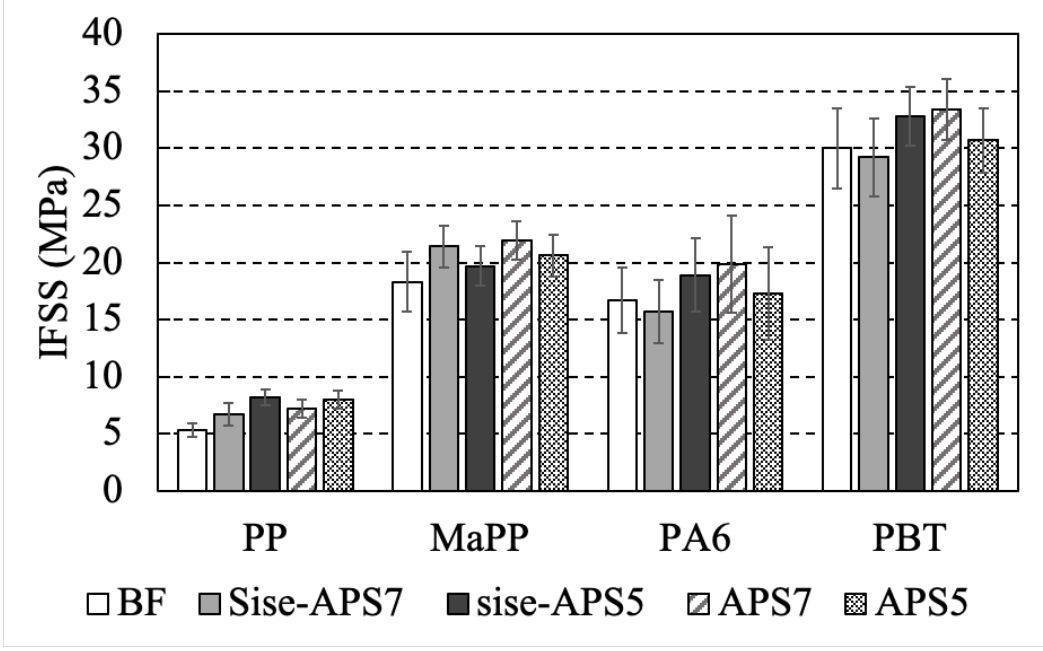

Figure 5.18. IFSS results for the industrial and dip coated APS sized fibre at different pH.

Table 5.5. Summary of microbond testing of industrial and dip coated APS sized fibre at different pH.

Designation	IFSS (MPa) PP	IFSS (MPa) MAPP	IFSS (MPa) PA6	IFSS (MPa) PBT
BF	5.1±0.6	18.3±2.6	16.7±2.9	30.0±3.5
Sise-APS	6.73±1.0	21.4±1.8	15.7±2.8	29.2±3.4
Sise-APS5	8.22±0.7	19.7±1.7	18.9±3.2	32.8±2.6
APS	7.2±0.8	21.9±1.6	19.82±4.2	31.9±3.9
APS5	8.0±0.8	20.6±1.8	17.3±4.0	30.8 ±2.8

Figure 5.19 and Table 5.6 show the IFSS results for BF and in-house dip coated APS sized fibres with the aim of evaluating the effect of different APS concentration, i.e., 1% and 0.2%,

and different pH levels with the investigated thermoplastics. Similar to the previous sections, the results show that the PBT system has the highest IFSS values, followed by MAPP, PA6 and PP systems. Microbond results for PBT systems stand as the highest value (approximately 30 MPa for BF and MPS, and 32 MPa for Sise-APS5). However, the improvement is small in APS sized fibres compared to BF, and the differences between the different APS pH solutions is not considerable.

It can be observed that IFSS for MAPP systems are much higher than PP systems for BF and APS sized fibre. The results show that the APS sized fibre at their natural pH either industrial or in house sized fibre had the statically highest IFSS value of around 21 MPa among all the samples in the MAPP system.

The IFSS results for PA6 systems show improvement in APS 0.2% with the IFSS value of 20.1 MPa, whereas Sise-APS has the lowest value 15.7 MPa. For PP systems, the application of all the APS sized except Sise-APS contributed to an improved IFSS significantly compared to the BF. The APS sized fibres generally exhibited IFSS in the region of around 6.7-8 MPa, which shows the improvement in IFSS compared to BF.

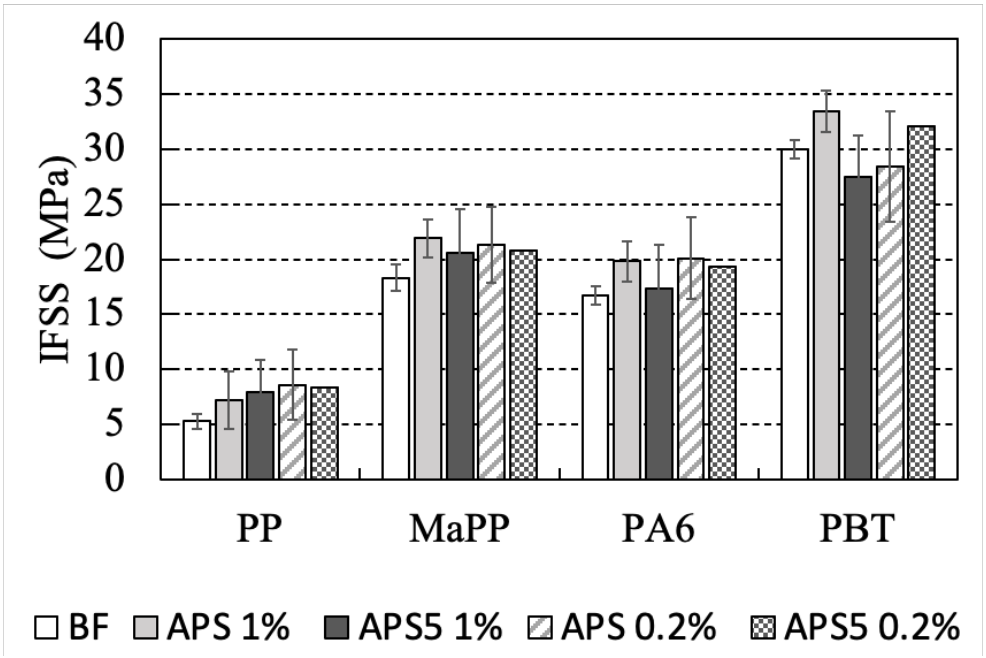

Figure 5.19. IFSS results for the dip coated APS sized fibre with different concentration pH levels.

Table 5.6. Summary of Microbond Testing Results of the dip coated APS sized fibre with different concentration and pH.

Designation	IFSS (MPa) PP	IFSS (MPa) MAPP	IFSS (MPa) PA6	IFSS (MPa) PBT
BF	5.1±0.6	18.3±2.6	16.7±2.9	30.0±3.2
APS 1%	7.2±1.2	21.9±1.8	19.8±3.8	33.4±3.4
APS5 1%	8.0±0.8	20.6±1.7	17.3±4.0	27.5±3.7
APS 0.2%	8.6±0.8	21.3±1.9	20.1±3.7	28.4±5
APS5 0.2%	8.4±1.0	20.8±2.5	19.3±4.7	32 ±5

5.4.5.3. IFSS of APS sized fibres using Spin coating technique

In order to evaluate the potential of the new spin coating method for silane sizing of the fibre, the IFSS results for the spin coated fibres sized with APS (1% concentration at the natural pH) are reported in Figure 5.20. A consistent trend is observed across different polymer systems, with the PBT system exhibiting the highest IFSS values, followed by MAPP, PA6, and PP. Table 5.7 compares the IFSS results of BF and those sized with APS through both dip and spin coating methods with the investigated thermoplastics.

There are evident differences between the IFSS values measured for the dip and spin coated fibres in the PP, MAPP, and PA6 matrices. An improvement in IFSS is seen when comparing the BF with spin coated fibres in PP and MAPP matrices, where the spin coated fibres exhibit higher values of 9.3 MPa for PP and 24.9 MPa for MAPP, respectively. This enhancement indicates that the spin coated fibres may have reached their maximum potential in these systems. Interestingly, a significant difference is observed in the PA6 system with spin coated fibres when compared to BF, a difference that was not apparent with dip coated fibres. This may be due to the more uniform and thinner layer of coating achieved with spin coating compared to dip coating. However, further investigation is needed to evaluate the uniformity of silane sizing applied via spin coating. Additional tests should also be conducted on silane-sized fibres using spin coating, particularly with thermoplastics such as PA6, to validate these findings.

For the PBT matrix, the IFSS values for dip coated (33.4 MPa) and spin coated (32.32 MPa) fibres are closely matching. In the PBT matrix, however, the IFSS results remain almost consistent between dip coating and spin coating, with no notable improvement over the BF.

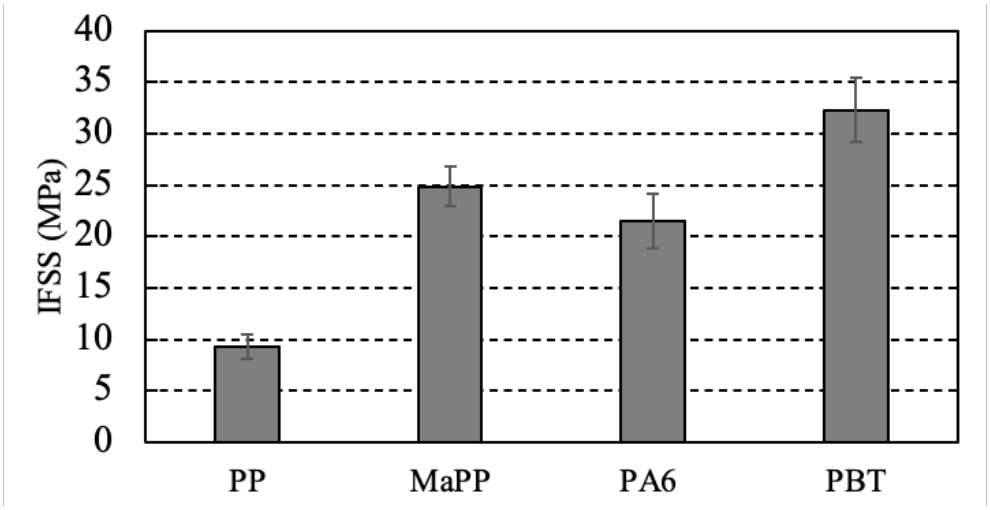

Figure 5.20. IFSS results for the APS spin coated fibre.

Table 5.7. IFSS results for the APS spin coated fibre.

Designation	IFSS (MPa) PP	IFSS (MPa) MAPP	IFSS (MPa) PA6	IFSS (MPa) PBT
BF	5.1±0.6	18.3±2.6	16.7±2.9	30.0±3.2
Dip APS 1%	7.2±1.2	21.9±1.8	19.8±3.8	33.4±3.4
Spin APS 1%	9.3±1.2	24.9±1.9	21.5±2.7	32.3±3.11

The observed improvements in IFSS with spin coated fibres could be attributed to the more uniform distribution of the sizing, leading to better fibre/matrix adhesion. Spin coating likely provides a closer distribution of the sizing on the fibre surface, compared to dip coating, and it better replicates the industrial sized fibre. This is investigated for full sizing in chapter 6 by SEM observations. This might be the reason in variations in coating thickness and possibly less optimal interfacial properties in the dip coating. The data suggests that while both dip and spin coating methods can enhance fibre/matrix adhesion relative to bare fibres, spin coating has the potential to achieve superior IFSS.

5.5. Conclusion

Chapter 5 has examined the degradation behaviours of various silane coatings applied to glass fibres, surface chemistry changes and the IFSS of the fibres when combined with different thermoplastics. Findings have revealed the influence of silane chemical groups on thermal stability, with MPS demonstrating the highest thermal resistance, followed by GPS and APS. The FTIR results showed the surface chemistry changes by silane coatings, however, no differences were noticed between different silane types.

The investigation into adhesion between fibres and various thermoplastic matrices revealed a strong dependence on the type of matrix and matrix modifications, such as introducing acid groups into the matrix, which can enhance interfacial strength.

The silane sized fibre/ thermoplastic systems demonstrated some IFSS improvements; however, this enhancement was not observed across all the studied thermoplastics, as summarised in Table 5.8. The application of all the silane improves the IFSS of PP and APS for MAPP systems in both dip coated and spin coated fibres. For PP, the improvements in IFSS are largely due to enhanced physical interactions like van der Waals forces, as the polymer itself has no functional groups to form chemical bonds with the silane. For MAPP, there may be stronger chemical interactions due to the presence of polar functional group (anhydride) that can form hydrogen bonds or covalent bonds with the APS silane's amine group. For the PA6 system, the improvement was only significant for the spin-coated fibres and the 0.2% APS dip-coated fibres. This may be attributed to the presence of polar functional groups (amide) in PA6, which contributed to some improvement in fibre performance. The PBT systems did not show any improvement in IFSS with different silanes or when changing the coating technique. It is noted that the PBT baseline IFSS is relatively high, and most silane treatments provide modest improvements. This indicates that PBT's polar nature interacts reasonably well with silane-coated fibres.

There are negligible IFSS differences between the various silane types used in the polymeric system, except MAPP. The difference is believed to be due to the nature of the bond, where the slight improvements in the APS/MAPP system is mainly due to physical interactions and basic chemical acid base interactions between basic amino groups at the silanized glass fibre surface and acidic groups of the maleic anhydride grafted matrix. Whereas the other polymers

might experience physical bonding, which justifies their similar IFSS in different silane systems.

The lower APS concentrations could also suffice for optimal adhesion properties. Furthermore, altering the pH of APS solutions does not appear to significantly affect the final adhesion properties across the thermoplastics studied. This outcome indicates that adjusting the pH is not a requisite step for APS application or its hydrolysis process, underscoring the robustness of APS as a silane coupling agent.

Table 5.8. Summary of all the microbond testing results.

Designation	PBT IFSS (MPa)	IFSS change (%)	PA6 IFSS (MPa)	IFSS change (%)	MAPP IFSS (MPa)	IFSS change	PP IFSS (MPa)	IFSS change (%)
BF	30.0	Baseline	16.7	Baseline	18.3	Baseline	5.1	Baseline
APS7 1%	31.9	6.3	19.82	18.7	21.9	19.7	7.2	41.2
APS 0.2%	28.4	-5.3	21.1	26.3	21.3	16.4	8.6	68.6
APS5 1%	30.8	2.7	17.3	3.6	20.6	12.6	8.0	56.9
APS5 0.2%	32.0	3.9	19.3	15.6	20.8	13.7	8.4	64.7
Sise-APS7	29.2	-2.7	15.7	-6.0	21.4	16.9	6.73	32.0
Sise-APS5	32.8	9.3	18.9	13.2	19.7	7.7	8.22	61.2
Spin APS	32.32	7.7	21.5	28.7	24.9	36.1	9.3	82.4
GPS	32.3	7.7	17.1	2.4	18.7	2.2	8.7	70.6
MPS	30.5	1.7	18.8	12.6	19.4	6.0	7.5	47.1

This chapter has tried to shed a light on the interaction of different thermoplastic systems and commonly used silanes. Compatibility of matrix and silane can be engineered with matrix modification such as introducing acid groups, and the use of various silane types to improve the interfacial properties of glass fibre composites. Future research is expected to explore the complex interplay between silane chemistry and polymer matrix to identify the nature of physical and chemical interactions and to optimise them to have an optimal fibre/matrix interfacial property

CHAPTER 6: CHARACTRIZING THE EFFECT OF FILM FORMER AND FULL SIZING IN GLASS FIBRE/PP, MAPP MATRICES

6.1. Introduction

This chapter investigates the role of film former and full-sizing (film former and silane) in compatible sizings for glass fibre with PP and MAPP matrices. PP was selected due to its reputation as one of the superior thermoplastic matrices for numerous industrial applications. Glass fibres are widely employed as reinforcing elements in PP and MAPP matrices because they offer superior mechanical properties at a reasonable cost. In this chapter industrial Homo polymer and Copolymer PP film formers were used with low and medium percentage of the Maleic Anhydride (MAH). Full sizing is composed of the film former and APS. APS was chosen as the silane component for our sizing formulation based on its established compatibility with PP composites. This is also confirmed in chapter 5, where an improvement in the IFSS was reported within PP and MAPP systems when APS was utilized. Surface chemistry, thermal stability and IFSS of the glass fibres sized with the film former and full sizing were characterised using FTIR, TGA and microbond tests. Furthermore, attempts were made to evaluate the possibility of making a thin film from the film former and full sizing, which can be used as an indication of the sizing quality.

Unlike silane coupling agents, there's no inherent assumption that film formers or other sizing components form chemical bonds with the fibre surface. For example, Thomason's research [179] demonstrated that a significant amount of epoxy based sizing could be removed by hot acetone extraction, suggesting that film formers make up a major portion of the removable substances in sizing. Confirmatory analyses such as NMR, FTIR, and elemental analysis have detected epoxy resin among other substances within these extracted materials. Furthermore, the early history of the research and development of composite materials is dominated by the use of chemically reactive thermosetting polymers. A natural consequence of this is that much of the published work relating to adhesion and stress transfer at the fibre/matrix interphase has been grounded in the assumption that the formation of chemical bonds plays a key role [4]. In the case of thermoplastic polymer matrices there is a substantially reduced level of chemical reaction present during composite processing. Consequently, there may often be little potential for chemical bonds to develop across the interphase in these systems. Both of these aspects of sizing and interphase adhesion are explored in this study. The microbond test, was used to

evaluate the IFSS of film former only coated fibre and full sizing with PP and MAPP. TGA was utilized to determine the thermal stability and composition of the film formers in the sizing. FTIR was used in this investigation to obtain molecular-level information on the chemical structure of the film former and its interaction with the glass fibre surface. Some approaches were also taken to investigate film former and full sizing film formations, which are reported in this chapter.

6.2. Literature review

6.2.1. The role of film former and full sizing in interphase

The primary function of the film former is to protect glass fibres during their manufacture and subsequent handling, as well as to promote the wetting of bundles by the reacting matrix during processing. It appears that this component could also enhance the properties of the fibres themselves and the fibre-reinforced polymers, such as tensile strength and impact resistance, without adversely affecting other material properties [180]. Scholtens and Brackman [177] demonstrated that by altering the film former chemical nature and molecular mass, and by omitting the silane coupling agent, the film former plays a crucial role in fibre/matrix adhesion, and its effect may be more significant than that of the silane. The interaction between the silane coupling agent and the film former is not purely additive but can be synergistic or even competitive depending on their composition and how they are applied. Ideally, the film former works in harmony with the silane to improve the fibre/matrix bond. The silane forms a strong chemical bond at the interface, while the film former enhances wetting and fibre protection, which can lead to better adhesion and stress transfer between the fibre and matrix. However, the interaction can be complex. Some studies suggest that the chemical nature and molecular mass of the film former can influence its role in fibre/matrix adhesion, sometimes even overshadowing the silane's effect.

In epoxy resin systems, the primary contribution to adhesion is attributed to covalent bonds. In thermoplastic composites it is still unclear if there is a chemical bond between the glass fibre and the matrix. So, there is a research gap in understanding the nature of bonding in the film former and full sizing when combined with thermoplastic matrices. Pisanova et al. demonstrated that in non-polar PP the adhesion strength determined from micromechanical tests can be effectively controlled by simultaneously modifying both the matrix and the fibre surfaces. This involves creating complementary acid and base sites on the contacting surfaces of the two materials. In another study, Mäder and Pisanova [181] concentrated on the

characterisation and design of interphases in glass fibre-PP, employing fibres sized with APS and fibres overcoated with PU or a MAPP film former dispersion. Their research found that silane-only sized fibres exhibited the highest IFSS levels when subjected to micromechanical testing. Notably, when the same sizing combinations were applied in a one-step process, IFSS values were significantly higher. They postulated that acid-base interaction and interdiffusion were competing bonding mechanisms, yet both contributed to an increase in mechanical strength of the interphase and the final composites. The one-step coating of APS/PP-film former sizing was notably effective, as the measured interfacial strengths correlated well with the macro-mechanical properties of the composites, suggesting that the sizing and interphase design provided a concurrent enhancement of both the tensile strength and the impact toughness in the composite materials. interfacial strength and the composite's macroscopic mechanical properties. The authors proposed that two bonding mechanisms, acid-base interaction and interdiffusion were overlapping and are the reason of the mechanical strength in interphase and composites.

Strategies to enhance interfacial properties of the glass fibre reinforced PP composites typically involve modification of sizing, matrix, or both. This is due to the non-polar nature of PP, therefore PP matrices and PP film former usually contains Homo PP or Copolymer PP and some percentage of MAH. Mäder and Freitag [182] observed through SFPO analysis that the application of different sizings to glass fibres did not alter their IFSS with PP. However, the interfacial strengths appeared to be considerably affected by the PP matrix modification. They investigated ten different sizing with 4 different PPs (PP, MAPP with 5% acrylic acid, PP with irradiated with electron and PP blended with 10 wt% modified PP. IFSS Improvements were noticed in all the modified PP and not in PP. Fraser et al. [183] employed an embedded single filament test to evaluate the effectiveness of various glass fibre sizings. They reported that when silane was used alone at high concentrations, it proved to be the most effective surface treatment for E-glass within resins such as PA6, polyethylene, and MAPP, in terms of IFSS and the protective capabilities of the surface coating. Notably, they pointed out that PVA is usually not considered a suitable film former for thermoplastic compatible glass fibres [1]. This is due to the hydrophilic nature of PVA, leading to poor adhesion with hydrophobic thermoplastics, and its limited thermal stability, which can cause degradation at typical thermoplastic processing temperatures. This study highlighted the efficacy of APS in promoting strong IFSS levels even at elevated temperatures with PA6 and acid-grafted PP, whereas MPS was particularly effective in enhancing IFSS with high-density polyethylene.

Nevertheless, none of the studied silanes, sizing agents, or lubricants were found to significantly improve IFSS with unmodified PP. Nygard et al. [178] explored the influence of sizing on IFSS in glass fibre-PP composites through fragmentation testing. The glass fibres sized with both single-component sizings and full sizings, incorporating APS and azidosilane coupling agents along with PU and PP film formers. They discovered that integrating MAPP into the PP matrix yielded superior IFSS results compared with PP. They concluded that introducing a functionalised PP is essential to fortify the bond strength between a PP matrix and an aminosilane sized glass fibre.

Some researchers focused mainly on the role of film former in sizing. For instance, Thomason and Schoolenberg [184] reported that sizing fibres solely with various silane coupling agents did not result in any improvement in IFSS of PP composites when compared to BF. However, they reported a significant difference in the IFSS results of the fully sized commercial fibres for the PP composites. The IFSS fluctuations were reflected in the flexural strength of unidirectional glass fibre-PP composites, which doubled based on the specific sizing utilised. This flexural strength was directly correlated with the IFSS, indicating a relationship between mechanical performance and the sizing formulation. Scholtens and Brackman [185] extended this line of investigation by examining the chemical nature and molecular mass of the film former on fibre/matrix adhesion. They used XPS and SEM to analyse unidirectional, continuous glass fibre reinforced PP composites. Their principal finding was that the film former is paramount in maintaining the level of fibre/matrix adhesion, attributing its significance to its inability to diffuse from the interface into the matrix. The study also found that most mechanical properties of short fibre reinforced compounds were augmented with an increase in fibre/matrix adhesion. Similarly, Mäder et al. [186] investigated the correlation between fibre surface treatment, interphase, and composite properties, concluding that contact angle and electrokinetic measurements allowed for detecting differences in glass fibre surface treatments. The results also indicated a potential relationship between the thermodynamic work of adhesion and the shear strength during debonding, which was supported by the data from pull-out and fibre fragmentation experiments. Mäder et al. [136] highlighted that an optimum concentration of PP film former is necessary to achieve high composite strength. With the use of SFPO tests and nanoindentation, they reported that the type of film former is a determinant factor for the adhesion strength and the interphase modulus, which in turn correlates with the tensile and Charpy impact strengths of the composites. Studies conducted by Rausch et al. [187] demonstrated that the absence of silane coupling agents in sizings generally results in

poor mechanical performance of composites. Conversely, no significant differences were seen between intermediate and high levels of silane concentration. The film former concentration and glass fibre diameter showed a negative correlation with the interphase strength, underscoring the complexity of sizing development. This suggests that increasing the film former concentration or fibre diameter may not always lead to better performance, and optimizing these variables is critical to achieving strong fibre/matrix bonding. Further, Zhuang et al. [188] showed that sizing E-glass fibres with a combination of APS and a PP film former, followed by boiling water treatment, led to a 30% increase in IFSS as measured by SFPO tests. They demonstrated that the higher IFSS is due to the more polar and hydrophilic surface of the boiled water-treated glass, with homogeneously distributed derivatives of the coupling agent.

The influence of the PP film former's molecular weight on composite bending properties has also been explored by Scholtens et al. [185]. Low molecular weight PP film formers exhibited an amide type bond with the coupling agent, leading to higher bending strength, suggesting that molecular weight plays a crucial role in the interfacial adhesion and, consequently, the mechanical properties of the composites. Larson and Drzal's [102] research into the sizing-matrix interactions and the interphase structure in a liquid composite moulding environment revealed that the chemical nature of the sizing components, including film formers, significantly affects the surface free energy and wettability of the glass fibres, which are critical for the fibre/matrix adhesion.

Thomason [189] has also pointed out that the composition of many commercial sizing agents used for the glass fibre reinforcement of thermoplastics creates a higher likelihood of silane reactions, especially with aminosilanes, among themselves or with other components, rather than with the glass fibre surface. It has also been noted that much of the perceived interfacial strength in thermoplastic composites may be attributed to physical phenomena, such as the residual compressive stresses at the interface of these materials [47, 190, 191], and has presented data on the temperature dependence of interfacial strength in glass fibre-PP composites which appears to support this hypothesis [161].

6.2.2. Sizing thermal stability and chemistry

The endurance of organic materials within sizings at the elevated temperatures required for processing high-performance composites is critical. Rudzinski et al. [86] delved into the thermal degradation behaviour of model E-glass fibre sizings, employing TGA-FTIR and

Pyrolysis-GC/MS. The sizings examined were tailored for polyamide compatible glass fibre reinforcements and used industry-standard concentrations to yield fibres with a LOI of 0.5 wt%. Despite challenges in consistently detecting weight loss from the minute organic sizing on fibres, their findings indicated a distinct peak in weight loss for sizing on the fibre surface during thermal degradation. Ramos et al. [192] scrutinised the stability of sizing raw materials for E-glass fibre production, focusing on an alkalimidazoline lubricant and a polyvinyl acetate (PVA) aqueous homopolymer dispersion acting as a film former. Through differential scanning calorimetry (DSC) and FTIR, they identified abnormalities such as contamination, ageing, or loss of volatiles, all of which could compromise the performance of sized fibreglass. Rheological analysis further revealed substantial changes in these materials after thirty days at room temperature. Yang and Thomason [83] utilised TGA to explore the thermal stability of a broad spectrum of commercial glass fibre products from various suppliers. They observed that sizings compatible with PP degraded when heated between 200 and 250 °C, a process that led to a complete loss of their adhesive qualities with PP. This degradation corresponded with a measured weight loss from aminosilane sized fibres at similar temperatures, suggesting that the reduction in the reinforcement effect of commercial fibres might stem from the thermal degradation of the aminosilane coupling agent. Jenkins et al. [84] and [85] corroborated these findings, noting the degradation of aminosilane on glass and basalt fibres within the 200–300 °C range in their TGA analysis of the thermal stability of epoxy compatible sizes.

Sizing surface chemistry is paramount in composite materials as it directly affects the bond strength between the fibre and the matrix, influencing the mechanical properties and durability of the composite. The effect of PP based sizing on surface chemistry of fibre were studied by some researchers, for instant Kitagawa et al. [193] leveraged Near-infrared (NIR) light-fibre optics spectroscopy to investigate sizing on glass fibres, specifically analysing the interaction between an aminosilane coupling agent and a MAPP binder. They examined two glass fibre samples with varying molecular weights of MAPP. Their study using NIR spectroscopy detecting the formation of an amide bond between the MAPP binder and the aminosilane on the glass fibre surface, offering insights into the chemical interactions at play on the sizing-coated glass fibres.

6.2.3. Sizing film formation

Research on the formation of sizing films has been relatively sparse, yet the process of creating film from polymer solutions is generally straightforward, given that the polymer exists in a

dissolved state. The film formation process involves spreading a polymer solution or emulsion onto a substrate, followed by the evaporation of the solvent, which allows the polymer chains to be build and form a continuous film. During this phase, the polymer transitions through a gel-like state before ultimately forming a solid film with continued drying. Film formation is influenced by several factors, including the composition of the polymer and substrate, as well as physical characteristics like particle size and the quality of the dispersion. Environmental conditions such as temperature and humidity also play a critical role, particularly because they affect the rate of solvent evaporation, a crucial aspect in the film formation process for both polymeric solutions and dispersions. McGravey [194] conducted an assessment of the film-forming capabilities of vinyl acetate-based sizing formulations, among other properties. In his observations, he noted that film formers consisting of larger particle sizes tended to create uneven films. This was attributed to the insufficient diffusion of particles during the film-forming process. Such unevenness in the film, caused by larger particle sizes, led to a film that was more optically active and exhibited a faster rate of wetting. Eriksson-Scott's research, as referenced in document [195], focused on the stabilization of trialkoxysilanes in aqueous solutions using surfactants to inhibit self-condensation. This study involved a comparative analysis of film quality derived from sixteen different trialkoxysilane emulsions/mixtures, with evaluations conducted via SEM, AFM, and electrochemical impedance spectroscopy. The chemical behaviours within the emulsions were monitored by observing the hydrolysis and condensation reactions of silanes in water. The study found that incorporating surfactants extended the working life of certain trialkoxysilane emulsions to beyond three weeks.

6.2.4. Literature conclusion

The collective research within the literature on thermoplastic sizing highlights the multifaceted role of film formers and full sizings in determining the mechanical performance of composite materials. Film formers are established as vital in protecting glass fibres during their production and handling, but they also significantly affect the interphase within thermoplastic matrices, directly influencing the strength and durability of the final composite product. It is also clear that both matrix and film former modification are required in order to improve the interfacial and mechanical properties of glass fibre/PP composites. However, it remains unclear whether the bond between the fibre and matrix, which includes sizing with a film former, is chemical or merely physical in nature.

The literature indicates that for PP-compatible sizings, factors such as the type of film former and silane, the molecular weight and particle size of the film former, and the concentration of the sizing, all influence the properties of thermoplastic composites. Additionally, the thermal stability of the sizing material is crucial for optimal composite performance. However, the research exploring these factors is limited and warrants more systematic investigation.

In addition, there is a notable lack of thorough published studies on the quality of sizing emulsions/solutions and the characterization of the sizing. Hence, there is considerable scope for further research in this area.

6.3. Experimental Procedure

6.3.1. Material

APS was purchased from Sigma-Aldrich. Film former aqueous emulsions were supplied by Sisecam who had sourced the emulsions from two different suppliers, i.e., Supplier 1 (S1) and Supplier 2 (S2), who are anonymous for confidentiality reasons. The fibre coating experiments were conducted using bare E-glass fibres taken from a large roving supplied by Sisecam. The PP (PETOPLEN EH102) and MAPP (Polybond® 3200) were supplied by Petkim and Addivant, respectively. Industry E-glass fibres sized with a proprietary sizing compatible with PP thermoplastic polymers were also used for comparison purposes. They were supplied by Sisecam and the sizing formulation was not declared due to the commercial sensitivity.

6.3.2. Film former and full sizing coating procedures

Prior to preparing 100 grams of sizing, the non-volatile content of the film formers and APS was measured by drying 10 gr of each of them in an oven. Due to the confidentiality of the components used in this study, the specific amounts of the non-volatile content cannot be disclosed. However, the formulations were designed to contain a total of 10% solids. To create 100 grams of sizing, the process involved the following steps: initially, 1.6 grams of APS were mixed with 50 gr deionised water and agitated for 10 minutes (Figure 6.1a). Subsequently, 24.2 grams of film former emulsion were added to the mixture along with deionised water, resulting in a total of 100 grams of sizing with a solids concentration of 10 wt% (Figure 6.1b). The solid content of the sizing for the spin coated and dip coated fibres was measured and maintained at 10%, which is also common for industrial sized fibres. Furthermore, the pH levels of the sizing solution were monitored and typically found to range from 9 to 10, as depicted in Figure 6.1c. The investigated fibres and sizing formulations are summarized in Table 6.1 As described in

chapter 4, dip coating and spin coating techniques were used for applying the in-house prepared sizes on the BF. For dip coating, 15 cm fibre bundles were left in the emulsion for about 15 min, and all the spin coated fibres (10 cm in length) were under 10000 rpm rotation speed. This speed gives the lowest LOI% (1.0%) which was close to the industrial sized fibre (0.8%) that was used in this thesis.

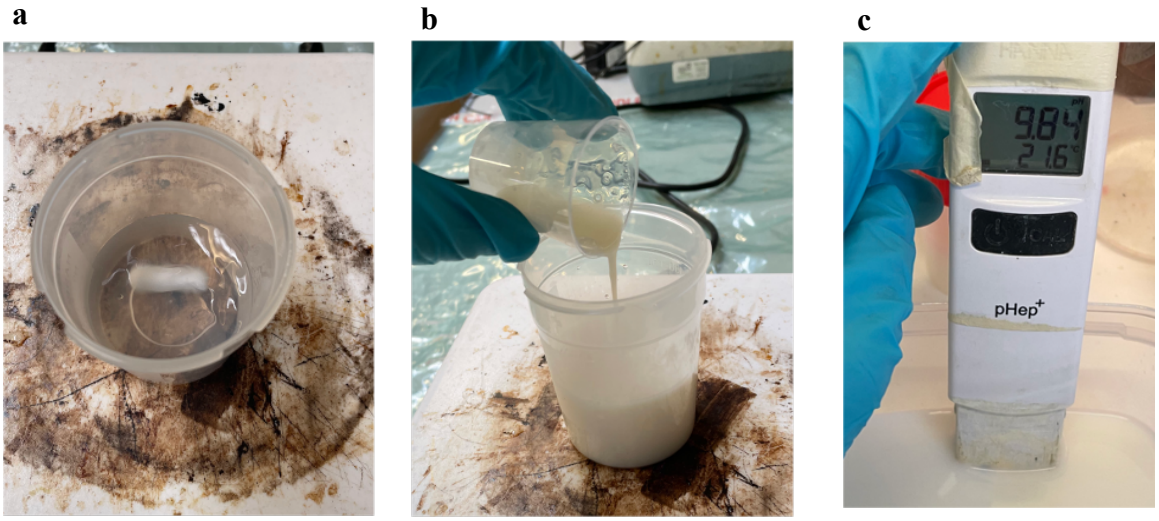

Figure 6.1.a) APS solution b) Film former added c) pH check.

Table 6.1. Summary of fully sized industrial and in house sized fibres.

Designation	Sizing		Molecular weight (g/mol)	Sizing concentration (wt%)	Sizing Solids (wt%)	Mean fibre diameter (µm)
BF	Bare (water size)		_	_	_	17.0
IS	Industry sized PP compatible	Unknown	_	_	_	17.5
S1A	Copolymer PP with medium percentage of Maleic Anhydride	APS	~30000	25.8%, 2.6%,	10%, 1%	17.0
S1B	Copolymer PP with low percentage of Maleic Anhydride	APS	~80000	25.8%	10%	17.0
S2A	HomoPP with low percentage of Maleic Anhydride	APS	~60000	25.8%	10%	17.0
S2B	Copolymer PP with low percentage of Maleic Anhydride	APS	~60000	25.8%	10%	17.0

6.3.3. Effect of silane on sizing emulsion stability

There is a lack of standardized assessment methodology for sizing stability. One way to assess the quality is to ensure that the sizing (combinations of film former, silane and other additives) remains stable in water. Additionally, it is imperative that every component of the sizing retains its initial composition for the whole of the sizing's useful life [196]. To assess the impact of APS concentration on sizing stability, a visual inspection was conducted using the S1A sizing at various APS concentrations. For each test, the amount of film former was kept constant at 24.2 grams, while the APS was varied at 0.2 grams, 1.6 grams (the original formulation with 10 wt% solids), 10 grams, 40 grams, and 60 grams. The process of preparing these mentioned sizings followed the same procedure as the original sizing preparation outlined in section 6.3.2. These emulsions were placed in closed glass bottle containers and observed over a period of two hours.

6.3.4. TGA

TGA analysis were performed on IS, dip coated and spin coated S1A, S1B, S2A and S2B fibres, as described in chapter 3.5.

6.3.5. FTIR

FTIR analysis were performed on IS, dip coated and spin coated S1A, S1B, S2A and S2B fibres and dried sizing films, as described in section 3.7.

6.3.6. Microbond

The microbond test, as outlined in chapter 3, Section 3.1, was conducted utilizing both IS, dip coated and spin coated S1A, S1B, S2A and S2B fibres, with two thermoplastic polymers: PP and MAPP.

6.3.7. Sizing film formation

To examine the possibility of making a thin film from the film formers and the complete sizing formulations, 5 grams of each diluted film former and full sizing (S1A, S1B, S2A, and S2B) were placed in aluminium cups and dried at two different temperatures, 110 °C and 165 °C, to assess film formation at varying temperatures. Efforts were also made to form sizing films on glass Petri dishes and microscope slides. The film formation capability of both the film formers

and sizing films is documented in this chapter. Furthermore, the structure of the dried sizing was observed using an optical microscope (Leitz Ergolux microscope) at 200x magnification. In addition, a crystallized structure was noticed in one of the sizing (S2A), captured using a polarized microscope (Olympus BX) with 100x and 200x magnification. Consequently, the sizing was applied to a bare glass fibre, and then microscopy observation was used to check if the same crystallization happening in the fibre surface. Images of normal and polarised microscopy of dried size are shown in Figure 6.2, showing the difference between these two techniques. The polarized imaging showed better crystalised structures, therefore only the polarised images are reported here.

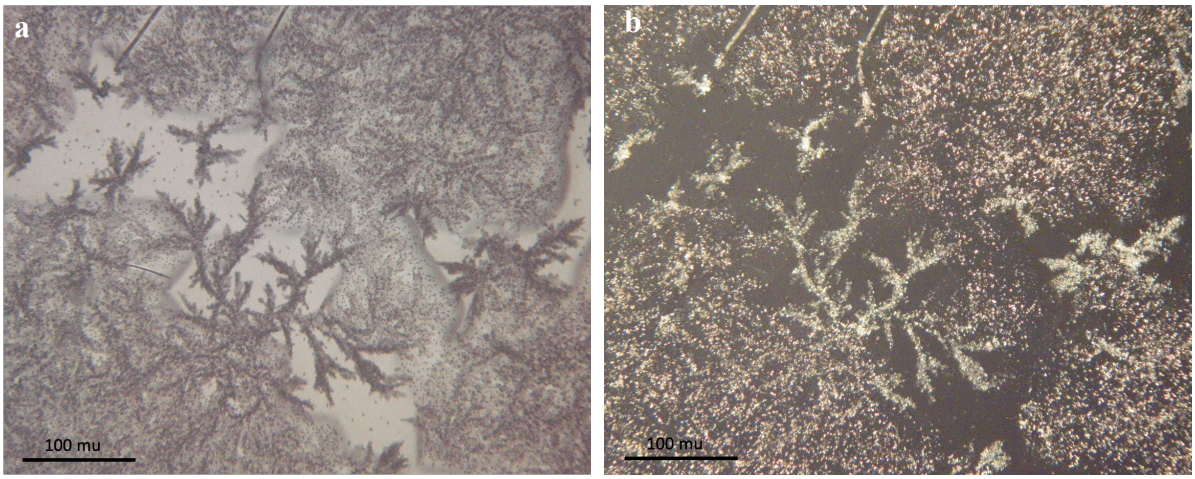

Figure 6.2. a) Nonpolarized and b) polarised microscope image comparison.

6.4. Results and discussion

6.4.1. Sizing emulsion stability characterization

A straightforward method for assessing emulsions, including those containing film formers and sizing agents, is through visual inspection. This section focuses on evaluating the stability of the full sizing by varying the concentration of the silane component, specifically APS, within the emulsion [197]. Figure 6.3 displays photographs of the sizing emulsion at differing concentrations of silane, captured immediately after placement in the container and again after resting undisturbed for two hours. From the pictures, a colour shift is noted at the sizing with 10% APS and higher, with a more pronounced phase change occurring at 60% APS concentration. The observed colour change, which was more obvious in sizing with 10% and more APS, could be a result of the chemical reactions taking place between APS and film former during the formation of the sizing solution. These reactions typically lead to the

formation of silanol groups and their subsequent condensation, which could cause a visual change in the solution.

Additionally, a correlation between APS concentration and temperature increase during the solution preparation process was observed. For instance, the temperature in solutions with 0.2% and 1.6% APS concentrations rose immediately from 23.5 °C to approximately 24.6 °C. Furthermore, a 10% APS solution reached 28 °C, while solutions with 40% and 60% APS showed more significant temperature rises to about 38.2 °C and 40.0 °C, respectively. Post-agitation, the solutions cooled slightly but exhibited another increase in temperature upon the addition of the MAPP film former. For example, the temperature of the 60% APS solution initially dropped to 34 °C before rising again to 37.9 °C.

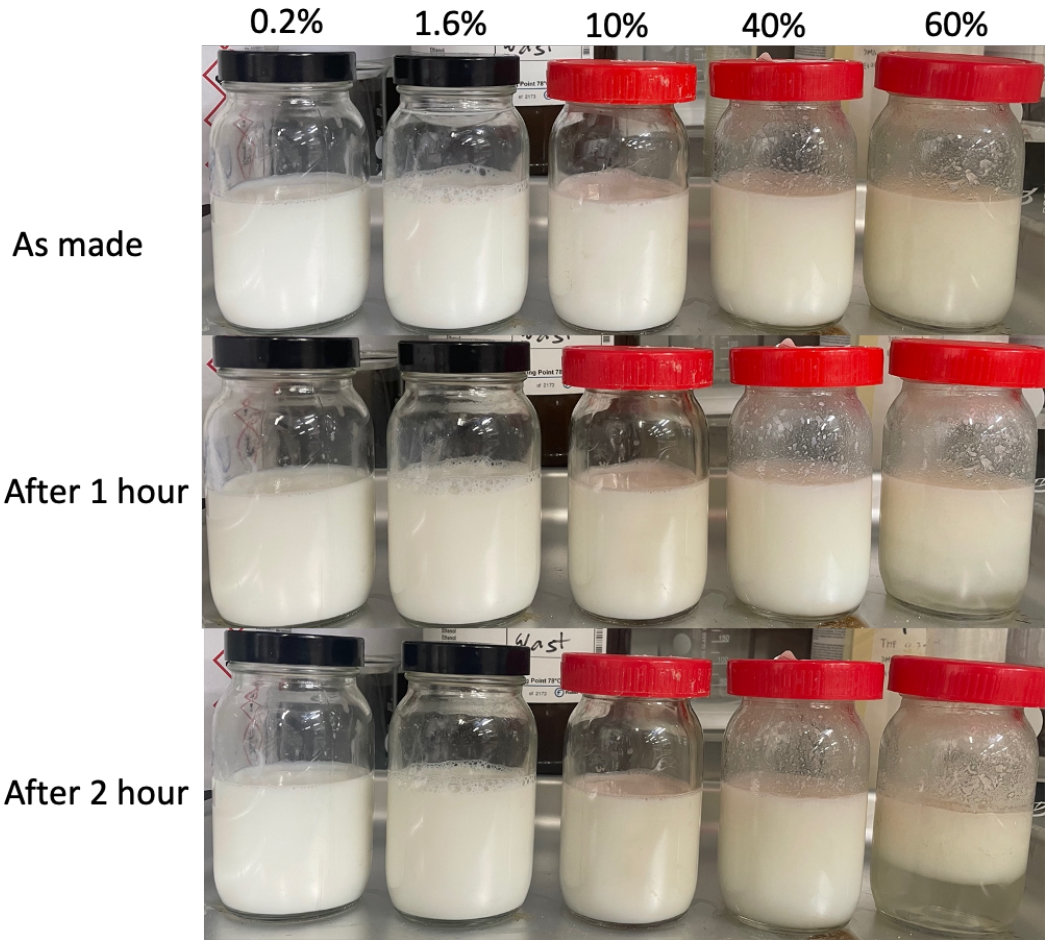

Figure 6.3. Sizing emulsion with different APS concentration at different times.

The increase in temperature is a consequence of the exothermic nature of the hydrolysis and condensation reactions of APS [198]. As the concentration of APS increases, the number of reactive sites multiplies, leading to more heat being released. This is why higher concentrations

of APS result in greater temperature rises. The initial drop in temperature after agitation is likely due to the dissipation of heat from the solution to the environment. When the film former, which may be at a lower temperature, is added to the high-concentration APS solution, it absorbs some of the heat. This temporarily lowers the solution's temperature, before the exothermic reactions of the film former with APS, causing the temperature to rise once more. This second temperature rise might be due to some interaction between APS and the film former.

The phase change observed at higher concentrations is indicative of a new chemical environment within the solution. As APS content increases, it may lead to a saturation point where the solution cannot maintain homogeneity, resulting in phase separation. Observing the colour and phase changes in the final sizing emulsion can serve as an effective method for assessing the quality of the sizing formulation. Before its application, such evaluation ensures that the sizing emulsion meets the required standards such as emulsion homogeneity which is crucial for maintaining consistency and performance in the finished composite product. These visual indicators, when coupled with temperature readings, provide a preliminary check that can prevent the use of suboptimal sizing mixtures, thereby safeguarding the integrity of the manufacturing process from the outset.

6.4.2. TGA of fully sized glass fibre

Figure 6.4 compares TGA and DTG results for the four-spin coated and dip coated fibres with different sizing formulation as mentioned in Table 6.1. All these fibre samples in Figure 6.4a exhibit a single major weight loss event in the temperature range 200–300 °C, and the graphs follow a very similar pattern. A slight weight increase observed in the 25–100 °C temperature range can be attributed to an experimental artifact. This effect was not fully eliminated by the baseline subtraction procedure, likely due to the extremely small sample mass involved in the measurement [16, 88]. The peak in the differential mass change data number for IS and spin coated fibres is between 223 °C and 228 °C, signifying the maximum rate of weight change. Thomason et al reported similar TGA degradation results from a range of industrial coated PP compatible glass fibre products and suggested that the majority of the weight loss between 200-300 °C appears to be due to degradation of the MAPP film former and the aminosilane coupling agent [83]. Given that the exact formulation of the sizing on IS, is unknown and that the exact composition of the film former emulsions used in this work are also unknown, due to industrial confidentiality, then the similarity in these results is notable. Thomason published a review of

industrial sizing formulation patents and also noted that the same two principal constituents of most PP compatible sizings (from different fibre manufacturers) does consistently appear to be MAPP and APS [1]. In the TGA graph of PP compatible sizing (see Figure 6.4c), for the dip coating, the weight loss is observed in the temperature range of 200–350 °C in all the sizing formulations. In all the DTG curves (Figure 6.4d) appear to exhibit two overlapping thermal degradation events, a “low temperature” event and a “high temperature” event peaking around 225 °C, and a “high temperature” event peaking around 280 °C. It is also interesting to note that there is a clear difference in the DTG curves of the dip coated and spin coated fibres. The dip coated samples have two peaks, while the spin coated sample has one peak, which is believed to be due to the sizing lost component or sizing sling off, during the higher speed spin coating. Further analysis such as XPS is required to better understand the reason behind this difference. Table 6.2 summarises all the LOI values, onset temperature and first derivative peak temperatures of the investigated fibres.

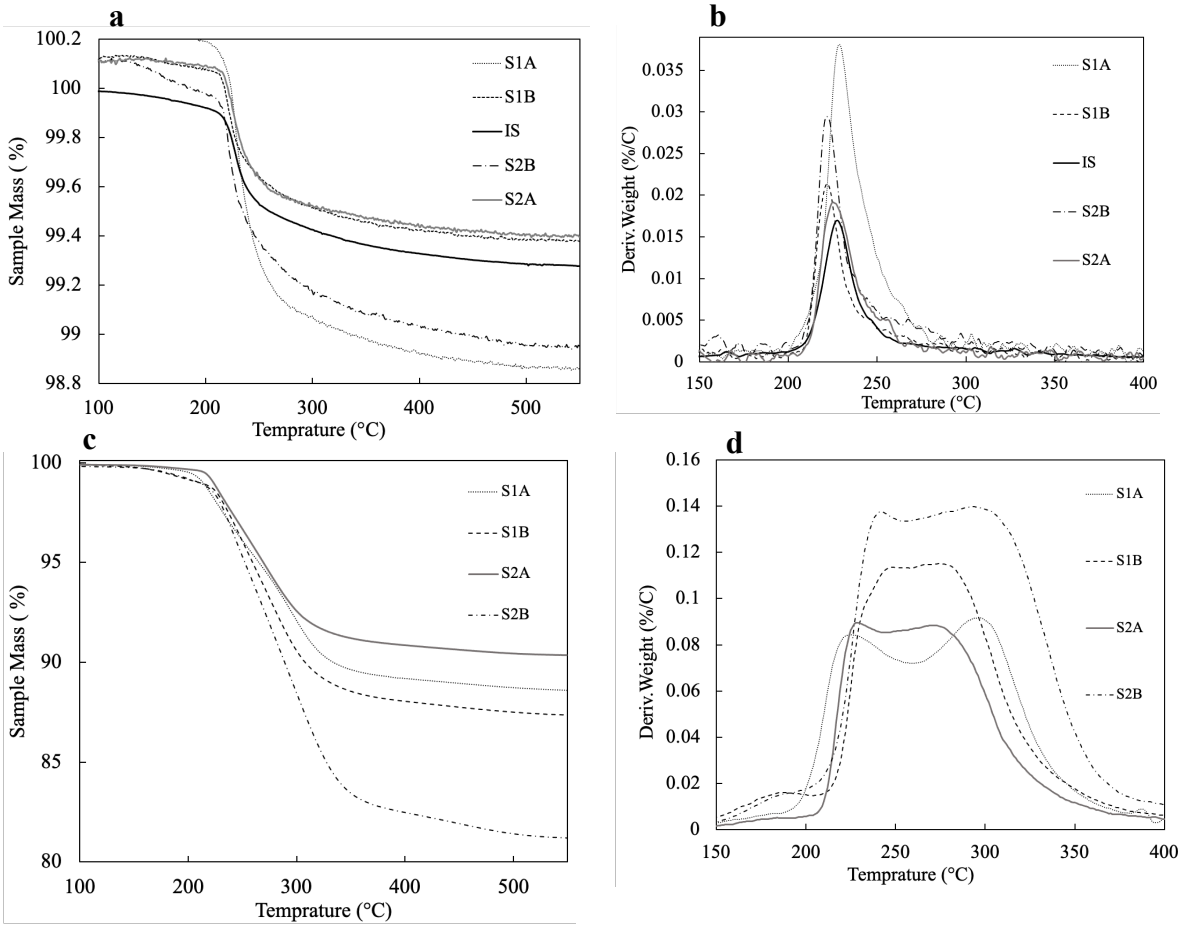

Figure 6.4. Comparison of TGA and DTG results i.e., a) TGA of 4 different spin coated fibre and IS, b) DTG of 4 different spin coated fibre and IS c) TGA of 4 different dip coated fibre and IS d) DTG of 4 different dip coated fibre and IS.

Table 6.2. TGA LOI of fully sized glass fibres using spin and dip coating.

Fibres	TGA LOI (%)	T_{onset} (°C)	Peak 1 (°C)	Peak 2 (°C)
IS	0.8	223	223	_
Spin S1A	1.0	212	225	_
Spin S1B	0.6	215	226	_
Spin S2A	0.6	217	228	_
Spin S2B	1.0	216	223	_
Dip S1A	11.3	211	227	303
Dip S1B	12.5	225	247	286
Dip S2A	9.6	220	237	284
Dip S2B	18.6	225	249	306

6.4.3. FTIR Analysis

FTIR spectra of the investigated IS, is shown in Figure 6.5. The PP existence of film former is validated through the formation of several prominent bands of 2950 cm^{-1}, 2918 cm^{-1} and 2870 cm^{-1}, which correspond to CH stretching, whereas, band 1375 cm^{-1} refers to stretching of CH_3. The spectral region between 1200–800 cm^{-1} prominently featured the high-intensity Si-O-Si signal originating from the glass fibres. In the case of IS fibres, the sizing thickness layer is notably low, rendering the MAPP spectral bands, typically found within the 1200–800 cm^{-1} range, invisible. Despite the lack of clarity regarding the formulation of the sizing for IS fibres, it can be assumed that MAPP should be present given its compatibility with PP. To delve deeper into the chemistry of PP-compatible sizing, an initial investigation involved applying the four film formers developed in this thesis to the fibre bundle through the dip coating technique. This approach was chosen to create a more substantial sizing layer, resulting in increased signal intensity in FTIR analyses. Figure 6.6 displays the spectra of the four dip coated fibres treated solely with film formers, namely S1A, S1B, S2A, and S2B.

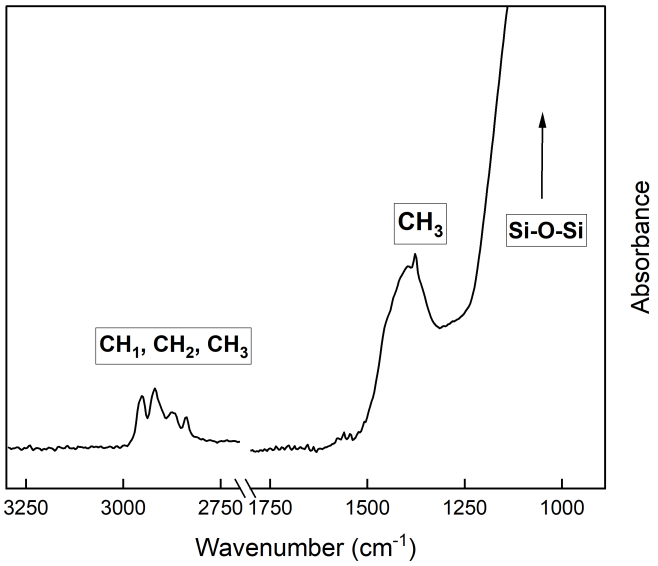

Figure 6.5. FTIR spectra of the PP compatible industrial sized (IS) fibre.

The MAPP film former-coated fibres exhibit distinct band assignments characterized by a triplet pattern with peaks at 2950, 2918, and 2836 cm^{-1}, corresponding to the C-H stretching vibrations of CH, CH_2, and CH_3 groups, respectively, which are indicative of PP. In chapter 5, section 5.4.2 the silane spectra featured doublet peaks at 2929 and 2856 cm^{-1}, and it is plausible that these peaks overlap with those associated with PP. The multipeak at 1800–1500 cm^{-1} (1703 cm^{-1}, 1646 cm^{-1}, 1560 cm^{-1}, 1545 cm^{-1}) were apparently due to the C=O vibration of the MA groups. The bands at 1450 cm−1 and 1373 cm^{-1}, and 998 cm^{-1} are characteristic peaks of PP which exhibit the $–CH_2$ bending vibration, $-CH_3$ bending vibration and $–CH_3$ rocking vibration, respectively [199]. The 1200–800 cm^{-1} spectral region was dominated by the high- intensity Si-O-Si signal from the glass fibres.

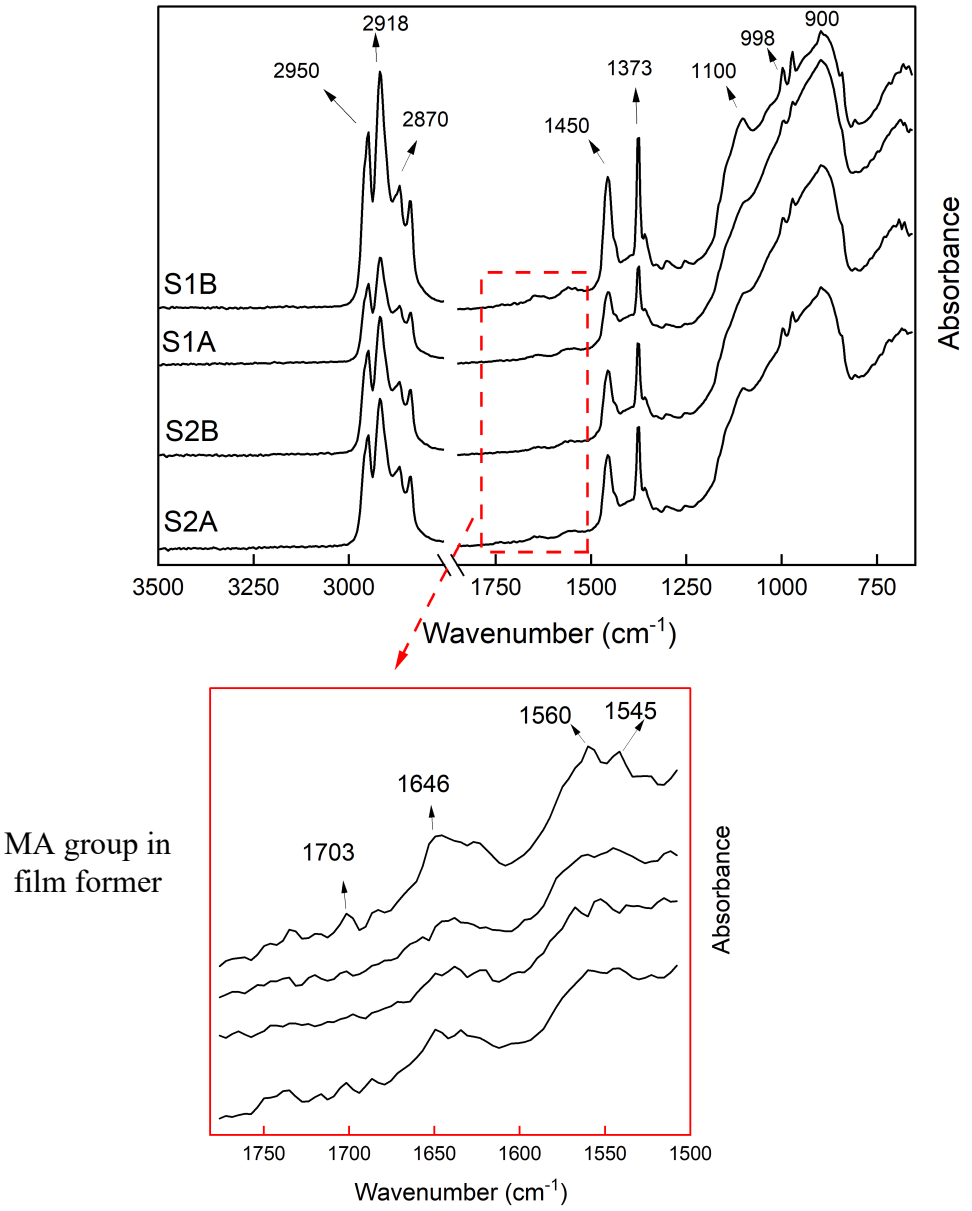

Figure 6.6. FTIR spectra of the dip coated MAPP film former only fibres.

Table 6.3. Spectral characteristics of film former coated glass fibres.

Band (cm^{-1})	Assignment
800–1200	Si-O-Si
998	$-CH_3-$ rocking
1373	$-CH_3-$ symmetric bending
1450	$–CH_2–$ symmetric bending
1545	C=O
1560	C=O
1646	C=O
1703	C=O
2950, 2918, 2836	C-H stretching of CH, CH_2 and CH_3

FTIR spectra of the investigated PP compatible sized glass fibres, which were dip and spin coated are shown in Figure 6.7. Band assignments attributable to all the PP coated fibres are a characteristic triplet showing peaks at 2950, 2918, and 2836 cm^{-1} assigned to the C-H stretching of CH, CH_2, and CH_3, respectively. Peaks at 1023 are attributable to C-O stretching of the Maleic anhydride. The 1200–800 cm^{-1} spectral region was dominated by the high- intensity Si-O-Si signal from the glass fibres. Accordingly, the fingerprint region was generally eclipsed for spin coated fibres which has a lower sizing thickness layer. MAPP spectral bands in the 1200–800 cm^{-1} range became visible as the sizing layer thickness approached the minimum penetration depth of the instrument (500 nm) in the dip coated fibres. Spectral bands associated with MAPP visible in the 1200–800 cm^{-1} region is 1032 cm^{-1} (assigned to the C-O-C stretching of ethers) and 910 cm^{-1} (assigned to the C-O stretching of the oxirane ring).

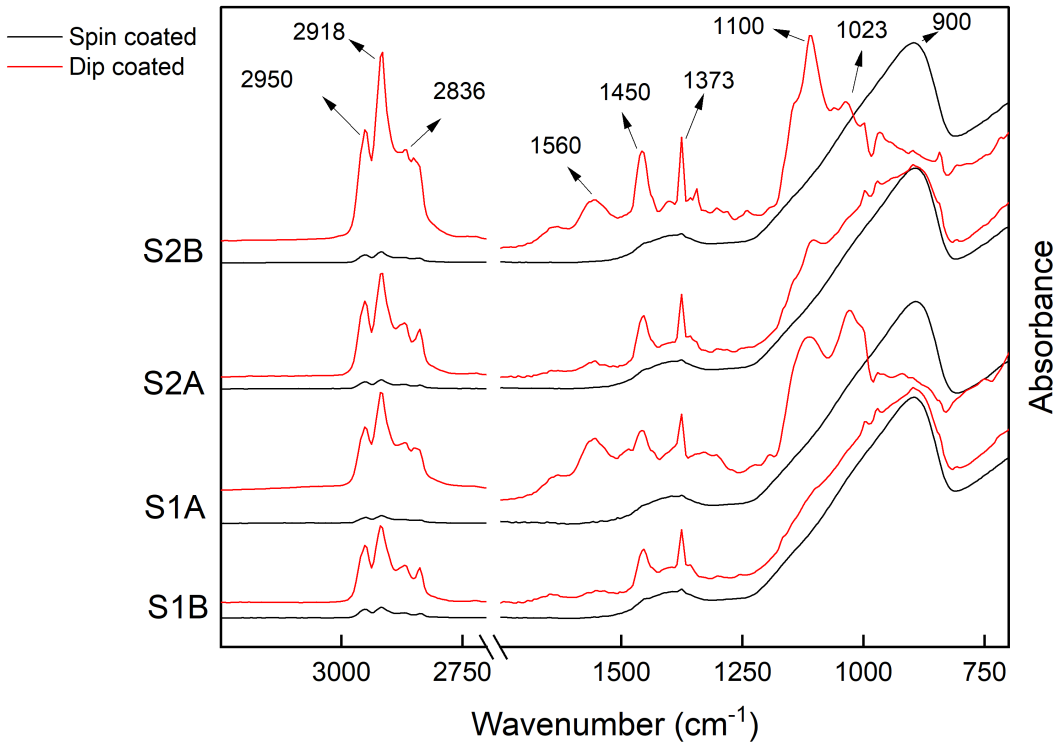

Figure 6.7. FTIR spectra of the investigated PP compatible sized glass fibres, which were dip and spin coated.

Table 6.4. Spectral characteristics of fully sized spin and dip coated glass fibres.

Band (cm^{-1})	Assignment
800–1200	Si-O-Si
1023	C-O stretching
1373	$-CH_3-$ symmetric bending
1450	$–CH_2–$ symmetric bending
1560	C=O stretching
2950, 2918, 2836	C-H stretching of CH_2, CH_3

To assess the chemical groups within the sizing, an alternative method was employed, involving the drying of the sizing material, without applying to the fibre, followed by FTIR analysis. The primary objective was to mitigate the presence of the high Si-O-Si signal (800-1200 cm-1) typically observed in sized glass fibres. By eliminating the silica peaks, the spectra

within this range became more discernible. Figure 6.8 illustrates the dried full sizings (film former and APS) under investigation.

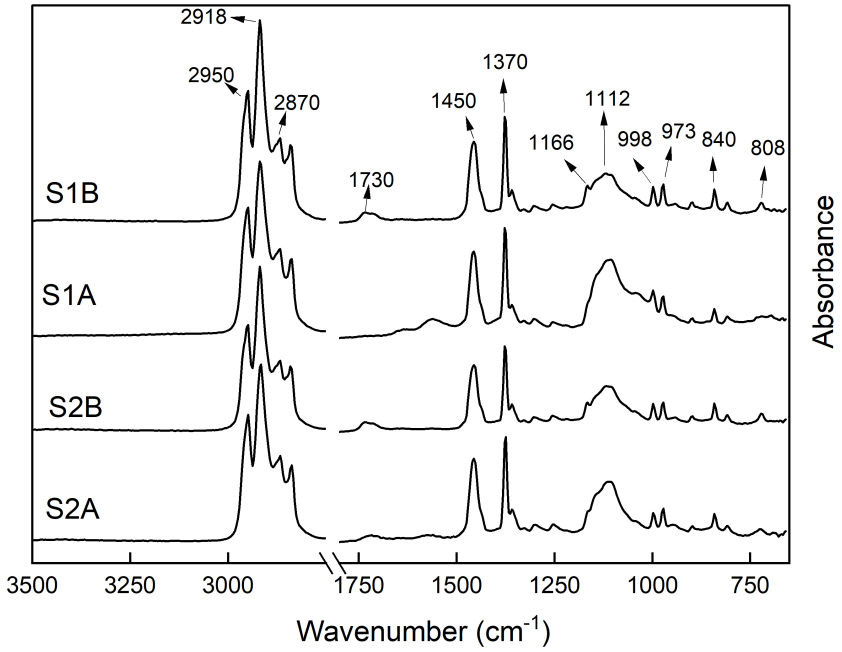

Figure 6.8. FTIR spectra of the investigated full sizing after drying.

The peaks at 2950, 2918, and 2836cm^{-1} assigned to the C-H stretching of CH, CH_2, and CH_3, respectively, can be also seen in all the dried full sizings as we had them in film former and fully sized fibres, which attributes to PP. The band at 1730 cm^{-1} is assigned to the absorption of carbonyl groups (C=O) of maleic anhydride. The two intensive peaks at 1450 cm^{-1} and 1370 cm^{-1} were assigned to the C–H bending vibration of PP backbone. The peaks between 800 to 1200 are also attribute to PP and MA. Table 6.5 summarizes and compares the peaks observed in APS sized fibres, as reported in chapter 5, with those of the fibres sized with film former only, fully sized fibres, and dried full sizing.

Table 6.5. Spectral characteristics summary of APS sized, FF only sized, fully sized spin and dip coated glass fibres and dried full sizing.

Band (cm-1)	Assignment	APS sized fibre	FF sized fibre	Fully sized fibre	Dried full sizings
800–1200	Si-O-Si	✓	✓	✓	
808	=C-H bending				✓
840	OH- symmetric stretching				✓
973	-CH_2- rocking				✓
998	-CH_3- rocking		✓		✓
1023	C-O stretching				✓
1112	C=O asymmetric stretching				✓
1166	-CH_3- symmetric deformation				✓
1370 and 173	-CH_3- symmetric bending		✓	✓	✓
1450	C–H bending		✓	✓	✓
1545	N-H stretching		✓		
1560	C=O stretching		✓	✓	
1646	C=O stretching		✓		
1703	C–H bending		✓		
1730	C=O stretching				✓
1740	C=O stretching	✓			
2856 and 2950	C-H stretching of CH_1	✓	✓	✓	✓
2918 and 2926	C-H stretching of CH_2	✓	✓	✓	✓
2836	C-H stretching of CH_3		✓	✓	✓

6.4.4. Microbond results

The IFSS BF, fibres sized with film former only, APS, and S1A-sized fibres, using spin coating technique, with both PP and matrices are evaluated and compared. Figure 6.9 illustrates the IFSS results for the investigated fibres.

The analysis reveals that glass fibres sized solely with film former demonstrated suboptimal IFSS values. Within the MAPP matrix, the IFSS for FF-sized fibres was recorded at 17.3 MPa, which is marginally lower than that of the BF at 18.3 MPa. A similar trend is observed in the PP matrix, where FF-sized fibres presented an IFSS of 6.7 MPa, compared to the BF's IFSS of 5.3 MPa. These results indicate that the application of a film former as the sole sizing agent is insufficient to significantly enhance the adhesion between the fibre and the matrix. In contrast, the inclusion of APS in the sizing formulation notably improved the IFSS in both the PP and MAPP matrices. For APS-sized fibres, the IFSS was elevated as 24.2 MPa in the MAPP matrix and to 12.3 MPa in the PP matrix. This substantial increase underscores the efficacy of APS as a sizing agent in strengthening the interfacial bond. Moreover, fibres subjected to the full S1A sizing exhibited an IFSS of 22.6 MPa in the MAPP matrix and 13.1 MPa in the PP matrix. This enhancement suggests that a comprehensive sizing strategy, likely including APS among other components, is more effective than the application of a film former alone. Scholtens et al. [185] demonstrated in their study on PP compatible sizing that the ideal film former and silane coupling agent promote enhanced fibre/matrix adhesion through some chemical reactions or strong (acid-base) interactions. This increased adhesion is achieved by the silane reacting chemically with the glass surface and by the interdiffusion of the film former and/or coupling additive into the matrix. Mäder and Pisanova [82] reported similar findings in glass fibre/ PP composites using a two-step fibre sizing approach. They coated glass fibres with APS, followed by an additional coating of either PU or MAPP film former dispersion. IFSS was assessed using a microbond test with PP and PP modified with 2% MAPP. In the two-step sizing process, fibres treated solely with silane demonstrated the highest IFSS levels in the microbond test. However, when the same sizing combinations were applied in a one-step process, IFSS values approximately doubled. The authors suggested that, in the one-step process, acid-base interactions and interdiffusion mechanisms were simultaneously at play, leading to increased interfacial strength and composite mechanical properties. Particularly effective was the one-step application of APS with a PP film former. The measured interfacial strengths were found to correlate closely with the overall mechanical properties of the composites. In a study by

Mäder et al. [200], the role of film formers in the mechanical performance of injection-moulded glass fibre/PP composite was investigated. They examined fibres treated with APS and coated with either PU dispersion or polypropylene PP dispersion film formers. The adhesion strength, assessed using SFPO tests, exhibited a notable dependence on the type of film former employed. For MAPP and differently sized glass fibres (APS/PU, APS/PP), the predominant mechanisms involved morphological changes in the interphase, in addition to a fundamental level of acid-base interaction between the basic amino groups on the silanized glass fibre surface and the acidic groups of the MaH in matrix. The choice of film former significantly altered the interphase, consequently affecting adhesion strength. The highest adhesion strengths observed with APS/PP-sized fibres corresponded with the highest tensile and impact strengths in the injection-moulded specimens. In another study by Mäder [136] the same results in glass fibre/epoxy composites, glass fibres were sized using only polyvinyl alcohol (PVOH) or a PVOH/PVA mix, solely with the APS coupling agent, or with full sizings that included APS along with a polyurethane or epoxy film former. Surface energy was evaluated using dynamic wetting measurements, and the pull-out test was employed to assess adhesion between the fibre and matrix. It was noted that fibres sized solely with a film former showed IFSS values 6–12 MPa lower than those of unsized fibres. In contrast, fibres with only the APS coupling agent displayed the strongest interfacial adhesion. The addition of APS with PU film former did enhance IFSS, though not as effectively as the coupling agent by itself, while the combination of APS with an epoxy film former resulted in IFSS values comparable to those of unsized fibres. The superior interfacial adhesion observed in the APS-only samples was ascribed to the robust interaction between the amino groups in APS and the epoxy matrix, coupled with the non-occurrence of film former swelling or dissolution.

The increased IFSS values associated with APS and S1A full sizing can be attributed to the morphological changes in the interphase, in addition to a fundamental level of acid-base interaction between the basic amino groups on the silanized glass fibre surface and the acidic groups of the MaH in MAPP matrix [200] . These alterations facilitate enhanced mechanical interlocking and chemical bonding with the matrix polymers. The difference in performance between the MAPP and PP matrices further suggests that the anhydride groups in MAPP provide additional reactive sites for chemical bonding with the sizing components specially APS.

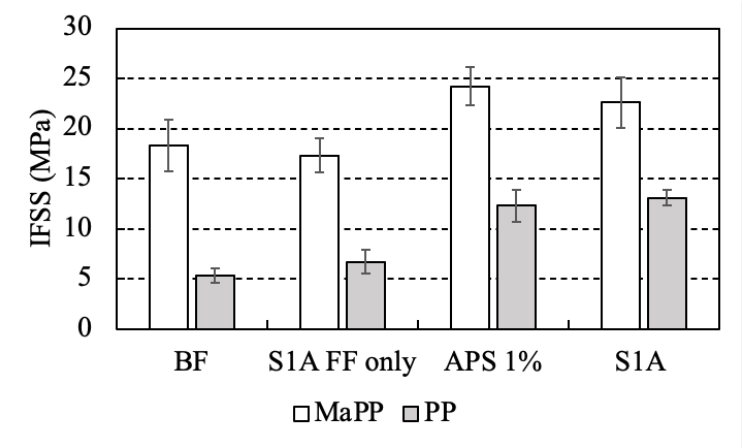

Figure 6.9. The IFSS BF, fibres sized with FF only, APS, and S1A-sized fibres, with PP and MAPP.

The IFSS results for sizing systems containing the different film former emulsions with MAPP are shown in Figure 6.10. In all the MAPP matrix systems, excluding S2A, it was observed that spin coated fibres exhibited a relatively higher average IFSS compared to the dip coated samples. At a 95% confidence level, no significant difference was found between the IFSS of spin coated fibres and IS, which had an IFSS value of 21.3 MPa. Comparing the spin coated fibres the S1A sizing have the highest IFSS value among all the spin coated fibres. This is because the amount of MAH is higher in S1A film former and sizing which could cause such a result. The SA1 also have the lowest molecular weight among the film formers, however it is still not clear if this factor plays a role for these results or not, and needs to be investigated more.

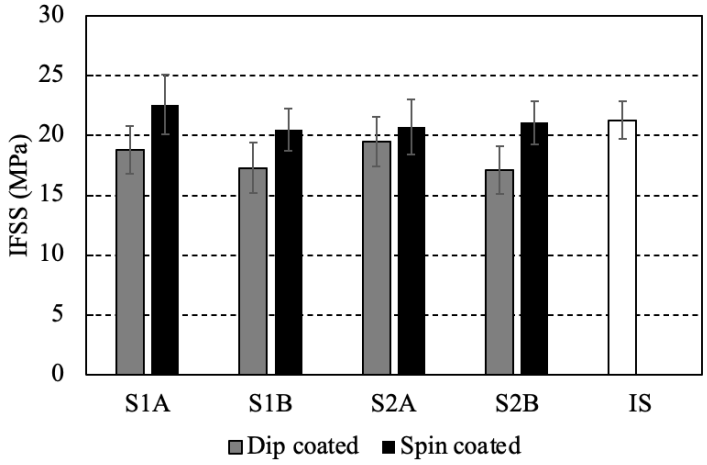

Figure 6.10. IFSS results for sizing systems containing the different film former emulsions with the MAPP matrix.

When analysing the IFSS results of the PP matrix systems (Figure 6.11) statistically, it was noted that spin coated S1A displayed a significantly (at 95% confidence level) higher IFSS compared to dip coated S1A. However, no significant differences were observed for the remaining systems. The IFSS value for IS, approximately 10.5 MPa, was closer to the IFSS of dip coated S1A and S2A fibres, and lower than that of spin coated fibres. The IFSS improvement in some systems might be due to the decrease in the thickness of the sizing layer. This is in agreement with previously published work [17], where in the thin sizing layer, a few random lumps of matrix on the sized fibres surface contribute to increased IFSS and increased friction. On the other hand, when the sizing layer is thick, the size acts as a cushion for the matrix lumps on the fibre thereby reducing the frictional stresses and IFSS.

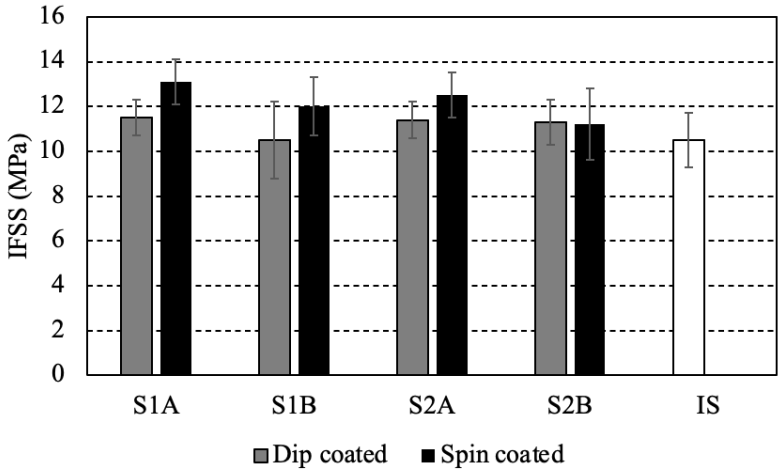

Figure 6.11. IFSS results for sizing systems containing the different film former emulsions with the PP matrix.

6.4.5. Film former and sizing film formation

6.4.5.1 film formation in aluminium container

This section investigated the film formation properties of MAPP film former emulsions and a full sizing mixture consisting of MAPP film former and APS silane, both using the original sizing formulation with 10% solids content. It was observed that heating the film formers and full sizing to temperatures below the melting point of MAPP, which is almost 160 °C, does not lead to film formation. This is illustrated in Figure 6.12, for film former emulsion, and 6.13, for full sizing, where no film was produced at temperatures below 160 °C. As the temperature exceeds 160 °C, the film formers begin to melt, as shown in Figure 6.13a, and upon cooling, a film is successfully formed (Figures 6.13b and c).

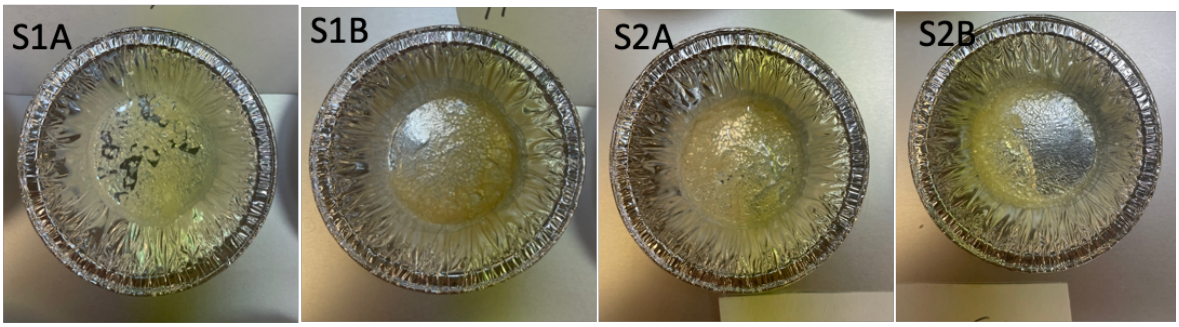

Figure 6.12. Film formers dried at 110 °C

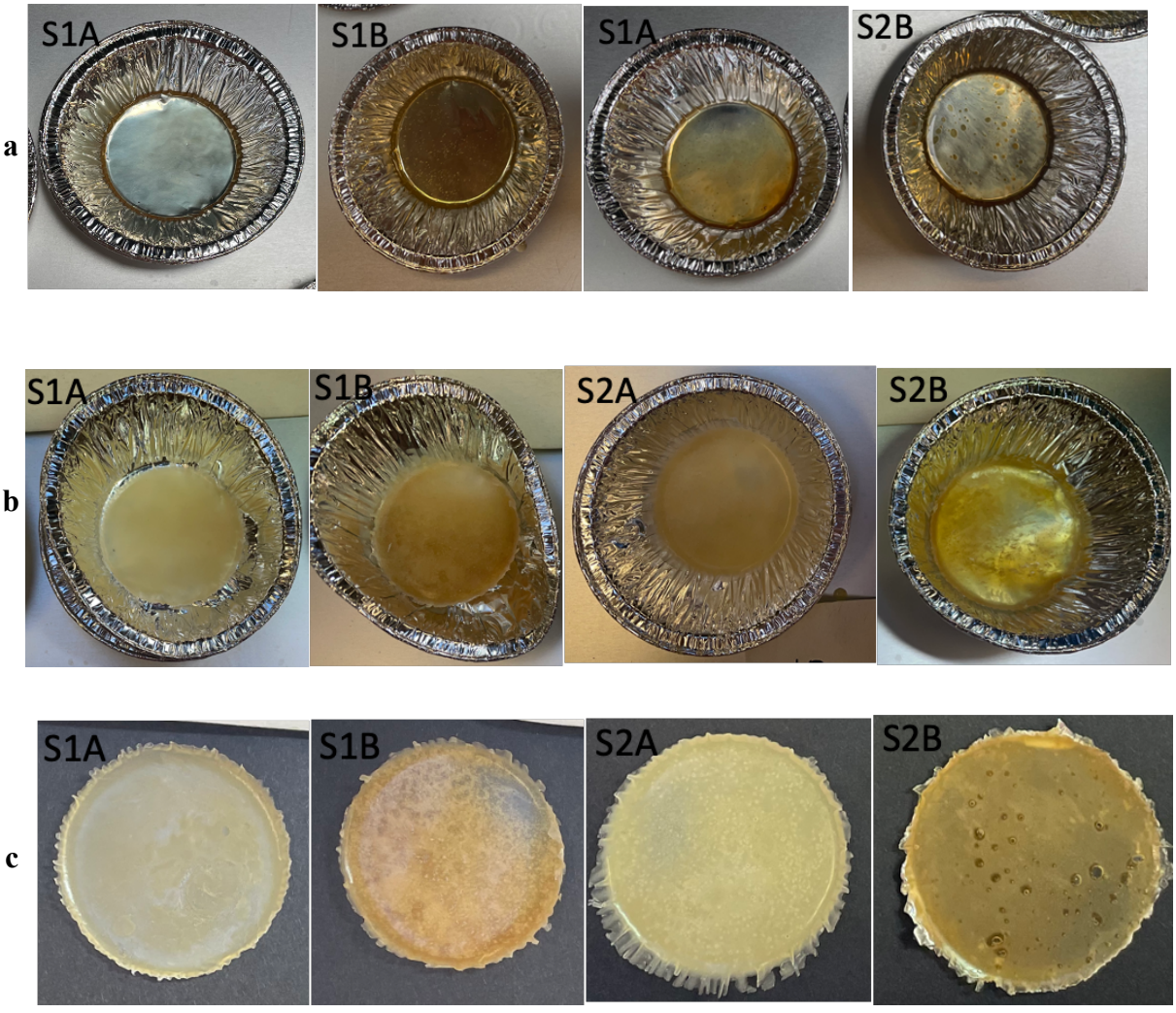

Figure 6.13. a) Film former melted at 165 °C b) After cooling c) final films.

However, adding APS to the film former did not result in film formation even at elevated temperatures. This lack of film formation in the full sizing could be due to chemical reactions induced by the addition of the silane, which might inhibit the film-forming process. Figure 6.14 (a and b) depicts the appearance of the fully sized mixture dried at 110 °C and 165 °C, respectively. Further experimental adjustments, such as altering the pH of the sizing emulsion

or varying the concentration of the sizing components, were attempted but failed to yield films from the full sizing. Silanes are known to engage in hydrolysis and condensation reactions that can lead to cross-linking, affecting the material's ability to form a continuous phase necessary for film formation. One theory would be Maleic anhydride groups in MAPP can react with the amino groups (-NH2) in APS through a chemical reaction that forms covalent bonds. This reaction creates additional cross-links between the APS and the MAPP, disrupting the typical polymer chain mobility. Additionally, the presence of APS could influence the viscosity and surface tension characteristics of the mixture, further complicating the film formation process. The precise mechanism, however, would require further investigation to elucidate the chemical dynamics at play.

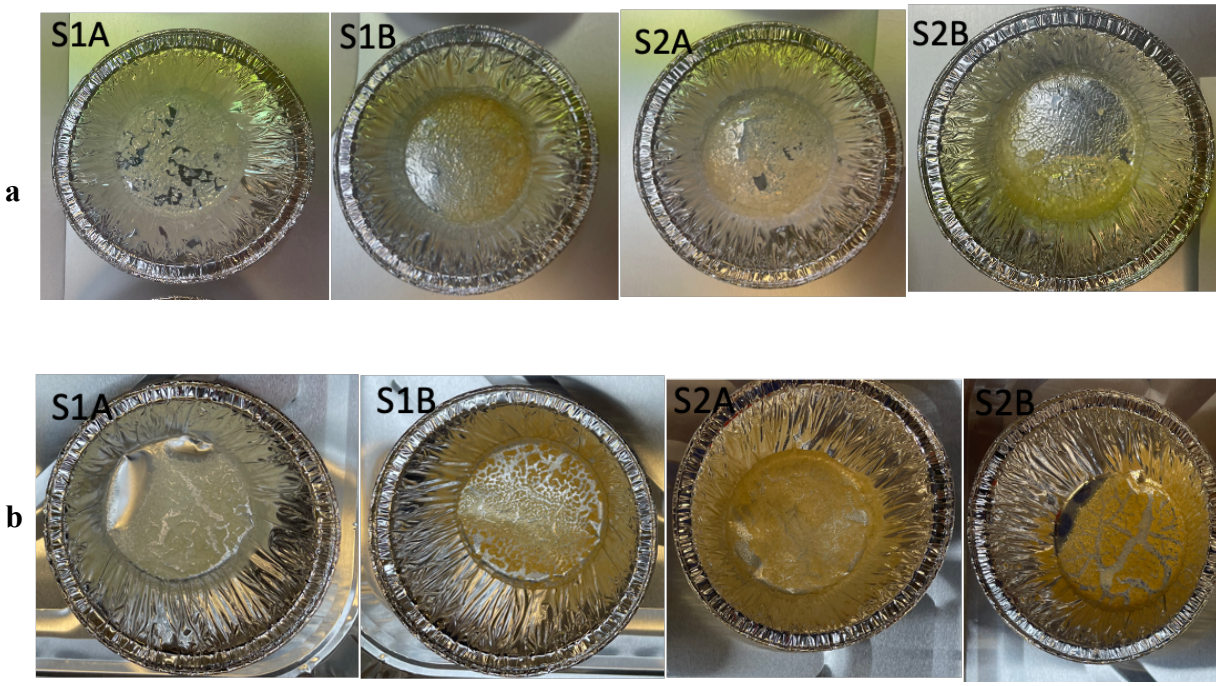

Figure 6.14. Full sizing dried at a) 110 and b)165 °C.

6.4.5.1. Sizing observation in glass container and on microscope slide

Additional efforts to produce a sizing film involved applying the sizing onto a glass substrate to determine whether direct contact with glass would alter the film formation behaviour. Figure 6.15 illustrates the appearance of the dried sizing within the glass container. Despite these efforts, a uniform film was not achieved. Nevertheless, the sizing exhibited strong adhesion to the glass substrate, which suggests the possibility of some chemical bonding occurring between the sizing components and the glass surface. This adherence could be due to the reactivity of

the APS silane with the glass, forming siloxane bonds that are known for their strong adhesive properties, particularly when paired with glass substrates.

Figure 6.15. S1A sizing in glass container.

The four investigated sizing formulations were applied to microscope slides and subsequently examined under an optical microscope after drying. Each sizing underwent both dip coating and spin coating to garner comprehensive details about their structures (Figure 6.16). As anticipated, each sizing exhibited a unique structure and particle morphology, with a more pronounced layer of sizing observed on the dip coated slides.

The differing molecular weights and concentrations of MAPP in the sizing formulations might be responsible for these variations. Heavier molecular weights and higher concentrations can lead to increased viscosity and, consequently, thicker coatings with more substantial particle agglomerations when dip coating is employed.

While it is challenging to confirm whether the exact structures observed on the slides will replicate on the surface of glass fibres, the microscopic analysis still provides valuable insights into the structure and homogeneity of the sizing films, as well as the crystallization behaviour of the dried sizing. These insights could be utilized to predict the quality of the sizing. The morphology seen on the slides can serve as an indicator of how the sizing might behave on a glass fibre surface, although the actual performance would need to be validated through direct application and testing on glass fibres.

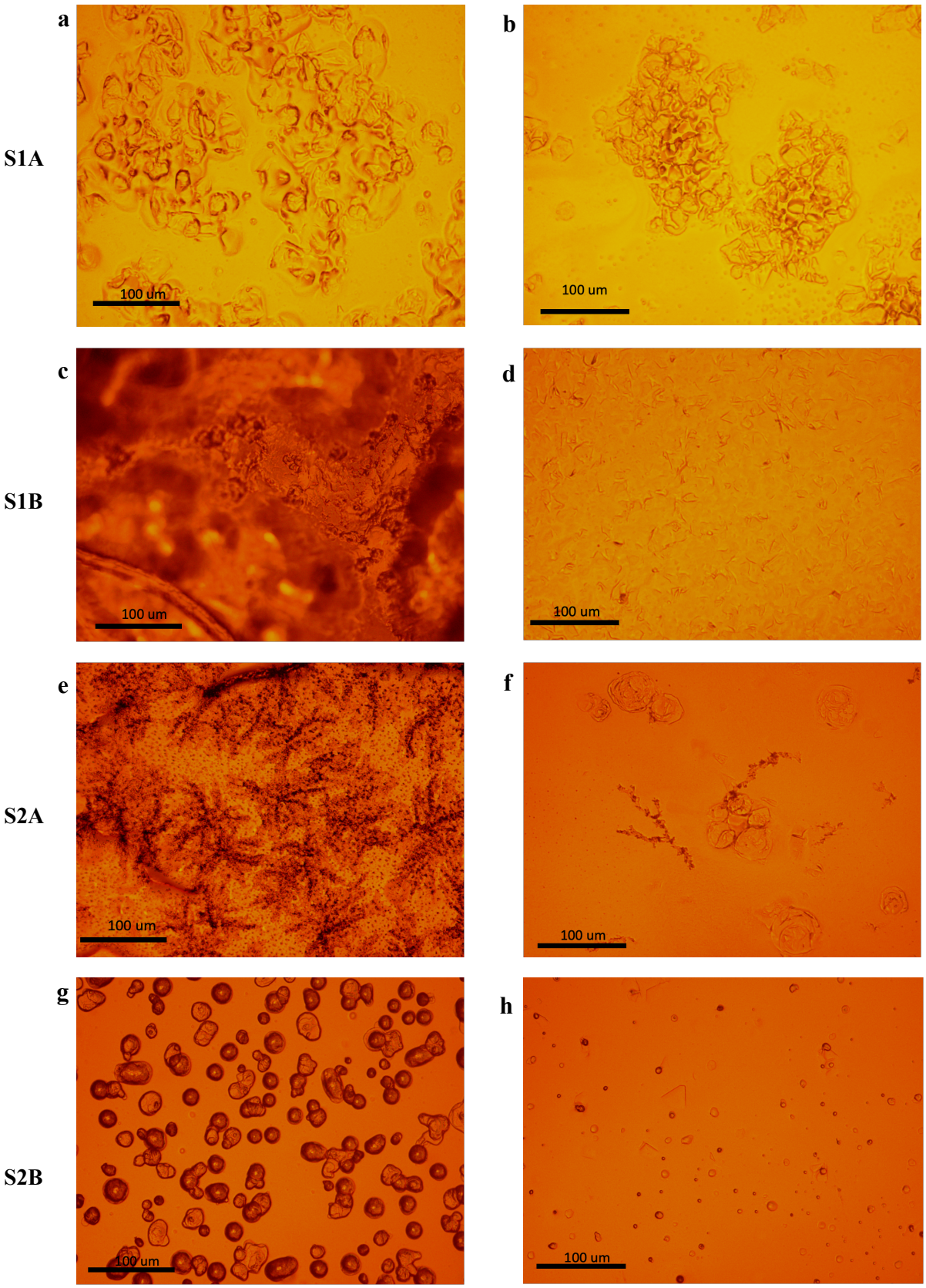

Figure 6.16. Investigated sizing structures on microscope slides, left 100x, right 200x.

The morphology of particle alignment within sizing S2A resembled a crystallized structure, prompting the capture of images using a polarized microscope to substantiate this hypothesis

(Figure 6.17). Furthermore, the same sizing formulations were applied to the bare fibre surface and subjected to drying in a hot stage chamber, as depicted in Figure 6.18. While it is not distinctly evident that crystallization occurs on the fibre surface in the same manner, the potential for such crystallization cannot be ruled out.

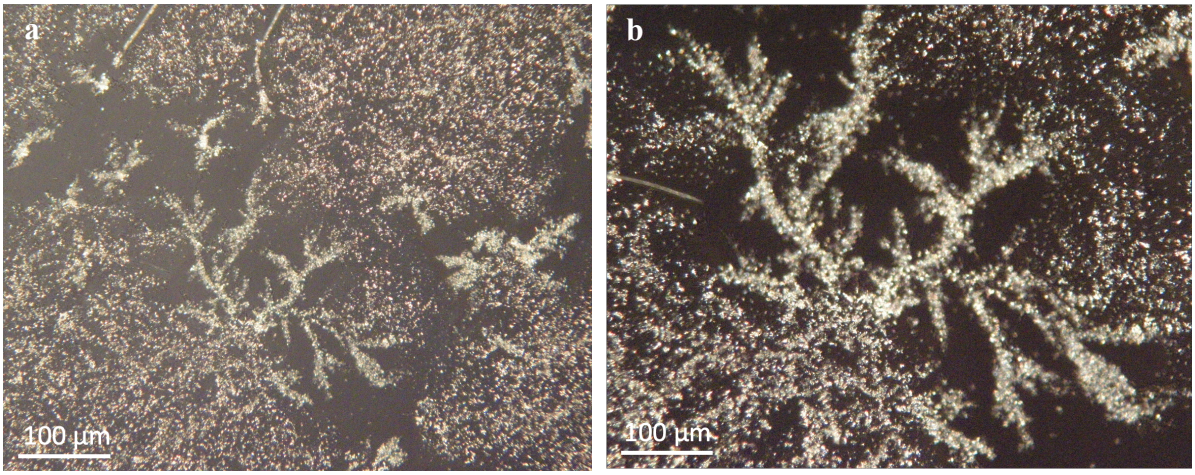

Figure 6.17. S2A sizing crystallisation a) 100x and b) 200x.

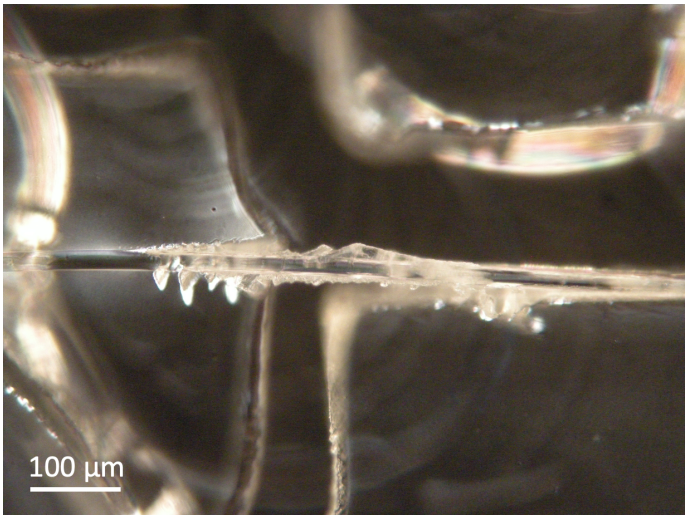

Figure 6.18. S2A sizing on bare glass fibre (200x).

There have been no previous reports addressing the potential crystallization of sizing and its potential implications on the properties of the final composite product, including whether such crystallization might occur on the glass fibre surface. However, this study has revealed that certain sizings do indeed undergo crystallization. The specific crystallization observed in S2A may be attributed to the use of a homoPP film former, unlike the other sizings which utilize a copolymer PP film former. HomoPP exhibits a highly uniform molecular chain structure,

resulting in elevated crystallinity levels. The Crystalline structures may prevent adequate matrix penetration, leading to compromised adhesion. Furthermore, the rigidity of crystalline polymers can lead to cracking or delamination under stress, further compromising the interface. This inherent characteristic leads to greater crystallinity compared to copolymer PP. This finding should be considered when formulating sizing materials in the future.

6.5. Conclusion

Chapter 6 has presented the analysis of the thermal and interfacial properties of glass fibres sized with various film formers and APS silane coupling agents, explaining their effects on adhesion with the PP and MAPP thermoplastic matrices. TGA of the sized glass fibres revealed a major weight loss event between 200–300 °C, consistent with the degradation of the MAPP film former and the aminosilane coupling agent. FTIR provided further insight into the chemical structure of the sizing agents, confirming the presence of characteristic functional groups such as Anhydride, PP and Amino groups.

Microbond testing results illustrated that the IFSS of glass fibres sized with only film former did not exhibit significant improvement compared to BF. However, the addition of APS to the sizing noticeably enhanced the IFSS in both PP and MAPP matrix systems, concluding that the silane coupling agents play the critical role in the interfacial properties of the glass fibre thermoplastic systems.

The study also explored the film formation capabilities of the sizing formulations. It was found that heating below the melting point of MAPP did not result in film formation, while heating above this temperature led to the formation of films upon cooling. The full sizing, including both PP film former and APS, did not form films even at elevated temperatures, suggesting that the chemical reactions between APS and MAPP may disrupt the film formation process. This could be due to the hydrolysis and condensation reactions of silanes leading to cross-linking, which affects the ability of the material to form a continuous phase.

Overall, chapter 6 significantly advances the understanding of how film formers and silane coupling agents influence the thermal and interfacial behaviours of glass fibre thermoplastic composites. The findings lay a foundation for future research to further explore the effect of other sizing components such as anti-static agents and lubricants on the interfacial properties of glass fibre thermoplastic systems.

CHAPTER 7: SUMMARY AND RECOMMENDATIONS FOR FUTURE WORK

7.1. Statement on the novelty of the work presented

Before going into the comprehensive conclusions detailed in the three results chapters (4-6), an assertion of the originality of the research conducted in this thesis is provided:

1. The development of a new lab-based fibre coating technique allowed to have sized fibres with properties such as LOI% and size thickness as close as industrial sized fibres. The developed method makes it possible to replicate the industry sizing process more closely than dip coating, which allows to have a better fundamental study in a laboratory environment.

2. The systematic study of fibre sized with three common silane coupling agents allowed to understand the role of silane more when combining with different thermoplastic matrices, and evaluate the compatibility of each silane with each thermoplastic. It was demonstrated that the APS/MAPP system exhibited enhanced performance compared to other polymeric systems. This improvement is attributed to both physical interactions and fundamental acid-base chemical interactions between the basic amino groups on the silanized glass fibre surface and the acidic groups of the maleic anhydride-grafted matrix.

3. A fundamental study of PP film former and PP compatible sized fibre allowed to understand more about the role of film former and full sizing. In addition, the developed lab-based spin coating method was found to be effective in providing results closer to the industrial sized fibres. It was noted that silane coupling agents play a key role in the interfacial properties, and film former only coated fibre did not show any improvement in the interfacial properties.

7.2. Summary of conclusions

7.2.1. Novel fibre coating method using spin coating technique

Chapter 4 of the thesis tackles the challenge of replicating industrial glass fibre sizing techniques within a laboratory setting, a step necessary for systematic research and to

democratise information on sizing. Historically, dip coating has been the default method when industrial means like bushing and sizing applicators were unavailable. However, dip coating typically results in a thick sizing layer and a high percentage of LOI%, which does not accurately reflect industrial product. Modifying the concentration of sizing components to alter the thickness is suboptimal and fails to replicate industrial formulations and procedures authentically.

Therefore, efforts were directed towards developing a more representative sizing technique similar to industrial sized fibre. Alternative methods employed in various sectors, such as brush or foam roller applications and spray techniques, were considered but dismissed due to the high risk of fibre damage and the challenge of achieving uniform coverage. Another method that was tried successfully in coating the fibre was spin coating. This technique, widely used in sectors like pharmaceuticals for film development, was adapted for the first time to the field of glass fibre sizing.

The spin coated, dip coated, and industrial sized fibres were evaluated for LOI% and thermal degradation. Additionally, the IFSS of the PP compatible sized fibres with PP and MAPP matrices were assessed. The IFSS of the epoxy compatible sizing were evaluated with epoxy resin. The conclusions summarised from chapter 4 are as follows:

1. Thermal degradation studies of the PP compatible sizing, using TGA demonstrate that spin coating can achieve a LOI% (0.8%) nearly identical to that of industrial-sized fibre (1%). In contrast, dip coating results in an excessively high LOI% around 11%, which remains significantly elevated (approximately 2.5%) even after a tenfold reduction in sizing concentration. The thermal degradation behaviour of industrial sized and spin coated fibres were also found to be closely aligned. The same behaviour of the thermal degradation was noticed in epoxy compatible sized fibres, with the achieved LOI% of as low as 0.5%, which is the same with the studied industrial fibre.
2. Experimental evidence indicates that spin coating possesses marked benefits over dip coating. It enables precise manipulation of the sizing layer's thickness and uniformity, facilitating an optimal fibre polymer interphase that is vital for the mechanical efficacy of composites.
3. Spin coating allows for the adjustment of LOI% and the investigation of different sizing layer thicknesses without the need to alter the sizing formulation concentration.

4. Microbond testing revealed that spin coated fibres generally exhibit higher apparent IFSS values compared to dip coated fibres, with IFSS figures approaching those of industrial sized fibres.

In essence, this work has led to the establishment of a new laboratory-based sizing method that is closer to the industrial process, enhancing accessibility and cost-efficiency for research purposes.

7.2.2. Study of silane and IFSS

Chapter 5 studied how different silane coupling agents (APS, GPS, and MPS) influence the performance of glass fibres within prevalent thermoplastic matrices such as PP, MAPP, PA6, and PBT. This chapter presents a comprehensive analysis of thermal degradation, chemical composition, and the adhesion-promoting properties of these silanes. The TGA findings indicate that among the three silanes, MPS exhibits superior thermal stability. FTIR spectroscopy of silane-sized glass fibre samples reveal a signature at 2926 and 2856 cm^{-1}, indicative of C-H stretching vibrations in CH_2 and CH_3 groups, respectively. Additionally, a notable peak at around 1740 cm^{-1} corresponds to C=O stretching vibrations of carbonyls, an observation consistent across all samples.

Application of the series of silane coupling agents (APS/GPS/MPS) on glass fibres significantly enhances the apparent IFSS with PP about 40% for APS and MPS, and 70% for GPS compared to BF. Spin coating with APS further amplifies this improvement to around 80%. A notable increase in IFSS is also observed with APS sized fibres in MAPP matrices, displaying an approximate 20% rise with dip coating and 36% with spin coating. However, for other silanes, the increases in IFSS are not substantial when compared to bare fibres. In PA6 and PBT systems, significant differences between silane-coated and bare fibres are largely absent, except for a 21% enhancement in IFSS with APS spin coated fibres in PA6. Overall, the IFSS findings indicate that modifications to the matrix are of paramount importance in affecting the adhesion properties between glass fibres and thermoplastic matrices. A clear example of this can be observed in the differences in IFSS between PP and MAPP.

The study also investigates the influence of APS concentration on adhesion properties. Interestingly, only a marked improvement is noted with a 0.2% APS concentration in the PA6 matrix, which surpassed the IFSS value obtained with a 1% concentration. This finding

suggests that lower APS concentrations could also suffice for optimal adhesion properties in silane only coated fibre.

Furthermore, altering the pH of APS solutions does not appear to significantly affect the final adhesion properties across the thermoplastics studied. This outcome indicates that adjusting the pH is not a requisite step for APS application or its hydrolysis process, underscoring the robustness of APS as a silane coupling agent in enhancing the adhesion properties of glass fibre-thermoplastics.

7.2.3. Study of PP compatible sizing and IFSS

In the chapter 6 the Study of the PP compatible sizing with different PP film former and their impact on IFSS were discussed. Also, the two laboratory-based coating methods i.e. dip coating and spin coating were employed in order to have comprehensive and good data set. A comprehensive evaluation of thermal degradation, chemical composition, and the adhesion-promoting properties of these sizings with PP and MAPP were reported. Furthermore, the details of the attempt for film formation of these sizings were mentioned.

The TGA results for spin coated and dip coated fibres with different sizing formulations indicate a major weight loss event between 200–300 °C, consistent with the degradation of both PP film former and the APS. This degradation profile is in line with previous studies and suggests the prominence of MAPP and APS as principal constituents in PP compatible sizings. The similarity in thermal degradation patterns between industrial and experimentally coated fibres, despite the confidentiality of exact sizing formulations, is notable and reinforces the understanding of the thermal behaviour of these key sizing components. The DTG analysis further reveals two stage thermal events in dip coated fibres, hinting at that some sizing components might sling off during sizing process in industrial process and spin coating.

The FTIR spectroscopy analysis of PP compatible sized glass fibres reveal distinctive spectral features associated with their chemical composition. The characteristic triplet peaks observed at 2950, 2918, and 2836 cm^{-1} correspond to the C-H stretching vibrations of CH, CH_2, and CH_3 groups respectively, which are typical of PP coatings. A peak at 1023 cm^{-1} is indicative of the C-O stretching vibrations from the Maleic anhydride component of the sizing. The region between 1200–800 cm^{-1} is largely dominated by the strong Si-O-Si signals emanating from the glass fibres themselves, making other signals less prominent, especially in spin coated fibres where the sizing layer is thinner. In dip coated fibres, where the sizing layer is thicker, spectral

bands of MAPP become discernible, such as the peak at 1032 cm^{-1} associated with the C-O-C stretching of ethers and the peak at 910 cm^{-1} related to the C-O stretching of the oxirane ring. These findings are crucial for understanding the chemical interactions and the composition of the sizing layers applied to glass fibres.

The IFSS demonstrates that glass fibres sized with just a film former yield insufficient adhesion values. For fibres sized with FF in a MAPP matric, the IFSS is slightly lower than that of BF, with the FF sized fibres showing an IFSS of 17.3 MPa compared to 18.3 MPa for the BF. The same pattern is seen in the PP matrix, where film former sized fibres have an IFSS of 6.7 MPa, only marginally higher than the 5.3 MPa for BF. These outcomes suggest that using film former alone does not markedly improve fibre/matrix adhesion. In contrast, the inclusion of APS in the sizing significantly boosts IFSS values in both PP and MAPP matrices. APS sized fibres show an IFSS of 24.2 MPa in MAPP and 12.3 MPa in PP, indicating the effectiveness of APS in enhancing interfacial bonding, due to its amino reactive group.

Furthermore, the application of a complete S1A sizing yields even better IFSS results, with fibres achieving 22.6 MPa in MAPP and 13.1 MPa in PP matrices. This improvement implies that a more comprehensive sizing approach, which incorporates APS and potentially other components, is superior in improving the fibre/matrix interface than the application of a film former by itself.

The research delved into the film-forming characteristics of MAPP film former emulsions and a comprehensive sizing blend that incorporated both MAPP film former and APS silane. It was observed that the process of heating these substances to temperatures below MAPP's melting point of approximately 160 °C did not result in the formation of a film. This remained consistent even with adjustments such as modifying the pH or altering the concentration of the sizing components, indicating a possible interference by the chemical reactions, particularly those involving the silane, which might impede the film formation.

Furthermore, attempts to form a film by applying the sizing directly onto a glass substrate did not yield a uniform film; however, strong adhesion to the glass was noted, suggesting potential chemical bonding, possibly through siloxane bonds known for their adhesive strength, especially to glass surfaces.

In addition to these findings, the examination of the four different sizing formulations, through both dip coating and spin coating, revealed distinct structures and particle morphologies on

microscope slides. A thicker layer of sizing was more evident on the dip coated slides. These structural differences are expected to significantly impact the interfacial properties, such as adhesion, which are crucial for the performance of composite materials comprising fibres and matrix.

7.3. Recommendations for future work

For future research directions, the introduction of a novel spin coating method for fibre coating, as presented in chapter 4, offers expansive potential for fundamental research into glass fibre sizings. It has been demonstrated that a higher Loss on Ignition (LOI%) value, which results from dip coating and leads to a thicker sizing layer, negatively impacts the IFSS between fibre and matrix. Conversely, the reduced LOI% values characteristic of industrial-sized and spin coated fibres contribute to enhanced IFSS. Future studies could focus on the influence of LOI% on glass fibre adhesion without altering the sizing concentration, leveraging the spin coating method. This approach allows for the exploration of more complex sizing formulations and their development. Additionally, refining the spin coating technique to accommodate the coating of larger fibre bundles could further enhance its applicability in industrial settings.

Chapter 5 revealed that APS, GPS, and MPS had a positive impact on improving the IFSS between the fibre and the PP matrix, particularly with APS showing an effect on IFSS in the MAPP matrix. From the IFSS results it was shown that spin coating technique would potentially be used for silane sizing of the fibres, however more investigation and characterization should be done in the future on the technique. Furthermore, future research is needed to look into the intricate interplay between silane chemistry and thermoplastic polymer matrices. This investigation aims to identify and optimize the nature of both physical and chemical interactions, ultimately enhancing the fibre/matrix interfacial properties to their optimal potential.

Chapter 6 explored the use of various PP film formers in conjunction with APS. Nonetheless, there remains ample room for additional research aimed at the development of more intricate sizing formulations that incorporate additives such as lubricants or anti-static agents. The objective is to gain a comprehensive understanding of the roles these additives play and to discover an optimized sizing formulation.

An analysis of FTIR results across dip coated, spin coated, and industrially-sized fibres reveals distinctive patterns. The thermogram of dip coated fibres exhibits certain peaks that are either

absent or less pronounced in the case of spin coated or industrially-sized fibres. A similar trend is observed in the TGA graphs, where dip coated fibres display a two-stage degradation process, whereas spin coated or industrially-coated fibres exhibit only one peak and stage of degradation. Further exploration of these distinctions using surface analysis techniques such as XPS could yield valuable insights.

To advance the characterization of sizing emulsions, more characterisation methods can be employed, such as evaluating viscosity using Viscometer or conducting particle size analyses. These approaches provide a deeper understanding of sizing materials and contribute to high-quality sizing characterization.

Efforts have been made to investigate the impact of different sizing formulations on deformation. However, consistent film quality has not been achieved. This aspect deserves further investigation to determine whether film quality directly affects sizing quality or if there are other factors at play.

References

1. Thomason, J.L., *Glass Fibre Sizing : A Review of Size Formulation Patents*. 2015: Blurb.co.uk.
2. Wang, S.-h., et al., *Effect of Nano SiO2 on Phase Structure and Properties of Impact Polypropylene Copolymer Resin.* Acta Polymerica Sinica, 2017(7): p. 1097-1104.
3. De Fazio, D., et al., *A Review on the Recycling Technologies of Fibre-Reinforced Plastic (FRP) Materials Used in Industrial Fields.* Journal of Marine Science and Engineering, 2023. **11**(4): p. 851.
4. Thomason, J.L., *Glass fibre sizing: A review.* Composites Part A: Applied Science and Manufacturing, 2019. **127**: p. 105619.
5. Acharya, A., *Chapter 16 - Metal oxide glass fibers*, in *Metal Oxide Glass Nanocomposites*, S. Bhattacharya, Editor. 2020, Elsevier. p. 273-278.
6. Thomason, J.L., *Glass fibre sizings : A review of the scientific literature*. 2012: Blurb.co.uk.
7. Thomason, J., *A review of the analysis and characterisation of polymeric glass fibre sizings.* Polymer Testing, 2020. **85**: p. 106421.
8. Reilly, S. and J. Thomason. *Effects of silane coating on the properties of glass fibre and glass fibre reinforced epoxy resin*. in *14th European conference on composite materials, ECCM14*. 2010.
9. Dibenedetto, A. and P. Lex, *Evaluation of surface treatments for glass fibers in composite materials.* Polymer Engineering & Science, 1989. **29**(8): p. 543-555.
10. Hamada, H., et al., *Effect of interfacial silane network structure on interfacial strength in glass fibre composites.* Composites, 1994. **25**(7): p. 512-515.

11. Berg, J. and F. Jones, *The role of sizing resins, coupling agents and their blends on the formation of the interphase in glass fibre composites.* Composites Part A: Applied Science and Manufacturing, 1998. **29**(9-10): p. 1261-1272.

12. Gao, X., et al., *Effect of fiber surface texture created from silane blends on the strength and energy absorption of the glass fiber/epoxy interphase.* Journal of Composite Materials, 2008. **42**(5): p. 513-534.

13. Thomason, J.L., *A note on the investigation of the composite interphase by means of thermal analysis.* Composites Science and Technology, 1992. **44**(1): p. 87-90.

14. Vazquez, A., et al., *Interphase modification in unidirectional glass-fiber epoxy composites.* Composites science and technology, 1998. **58**(3-4): p. 549-558.

15. Tan, C., et al., *L-DOPA coating improved phosphate glass fibre strength and fibre/matrix interface.* Journal of the Mechanical Behavior of Biomedical Materials, 2022. **136**: p. 105480.

16. Bryce, D., *Investigation of a micromechanical methodology for assessing the influence of processing variables and fibre sizing on composite interphase*, in *Aerospace and Mechnical Department*. University of Stratclyde.

17. Yue, C.Y. and M.Y. Quek, *The interfacial properties of fibrous composites.* Journal of Materials Science, 1994. **29**(9): p. 2487-2490.

18. Mazumdar, S., Karthikeyan, D., Pichler, D., Benevento, M., *State of the composites industry report for 2017*, in *Composites Manufacturing Magazine*. 2017.

19. Morampudi, P., et al., *Review on glass fiber reinforced polymer composites.* Materials Today: Proceedings, 2021. **43**: p. 314-319.

20. Pirzada, M.M., *Recent Trends and Modifications in Glass Fibre Composites–A Review.* Int. J. Mater. Chem, 2015. **5**: p. 117-122.

21. museum, T.a.o. *Composite Materials*. 2010; Available from: http://www.aviation-history.com/theory/composite.htm.

22. *100% recyclable wind turbine blades*, in *Plasticlemag*. 2022.

23. Tan, W., et al., *The role of interfacial properties on the intralaminar and interlaminar damage behaviour of unidirectional composite laminates: Experimental characterization and multiscale modelling.* Composites Part B: Engineering, 2018. **138**: p. 206-221.

24. Jones, F.R. and N.T. Huff, *The structure and properties of glass fibers*, in *Handbook of properties of textile and technical fibres*. 2018, Elsevier. p. 757-803.

25. Mahltig, B. and Y. Kyosev, *Inorganic and composite fibers: production, properties, and applications*. 2018: Elsevier.

26. Jones, F., X. Liu, and J. Thomason, *The differential adsorption of silanes from solution onto model E-glass surfaces using high-resolution XPS.* Silanes and other coupling agents. Vol. 4. 2007: CRC Press. 29-37.

27. Loewenstein, K.L., *The manufacturing technology of continuous glass fibres*. 1973: Elsevier.

28. Thomason, J., *Interfaces and interfacial effects in glass reinforced thermoplastics-Keynote Presentation.* In: Proceedings of the 28th Risø International Conference on Materials Science. , 2007.

29. Petersen, H.N., *Investigation of sizing-from glass fibre surface to composite interface.* Materials Science, Engineering, 2017.

30. Park, S.-J., J.-S. Jin, and J.-R. Lee, *Influence of silane coupling agents on the surface energetics of glass fibers and mechanical interfacial properties of glass fiber-reinforced composites.* Journal of Adhesion Science and Technology, 2000. **14**(13): p. 1677-1689.

31. Maity, P., et al., *Improvement in surface degradation properties of polymer composites due to pre-processed nanometric alumina fillers.* IEEE Transactions on Dielectrics and Electrical Insulation, 2008. **15**(1): p. 63-72.

32. Witucki, G.L., *A silane primer: chemistry and applications of alkoxy silanes.* Journal of coatings technology, 1993. **65**: p. 57-57.

33. Liu, Z., F. Zhao, and F.R. Jones, *Optimising the interfacial response of glass fibre composites with a functional nanoscale plasma polymer coating.* Composites science and technology, 2008. **68**(15-16): p. 3161-3170.

34. MELITO, S., *Thermoplastics vs. Thermoset Plastics: Material Properties Overview*, in *Fictive*. 2022.

35. Arias, F., *Assessment of present/future decommissioned wind blade fiber-reinforced composite material in the United States*, in *Dept. of Civil Engineering, City College of New York, United States*. 2016.

36. Jacob, A., *Composites can be recycled.* Reinforced Plastics, 2011. **55**(3): p. 45-46.

37. *Council Directive 1999/31/EC of 26 April 1999 on the landfill of waste*, in *31999L0031*, T.C.O.T.E. UNION, Editor. 1999: Official website of the European Union.

38. Wong, J., *Processing of high performance thermoplastic composites*, in *ETH Zürich, Laboartory of Composite Materials and Adaptronic Structures*. 2017.

39. Maddah, H.A., *Polypropylene as a promising plastic: A review.* J. Polym. Sci, 2016. **6**(1): p. 1-11.

40. Zhou, X., et al., *Effects of maleic anhydride-grafted polypropylene (MAPP) on the physico-mechanical properties and rheological behavior of bamboo powder-polypropylene foamed composites.* BioResources, 2013. **8**(4): p. 6263-6279.

41. Kondo, M.Y., et al., *Recent advances in the use of Polyamide-based materials for the automotive industry.* Polímeros, 2022. **32**.

42. Zohuri, G., *Polymer science: a comprehensive reference*. 2012: Elsevier.

43. Herrera-Franco, P. and L. Drzal, *Comparison of methods for the measurement of fibre/matrix adhesion in composites.* Composites, 1992. **23**(1): p. 2-27.

44. Pitkethly, M.J., *The use of interfacial test methods in composite materials development*, in *Fiber, matrix, and interface properties*. 1996, ASTM International.

45. Zhuang, R.-C., et al., *Affecting glass fibre surfaces and composite properties by two stage sizing application.* eXPRESS Polymer Letters, 2010. **4**(12).

46. Thomason, J.L., *Interfacial strength in thermoplastic composites - at last an industry friendly measurement method?* Composites Part A: Applied Science and Manufacturing, 2002. **33**(10): p. 1283-1288.

47. Thomason, J., *Micromechanical parameters from macromechanical measurements on glass reinforced polypropylene.* Composites Science and Technology, 2002. **62**(10-11): p. 1455-1468.

48. Miller, B., P. Muri, and L. Rebenfeld, *A microbond method for determination of the shear strength of a fiber/resin interface.* Composites Science and Technology, 1987. **28**(1): p. 17-32.

49. Gaur, U. and B. Miller, *Microbond method for determination of the shear strength of a fiber/resin interface: Evaluation of experimental parameters.* Composites Science and Technology, 1989. **34**(1): p. 35-51.

50. Blacks, J., R. Latour, and B. Miller, *Failure of desiccator storage to maintain interfacial bond strength in some thermoplastic/fiber systems.* Journal of adhesion science and technology, 1989. **3**(1): p. 65-67.

51. Miller, B., U. Gaur, and D.E. Hirt, *Measurement and mechanical aspects of the microbond pull-out technique for obtaining fiber/resin interfacial shear strength.* Composites science and technology, 1991. **42**(1-3): p. 207-219.

52. Chou, C., U. Gaur, and B. Miller, *The effect of microvise gap width on microbond pull-out test results.* Composites science and technology, 1994. **51**(1): p. 111-116.

53. McDonough, W.G., J.M. Antonucci, and J.P. Dunkers, *Interfacial shear strengths of dental resin-glass fibers by the microbond test.* Dental Materials, 2001. **17**(6): p. 492-498.

54. Kang, S.-K., D.-B. Lee, and N.-S. Choi, *Fiber/epoxy interfacial shear strength measured by the microdroplet test.* Composites Science and Technology, 2009. **69**(2): p. 245-251.

55. Ozzello, A., et al., *Interfacial shear strength of ion beam modified UHMW-PE fibers in epoxy matrix composites.* MRS Online Proceedings Library (OPL), 1989. **153**.

56. Sheu, G. and S. Shyu, *Surface properties and interfacial adhesion studies of aramid fibres modified by gas plasmas.* Composites science and technology, 1994. **52**(4): p. 489-497.

57. Liu, F.P., et al., *Characterization of the interface between cellulosic fibers and a thermoplastic matrix.* Composite Interfaces, 1994. **2**(6): p. 419-432.

58. Craven, J., R. Cripps, and C. Viney, *Evaluating the silk/epoxy interface by means of the microbond test.* Composites Part A: Applied Science and Manufacturing, 2000. **31**(7): p. 653-660.

59. Liu, Z., et al., *Analysis of a modified microbond test for the measurement of interfacial shear strength of an aqueous-based adhesive and a polyamide fibre.* Composites Science and Technology, 2011. **71**(13): p. 1529-1534.

60. Koyanagi, J., et al., *Time and temperature dependence of carbon/epoxy interface strength.* Composites Science and Technology, 2010. **70**(9): p. 1395-1400.

61. Yang, L. and J. Thomason, *Interface strength in glass fibre–polypropylene measured using the fibre pull-out and microbond methods.* Composites Part A: Applied Science and Manufacturing, 2010. **41**(9): p. 1077-1083.

62. Dirand, X., et al., *Interfacial shear strength in glass-fiber/vinylester-resin composites.* Composites science and technology, 1996. **56**(5): p. 533-539.

63. Chizyuka, C.G., G.M. Munakaampe, and S.B. Kanyanga, *Effects of Hydrothermal Ageing on the Microbond Interfacial Shear Strength of NaOH Treated Sisal Fibre Reinforced Polyester Composites.* Journal of Natural and Applied Sciences, 2016. **2**(1): p. 39-54.

64. Yang, L. and J. Thomason, *Development and application of micromechanical techniques for characterising interfacial shear strength in fibre-thermoplastic composites.* Polymer Testing, 2012. **31**(7): p. 895-903.

65. Zhi, C., H. Long, and M. Miao, *Influence of microbond test parameters on interfacial shear strength of fiber reinforced polymer-matrix composites.* Composites Part A: Applied Science and Manufacturing, 2017. **100**: p. 55-63.

66. Wagner, H., H.E. Gallis, and E. Wiesel, *Study of the interface in Kevlar 49-epoxy composites by means of microbond and fragmentation tests: effects of materials and testing variables.* Journal of Materials Science, 1993. **28**: p. 2238-2244.

67. Minty, R.F., L. Yang, and J.L. Thomason, *The influence of hardener-to-epoxy ratio on the interfacial strength in glass fibre reinforced epoxy composites.* Composites Part A: Applied Science and Manufacturing, 2018. **112**: p. 64-70.

68. Downes, K.A. and J.L. Thomason, *A method to measure the influence of humidity and temperature on the interfacial adhesion in polyamide composites.* Composite Interfaces, 2015. **22**(8): p. 757-766.

69. Thomason, J., *An overview of some scaling issues in the sample preparation and data interpretation of the microbond test for fibre-matrix interface characterisation.* Polymer Testing, 2022. **111**: p. 107591.

70. Haaksma, R.A. and M.J. Cehelnik, *A critical evaluation of the use of the microbond method for determination of composite interfacial properties.* MRS Online Proceedings Library (OPL), 1989. **170**: p. 71.

71. Bryce, D., J.L. Thomason, and L. Yang, *Thermoset droplet curing performance in the microbond test.* Composite Interfaces, 2023.

72. Yang, L., J.L. Thomason, and W. Zhu, *The influence of thermo-oxidative degradation on the measured interface strength of glass fibre-polypropylene.* Composites Part A: Applied Science and Manufacturing, 2011. **42**(10): p. 1293-1300.

73. Pawlak, A. and E. Piorkowska, *Crystallization of isotactic polypropylene in a temperature gradient.* Colloid and Polymer Science, 2001. **279**: p. 939-946.

74. Thomason, J.L. and G. Porteus, *An investigation of glass–fiber reinforced polyamide 66 during conditioning in various automotive fluids.* Polymer composites, 2011. **32**(9): p. 1369-1379.

75. Pandey, G., C. Kareliya, and R. Singh, *Effect of Testing Parameters on Data Scatter in Microbond Testing.* Society for Experimental Mechanics - SEM Annual Conference and Exposition on Experimental and Applied Mechanics 2009, 2009. **4**.

76. Zhandarov, S. and E. Mäder, *Peak force as function of the embedded length in pull-out and microbond tests: effect of specimen geometry.* Journal of Adhesion Science and Technology, 2005. **19**(10): p. 817-855.

77. Nagel, U., et al., *Effects of thermal recycling temperatures on the reinforcement potential of glass fibers.* Polymer Composites, 2018. **39**(4): p. 1032-1040.

78. Kumar, A., P. Singh, and A. Nanda, *Hot stage microscopy and its applications in pharmaceutical characterization.* Applied Microscopy, 2020. **50**(1): p. 12.

79. McCrone, W.C., *Polarized light microscopy / Walter C. McCrone, Lucy B. McCrone, John Gustav Delly*, ed. L.B. McCrone, J.G. Delly, and I. McCrone Research. 1984: McCrone Research Institute.

80. Vitez, I.M., et al., *The evolution of hot-stage microscopy to aid solid-state characterizations of pharmaceutical solids.* Thermochimica acta, 1998. **324**(1-2): p. 187-196.

81. Minty, R.F., et al., *Development and application of novel technique for characterising the cure shrinkage of epoxy resins.* Polymer Testing, 2019. **73**: p. 316-326.

82. Coats, A.W. and J.P. Redfern, *Thermogravimetric analysis. A review.* Analyst, 1963. **88**(1053): p. 906-924.

83. Thomason, J.L., et al., *A study of the thermal degradation of glass fibre sizings at composite processing temperatures.* Composites Part A: Applied Science and Manufacturing, 2019. **121**: p. 56-63.

84. Jenkins, P., et al. *Investigation of the strength of thermally conditioned basalt and E-glass fibres*. in *20th International Conference on Composite Materials*. 2015.

85. Jenkins, P., *Investigation of the strength loss of heat treated glass fibre*, in *Department of Mechanical and Aerospace Engineering*. 2016, University of Strathclyde.

86. Rudzinski, S., et al., *Glass fibre reinforced polyamide composites: Thermal behaviour of sizings.* Composites Part A: Applied Science and Manufacturing, 2011. **42**(2): p. 157-164.

87. Gao, P., et al., *Effects of chemical composition and thermal stability of finishes on the compatibility between glass fiber and high melting temperature thermoplastics.* Polymer Composites, 2000. **21**(2): p. 312-321.

88. Feih, S., et al., *Mechanical properties of thermally-treated and recycled glass fibres.* Composites Part B: Engineering, 2011. **42**(3): p. 350-358.

89. McMullan, D., *Scanning electron microscopy 1928–1965.* Scanning, 1995. **17**(3): p. 175-185.

90. Bledzki, A.K., et al., *Characterization of the surfaces of treated glass fibres with different methods of investigation.* Composite Interfaces, 1997. **5**(1): p. 41-53.

91. Le-Huy, C.C., L.G. Britcher, and J.G. Matisons, *The effect of silane concentration on the adsorption of poly (vinyl acetate-co-maleate) and γ-methacryloxypropyl-trimethoxysilane onto E-glass fibers.* Silicon Chemistry, 2002. **1**: p. 195-205.

92. Kiio, T.M. and S. Park, *Nano-scientific Application of Atomic Force Microscopy in Pathology: from Molecules to Tissues.* Int J Med Sci, 2020. **17**(7): p. 844-858.

93. Rädlein, E. and G.H. Frischat, *Atomic force microscopy as a tool to correlate nanostructure to properties of glasses.* Journal of non-crystalline solids, 1997. **222**: p. 69-82.

94. El Achari, A., et al., *Topographic Study of Glass Fibers by Atomic Force Microscopy.* Textile Research Journal, 1996. **66**(8): p. 483-490.

95. Turrión, S.G., D. Olmos, and J. González-Benito, *Complementary characterization by fluorescence and AFM of polyaminosiloxane glass fibers coatings.* Polymer Testing, 2005. **24**(3): p. 301-308.

96. Behary, N., et al., *Tribology of Sized Glass Fibers: Part I: Friction Analysis by Lateral Force Microscopy and Electronic Microbalance Technique.* Textile Research Journal, 2000. **70**(8): p. 700-708.

97. Gupta, P.K., et al., *Nanoscale roughness of oxide glass surfaces.* Journal of Non-Crystalline Solids, 2000. **262**(1): p. 200-206.

98. Mai, K., E. Mäder, and M. Mühle, *Interphase characterization in composites with new non-destructive methods.* Composites Part A: Applied Science and Manufacturing, 1998. **29**(9): p. 1111-1119.

99. Chiang, C.-H., H. Ishida, and J.L. Koenig, *The structure of γ-aminopropyltriethoxysilane on glass surfaces.* Journal of Colloid and Interface Science, 1980. **74**(2): p. 396-404.

100. Naviroj, S., et al., *Structure and adsorption characteristics of silane coupling agents on silica and E-glass fiber; dependence on pH.* Journal of Colloid and Interface Science, 1984. **97**(2): p. 308-317.

101. Bikiaris, D., et al., *Use of silane agents and poly (propylene-g-maleic anhydride) copolymer as adhesion promoters in glass fiber/polypropylene composites.* Journal of applied polymer science, 2001. **81**(3): p. 701-709.

102. Larson, B. and L. Drzal, *Glass fibre sizing/matrix interphase formation in liquid composite moulding: effects on fibre/matrix adhesion and mechanical properties.* Composites, 1994. **25**(7): p. 711-721.

103. International, A., *Standard Test Methods for Loss on Ignition (LOI) of Solid Combustion Residues: ASTM D7348-13*. 2013: ASTM International.

104. Dibenedetto, A.T. and P.J. Lex, *Evaluation of surface treatments for glass fibers in composite materials.* Polymer Engineering & Science, 1989. **29**(8): p. 543-555.

105. Scriven, L.E., *Physics and Applications of DIP Coating and Spin Coating.* MRS Online Proceedings Library, 1988. **121**(1): p. 717-729.

106. Dong, Y., et al., *Enhance interfacial properties of glass fiber/epoxy composites with environment-friendly water-based hybrid sizing agent.* Composites Part A: Applied Science and Manufacturing, 2017. **102**: p. 357-367.

107. Dwight, D.W., et al., *Acid-base interfaces in fiber-reinforced polymer composites.* Journal of adhesion science and technology, 1990. **4**(1): p. 619-632.

108. Frey, M. and A.J. Brunner, *Assessing glass-fiber modification developments by comparison of glass-fiber epoxy composites with reference materials: Some thoughts on relevance.* Proceedings of the Institution of Mechanical Engineers, Part L: Journal of Materials: Design and Applications, 2017. **231**(1-2): p. 49-54.

109. Tyona, M.D., *A theoritical study on spin coating technique.* Advances in materials research, 2013. **2**: p. 195-208.

110. Nguyen, N.-T., *Chapter 4 - Fabrication technologies*, in *Micromixers (Second Edition)*, N.-T. Nguyen, Editor. 2012, William Andrew Publishing: Oxford. p. 113-161.

111. Nandy, S. and K.H. Chae, *17 - Chemical synthesis of ferrite thin films*, in *Ferrite Nanostructured Magnetic Materials*, J. Pal Singh, et al., Editors. 2023, Woodhead Publishing. p. 309-334.

112. Öz, S., et al., *5 - Industrial perspectives on the upscaling of perovskite materials for photovoltaic applications and its environmental impacts*, in *Metal Halide Perovskites for Generation, Manipulation and Detection of Light*, J.P. Martínez-Pastor, P.P. Boix, and G. Xing, Editors. 2023, Elsevier. p. 117-142.

113. Amokrane, G., et al., *A simple method to functionalize PCL surface by grafting bioactive polymers using UV irradiation.* Irbm, 2018. **39**(4): p. 268-278.

114. Zinck, P., et al., *Mechanical characterisation of glass fibres as an indirect analysis of the effect of surface treatment.* Journal of Materials Science, 1999. **34**(9): p. 2121-2133.

115. Xu, L., *Interfacial engineering of the interphase between carbon fibers and vinyl ester resin*. 2003: Michigan State University.

116. Petersen, H.N., et al. *Analysis of glass fibre sizing*. in *Proceedings of the 28th international conference on surface modification technol-ogies*. 2014.

117. Plueddemann, E.P., *Silane Coupling Agents*. 1991, Boston, MA: Springer US. 1-28.

118. Ishida, H., *A review of recent progress in the studies of molecular and microstructure of coupling agents and their functions in composites, coatings and adhesive joints.* Polymer Composites, 1984. **5**(2): p. 101-123.

119. Park, S.-J. and M.-K. Seo, *Chapter 9 - Modeling of Fiber–Matrix Interface in Composite Materials*, in *Interface Science and Technology*, S.-J. Park and M.-K. Seo, Editors. 2011, Elsevier. p. 739-776.

120. Nishikawa, M., et al., *Micromechanical modeling of the microbond test to quantify the interfacial properties of fiber-reinforced composites.* International Journal of Solids and Structures, 2008. **45**(14): p. 4098-4113.

121. Dai, S.-R. and M. Piggott, *The strengths of carbon and Kevlar fibres as a function of their lengths.* Composites science and technology, 1993. **49**(1): p. 81-87.

122. Nairn, J.A., Y.C. Liu, and C. Galiotis, *Analysis of stress Transfer from the Matrix to the fiber Through an imperfect Interface: Application to Raman Data And the Single-Fiber Fragmentation test.* ASTM special technical publication, 1996. **1290**: p. 47-66.

123. Tripathi, D. and F. Jones, *Single fibre fragmentation test for assessing adhesion in fibre reinforced composites.* Journal of materials science, 1998. **33**: p. 1-16.

124. Kelly, A. and a.W. Tyson, *Tensile properties of fibre-reinforced metals: copper/tungsten and copper/molybdenum.* Journal of the Mechanics and Physics of Solids, 1965. **13**(6): p. 329-350.

125. Piggott, M. and Y. Xiong, *Direct observation of debonding in fiber pull-out specimens*, in *Fiber, Matrix, and Interface Properties*. 1996, ASTM International.

126. Aziz, S.H. and M.P. Ansell, *The effect of alkalization and fibre alignment on the mechanical and thermal properties of kenaf and hemp bast fibre composites: Part 1 – polyester resin matrix.* Composites Science and Technology, 2004. **64**(9): p. 1219-1230.

127. Medina M, C., et al., *Comparison of push-in and push-out tests for measuring interfacial shear strength in nano-reinforced composite materials.* Journal of Composite Materials, 2016. **50**(12): p. 1651-1659.

128. Mandell, J.F., et al. *Modified mircodebonding test for direct in situ fiber/matrix bond strength determination in fiber composites*. in *Composite materials: testing and design (seventh conference)*. 1986. ASTM International.

129. Afrizal, A., et al., *Investigation of Meniscus Effect on Microbond Test of Typha Fiber/Epoxy Matrix.* Defect and Diffusion Forum, 2020. **402**: p. 14-19.

130. Greene, J.P., *12 - Polymer Composites*, in *Automotive Plastics and Composites*, J.P. Greene, Editor. 2021, William Andrew Publishing. p. 191-222.

131. Favre, J.-P. and D. Jacques, *Stress transfer by shear in carbon fibre model composites: Part 1 Results of single-fibre fragmentation tests with thermosetting resins.* Journal of Materials Science, 1990. **25**: p. 1373-1380.

132. Mittal, K.L., *Silanes and Other Coupling Agents, Volume 4*. Vol. 4. 2007: CRC Press.

133. Mittal, K.L., *Silanes and other coupling agents, vol. 2.* VSP, Utrecht, 2000.

134. Mittal, K., *Silanes and other coupling agents: festschrift in honor of the 75th birthday of Dr. Edwin P. Plueddemann.* (No Title), 1992.

135. Tanoglu, M., et al., *The effects of glass-fiber sizings on the strength and energy absorption of the fiber/matrix interphase under high loading rates.* Composites science and technology, 2001. **61**(2): p. 205-220.

136. Mäder, E., *Study of fibre surface treatments for control of interphase properties in composites.* Composites science and technology, 1997. **57**(8): p. 1077-1088.

137. Zhao, F. and N. Takeda, *Effect of interfacial adhesion and statistical fiber strength on tensile strength of unidirectional glass fiber/epoxy composites. Part I: experiment results.* Composites Part A: Applied Science and Manufacturing, 2000. **31**(11): p. 1203-1214.

138. Mäder, E., S.-l. Gao, and R. Plonka, *Static and dynamic properties of single and multi-fiber/epoxy composites modified by sizings.* Composites science and technology, 2007. **67**(6): p. 1105-1115.

139. Koenig, J.L. and H. Emadipour, *Mechanical characterization of the interfacial strength of glass-reinforced composites.* Polymer composites, 1985. **6**(3): p. 142-150.

140. Gao, X., et al., *Effect of Fiber Surface Texture Created from Silane Blends on the Strength and Energy Absorption of the Glass Fiber/Epoxy Interphase.* Journal of Composite Materials, 2008. **42**(5): p. 513-534.

141. Feresenbet, E., D. Raghavan, and G.A. Holmes, *The influence of silane coupling agent composition on the surface characterization of fiber and on fiber-matrix interfacial shear strength.* The Journal of Adhesion, 2003. **79**(7): p. 643-665.

142. Gomez, J. and J. Kilgour. *The effect of temperature on silane coupling agent performance at the glass fiber/resin interface*. in *TECHNICAL SESSIONS OF THE*

ANNUAL CONFERENCE-COMPOSITES INSTITUTE. 1993. SOCIETY OF THE PLASTICS INDUSTRY, INC.

143. Feresenbet, E., D. Raghavan, and G. Holmes, *The influence of silane coupling agent composition on the surface characterization of fiber and on fiber-matrix interfacial shear strength.* The Journal of Adhesion, 2003. **79**(7): p. 643-665.

144. Olmos, D., R. Lopez-Moron, and J. Gonzalez-Benito, *The nature of the glass fibre surface and its effect in the water absorption of glass fibre/epoxy composites. The use of fluorescence to obtain information at the interface.* Composites science and technology, 2006. **66**(15): p. 2758-2768.

145. Sahin, M., et al., *Tailoring the interfaces in glass fiber-reinforced photopolymer composites.* Polymer, 2018. **141**: p. 221-231.

146. Peters, L., *Influence of glass fibre sizing and storage conditions on composite properties.* Durability of composites in a marine environment 2, 2018: p. 19-31.

147. Gu, S., et al., *Interfacial designing of PP/GF composites by binary incorporation of MAH-g-PP and lithium bis(trifloromethanesulfonyl)imide: Towards high strength composites with excellent antistatic performance.* Composites Science and Technology, 2018. **156**: p. 247-253.

148. Periasamy, K., et al., *Interfacial Engineering Methods in Thermoplastic Composites: An Overview.* Polymers, 2023. **15**(2): p. 415.

149. Shokoohi, S. and A. Aref Azar, *Effect of coupling agents on polymer-filler surface interactions, morphology and properties of fiber-reinforced thermoplastics.* Journal of reinforced plastics and composites, 2009. **28**(17): p. 2131-2142.

150. Lee, N.-J. and J. Jang, *The use of a mixed coupling agent system to improve the performance of polypropylene-based composites reinforced with short-glass-fibre mat.* Composites science and technology, 1998. **57**(12): p. 1559-1569.

151. Zykaite, R., et al., *Microdebond test development and interfacial shear strength evaluation of basalt and glass fibre reinforced polypropylene composites.* Journal of Composite Materials, 2017. **51**(29): p. 4091-4099.

152. Hoecker, F. and J. Karger-Kocsis, *On the effects of processing conditions and interphase of modification on the fiber/matrix load transfer in single fiber polypropylene composites.* The Journal of Adhesion, 1995. **52**(1-4): p. 81-100.

153. Laura, D., et al., *Effect of glass fiber surface chemistry on the mechanical properties of glass fiber reinforced, rubber-toughened nylon 6.* Polymer, 2002. **43**(17): p. 4673-4687.

154. Yun, S.H., et al., *Effect of silane coupling agents with different organo-functional groups on the interfacial shear strength of glass fiber/Nylon 6 composites.* Journal of materials science letters, 2003. **22**(22): p. 1591-1594.

155. Jenneskens, L., et al., *Molecular mechanisms of adhesion promotion by silane coupling agents in glass bead-reinforced polyamide-6 model composites.* Composites, 1994. **25**(7): p. 504-511.

156. Noda, K., et al., *Aggregation structure and molecular motion of (glass-fiber/matrix nylon 66) interface in short glass-fiber reinforced nylon 66 composites.* Polymer, 2002. **43**(14): p. 4055-4062.

157. Wagner, H. and J. Nairn, *Residual thermal stresses in three concentric transversely isotropic cylinders: application to thermoplastic-matrix composites containing a transcrystalline interphase.* Composites Science and Technology, 1997. **57**(9-10): p. 1289-1302.

158. Di Landro, L. and M. Pegoraro, *Evaluation of residual stresses and adhesion in polymer composites.* Composites Part A: Applied Science and Manufacturing, 1996. **27**(9): p. 847-853.

159. Thomason, J.L., L. Yang, and R. Meier, *The properties of glass fibres after conditioning at composite recycling temperatures.* Composites Part A: Applied Science and Manufacturing, 2014. **61**: p. 201-208.

160. Nairn, J.A., *Thermoelastic analysis of residual stresses in unidirectional, high-performance composites.* Polymer Composites, 1985. **6**(2): p. 123-130.

161. Thomason, J. and L. Yang, *Temperature dependence of the interfacial shear strength in glass–fibre polypropylene composites.* Composites Science and Technology, 2011. **71**(13): p. 1600-1605.

162. Wang, X., et al., *Effects of thermal residual stress on interfacial properties of polyphenylene sulphide/carbon fibre (PPS/CF) composite by microbond test.* Journal of materials science, 2016. **51**: p. 334-343.

163. Park, B.J., *Attachment Energy of Janus Particles at Fluid-Fluid Interfaces.* Korean Chemical Engineering Research, 2013. **51**(6): p. 655-660.

164. Mittal, K.L.E., *Silanes and Other Coupling Agents, .* CRC Press., 2004. **Volume 3 (1st ed)**.

165. Lessa Belone, M.C., *Thermogravimetric analysis of resized glass and carbon fibers*. 2019.

166. Li, Z., et al., *Effects of surface fluoride-functionalizing of glass fiber on the properties of PTFE/glass fiber microwave composites.* RSC advances, 2017. **7**(37): p. 22810-22817.

167. Guo, Z., et al., *Surface functionalized alumina nanoparticle filled polymeric nanocomposites with enhanced mechanical properties.* Journal of Materials Chemistry, 2006. **16**(27): p. 2800-2808.

168. Petersen, H.N., et al. *Preliminary characterization of glass fiber sizing*. in *Proceedings of the Risø international symposium on materials science*. 2013. Risø National Laboratory.

169. Thomason, J., *The interface region in glass fibre-reinforced epoxy resin composites: 3. Characterization of fibre surface coatings and the interphase.* Composites, 1995. **26**(7): p. 487-498.

170. Ishida, H. and J.L. Koenig, *Fourier transform infrared spectroscopic study of the structure of silane coupling agent on E-glass fiber.* Journal of Colloid and Interface Science, 1978. **64**(3): p. 565-576.

171. Bashir, S.T., *A chemical approach to regenerating the performance of thermally damaged glass fibres*, in *Aerospace and Mechnical Department*. 2019, University of Stratclyde.

172. Xiang, Q., et al., *Effects of melt reprocessing on volatile emissions and structural/rheological changes of unstabilized polypropylene.* Polymer Degradation and Stability, 2002. **77**(1): p. 93-102.

173. DePolo, W.S., *Dimensional Stability and properties of thermoplastics reinforced with particulate and fiber fillers.* 2005.

174. Minty, R.F., *The influence of matrix stoichiometry on interfacial adhesion in composites for wind turbine applications.* 2018.

175. Pearson, A., et al., *Effect of temperature on the fiber-matrix adhesion in glass fiber reinforced thermoplastics.* Composites Science and Technology, 2022. **230**: p. 109782.

176. Jia, N. and V.A. Kagan, *Mechanical Performance of Polyamides with Influence of Moisture and Temperature – Accurate Evaluation and Better Understanding*, in

Plastics Failure Analysis and Prevention, J. Moalli, Editor. 2001, William Andrew Publishing: Norwich, NY. p. 95-104.

177. McKeen, L.W., *Chapter 1 - Introduction to Plastics and Polymers*, in *Film Properties of Plastics and Elastomers (Third Edition)*, L.W. McKeen, Editor. 2012, William Andrew Publishing: Boston. p. 1-18.

178. Nygård, P., K. Redford, and C.-G. Gustafson, *Interfacial strength in glass fibre-polypropylene composites: influence of chemical bonding and physical entanglement.* Composite Interfaces, 2002. **9**(4): p. 365-388.

179. Thomason, J.L., *The interface region in glass fibre-reinforced epoxy resin composites: 3. Characterization of fibre surface coatings and the interphase.* Composites, 1995. **26**(7): p. 487-498.

180. Tillie, M., T. Lam, and J. Gerard, *Insertion of an interphase synthesised from a functionalised silicone into glass-fibre/epoxy composites.* Composites science and technology, 1998. **58**(5): p. 659-663.

181. Mäder, E. and E. Pisanova, *Characterization and design of interphases in glass fiber reinforced polyproplyene.* Polymer composites, 2000. **21**(3): p. 361-368.

182. Mäder, E. and K. Freitag, *Interface properties and their influence on short fibre composites.* Composites, 1990. **21**(5): p. 397-402.

183. Fraser, W., et al., *Evaluation of surface treatments for fibers in composite materials.* Polymer Composites, 1983. **4**(4): p. 238-248.

184. Thomason, J.L. and G.E. Schoolenberg, *An investigation of glass fibre/polypropylene interface strength and its effect on composite properties.* Composites, 1994. **25**(3): p. 197-203.

185. Scholtens, B.J. and J.C. Brackman, *Influence of the film former on fibre-matrix adhesion and mechanical properties of glass-fibre reinforced thermoplastics.* The Journal of Adhesion, 1995. **52**(1-4): p. 115-129.

186. Mäder, E., et al., *Surface, interphase and composite property relations in fibre-reinforced polymers.* Composites, 1994. **25**(7): p. 739-744.

187. Rausch, J., R. Zhuang, and E. Mäder, *Systematically varied interfaces of continuously reinforced glass fibre/polypropylene composites: Comparative evaluation of relevant interfacial aspects.* eXPRESS Polymer Letters, 2010. **4**(9).

188. Zhuang, R.-C., T. Burghardt, and E. Mäder, *Study on interfacial adhesion strength of single glass fibre/polypropylene model composites by altering the nature of the surface of sized glass fibres.* Composites Science and Technology, 2010. **70**(10): p. 1523-1529.

189. Thomason, J.L. and L.J. Adzima, *Sizing up the interphase: an insider's guide to the science of sizing.* Composites Part A: Applied Science and Manufacturing, 2001. **32**(3): p. 313-321.

190. Thomason, J., *Interfacial strength in thermoplastic composites-at last an industry friendly measurement method?* Composites Part A: Applied Science and Manufacturing, 2002. **33**(10): p. 1283-1288.

191. Raghava, R., *Thermal expansion of organic and inorganic matrix composites: A review of theoretical and experimental studies.* Polymer Composites, 1988. **9**(1): p. 1-11.

192. Ramos, G., A. Gomez, and J. Guardiola, *The influence of stability of raw materials used in sizings for E and AR fiberglass manufacture.* Polymer degradation and stability, 1996. **51**(3): p. 361-365.

193. Kitagawa, K., S. Hayasaki, and Y. Ozaki, *In situ analysis of sizing agents on fibre reinforcements by near-infrared light-fibre optics spectroscopy.* Vibrational spectroscopy, 1997. **15**(1): p. 43-51.

194. McGravey, M.P., *An investigation into the structure and performance of a glass fibre size*. 2008, Durham University.

195. Eriksson-Scott, K., *How surfactants affect trialkoxysilanes in aqueous emulsions*. 2015, University of Western Sydney (Australia).

196. McMican, R., *Sizing stability is a key element for glass fibre manufacturing.* Reinforced Plastics, 2012. **56**(5): p. 29-32.

197. Inc, M. *Glass Fibre Manufacturing and Sizing Stability*. 2018.

198. Chemical, D. *Silane recation with water, The role of catalysts*. 2024; Available from: https://www.dakenchem.com/silane-reaction-with-water/#:~:text=Catalysts%20in%20Silane%2DWater%20Reaction,silane%20and%20water%20reaction%20mechanism.

199. Koay, S.C., S. Husseinsyah, and H. Osman, *Modified cocoa pod husk-filled polypropylene composites by using methacrylic acid.* BioResources, 2013. **8**(3): p. 3260-3275.

200. Mäder, E., E. Moos, and J. Karger-Kocsis, *Role of film formers in glass fibre reinforced polypropylene — new insights and relation to mechanical properties.* Composites Part A: Applied Science and Manufacturing, 2001. **32**(5): p. 631-639.